

Chapter 2

Characterisation of Colloidal Suspensions

Working with colloidal suspensions means to adjust or to monitor certain properties of the single particles and of the whole disperse system. This may concern the generation and modification of colloidal particles, the preparation and processing of suspensions from such particles, or the observation of the colloids' behaviour in physiological and environmental media. Each of these tasks requires appropriate techniques for the determination of the relevant particle or suspension properties. There are various potentially interesting properties which may be classified as follows (Polke et al. 2003; Stintz et al. 2010):

- particle morphology (size, shape, structure)
- particle properties based on hydrodynamics or specific interactions with external fields that relate to morphology (e.g. diffusion, settling, scattering)
- surface area of the dispersed phase
- interfacial properties which depend on solvents (e.g. surface charge, zeta-potential)
- concentration of particles (e.g. mass or number concentration, total or per size fraction)
- suspension properties (e.g. turbidity, viscosity, stability)
- bulk properties of the dispersed phase and its interaction with the solvent (e.g. solubility and dissolution kinetics)

Each point corresponds to numerous measurands and even more characterisation techniques. In practice, however, only a few parameters are important for evaluating process performance or product quality. This chapter will focus on characterisation techniques that allow for a quantification of particle size and aggregate structure, which are of fundamental importance in describing any colloidal suspension. Besides this, relevant techniques for the quantification of interfacial properties are presented.

2.1 Particle Size Distribution

Particle size is one of the most important parameters when describing colloidal suspensions. It is the only criterion for classifying a particle as a *colloidal particle* or even *nanoparticle*, it changes during aggregation processes or during dispersion and comminution and it is related to other properties like surface area or settling velocity. For this reason, particle size serves as one of the fundamental parameters when characterising colloidal suspensions.

However, the term *particle size* does not describe an unambiguous quantity, but rather a variety of measurands which are related to the outer particle dimensions. Indeed, particle size is always derived from a geometrical or physical property. If the property is not a length, it is usually converted to a diameter of a sphere being equivalent to the particle with regard to this property. The corresponding diameter is called equivalent diameter (e.g. equivalency in volume V leads to volume equivalent diameter x_V). Table 2.1 lists some of these properties and the associated equivalent diameters.

In general, particle properties vary within a particle system and the particle size x should be regarded as a distributed parameter. Size distributions can be depicted by the cumulative function Q_r , the density function q_r , or the transformed density function q_r^* :

$$dQ_r = q_r dx = q_r^* d \ln x = \frac{\text{amount of particles in } x \cdot x + dx}{\text{total amount of particles}}, \quad (2.1)$$

where the index r characterises the type of quantity¹ which is employed to weigh the individually size fractions (Rumpf and Ebert 1964; Leschonski 1984; ISO 9276-1 2004).

The details of size distributions are frequently summarised in a few parameters that reflect the “average size” or the polydispersity of the particle system:

- modal value(s) $x_{\text{mod},r}$ or $x_{\text{mod}^*,r}$ of the density functions q_r and q_r^* , respectively
- median $x_{50,r}$: of Q_r
- mean size $\bar{x}_{k,r} = (\int x^k dQ_r)^{1/k}$ requires complete knowledge of q_r or Q_r (important: $k = -1, 0, 1, 2 \rightarrow$ harmonic, geometric, arithmetic mean and rms value)
- percentile (or: quantile) $x_{p,r}$: inverted cumulative distribution, $Q_r(x_{p,r}) = p\%$
- standard deviation: $s_r = \int (x - \bar{x}_{1,r})^2 dQ_r$

All three types of location parameters—modes, medians and means—are frequently used in practice; yet their meaning and robustness is not identical.

The *modal values* are characteristic values of the density functions q and q^* , which appear to be the immediate result of most sizing techniques (e.g. line-start disc centrifugation, spectroscopic techniques). Modal values represent the most

¹A cumulable quantity like volume, number, or scattering intensity of a dilute particle system.

Table 2.1 Particle properties, in brackets the associated equivalent diameters (if existing)

Geometric properties	Properties related to mobility	Interaction with external fields
Volume (x_V)	Settling velocity (x_{Stokes})	Weight/inertia (x_m)
Surface (x_S)	Translational diffusion coefficient ($x_{h,t}$)	Extinction cross section with regard to light or sound
Characteristic length at 2D projection (e.g. x_{Feret})	Acoustophoretic mobility (x_{ap})	Scattering cross section with regard to light or sound

frequent particle size(s) and, thus, bear a relatively low statistical uncertainty (provided the sizing technique allows to resolve modal values). Moreover, they are usually not affected by the relatively large measurement uncertainties of rare size fractions or by a lacking sensitivity to very fine or very coarse particles. Note, that $x_{\text{mod},r}$ and $x_{\text{mod}^*,r}$ are not identical and that the latter—derived from q_r^* —is usually employed for very broad size distributions. Last but not least, modal values do not offer an unambiguous characterisation, since a size distribution can consists of several modes.

Median values split the particle population into a fine and a coarse fraction of equal weight (in the selected type of quantity). They are obtained from the cumulative function Q_r , which commonly has to be computed from the originally measured density functions q or q^* . Only a few methods directly reflect the cumulatively function Q_r in their results (e.g. cuvette centrifugation). Unlike modal values, the median is adversely affected if the weights of certain size classes, in particular at the lower and upper end of the size distribution, are not accurately quantified. However, the exact knowledge of, e.g., x_{\min} or x_{\max} is not required. Medians are unequivocally defined and reliably reflect global changes in the size distribution.

A *mean* particle size corresponds to the expectation value of a certain power k of x , i.e. to a certain moment of the distribution function. It is affected by the main modes of distribution as well as by the rare fractions at the ends of the size distribution. In the case of arithmetic means all size classes are equally weighted (with given type of quantity), whereas quadratic means (rms values) are more sensitive to coarse particles, and harmonic means are more affected by the fine ones. The accurate calculation of means values from a distribution function, therefore, requires the exact knowledge of q_r for the total size range including the size and frequency of the finest and coarsest size fractions. The major advantage of mean values is that they correspond to effective properties of the dispersed phase (e.g. to its specific surface area, or to the suspension turbidity). They can, thus, be measured directly without the necessity of resolving the size distribution. Such values (e.g. the intensity weighted harmonic mean $x_{-1,\text{int}}$ or x_{cum} in the case of dynamic light scattering) can be measured with higher reliability and lower uncertainty than even modal or median values.

Other characteristic size parameters of the distribution function are the *percentiles* (also: *quantiles*) other than $x_{50,r}$. They are commonly used to quantify the

polydispersity, either as indicators for the minimum or maximum particle size (e.g. by $x_{10,r}$ and $x_{90,r}$, respectively) or as the difference between high and low order percentiles (e.g. $x_{90,r}-x_{10,r}$). In contrast, the standard deviation s_r is rarely computed for a size distribution q_r . Yet, it may be employed as a regression parameter when describing a given measurement result by means of an analytical distribution function.

Note that all mentioned distribution parameters are subject to the specific type of quantity in which the size distribution is weighted. Conversion between different types of quantity requires (i) models that correlate the detected particle properties with the types of quantity and (ii) the accurate quantification of q_r over the entire size range. Solving the two points is prerequisite for comparing measured size distributions. They can be, therefore, considered as fundamental challenges to any particle sizing technique.

2.2 Particle Sizing

The strict differentiation of particle size distributions with regard to the particle property and the type of quantity is not just an academic issue but indispensable when coping with the huge variety of particle sizing techniques. There are several means and physical phenomena that allow for the determination of size distributions (e.g. imaging, sedimentation, extinction). A more general distinction of particle sizing techniques is based on how the weights of the individual size fractions are determined (Fig. 2.1; cf. Stintz 2005; Stintz et al. 2010):

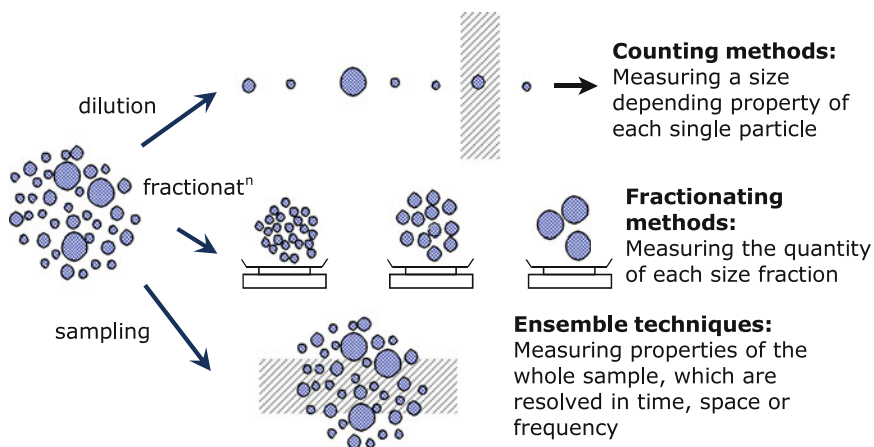


Fig. 2.1 Classification of particle sizing techniques

- counting techniques (measuring particle properties at individual particles)
- fractionating techniques (measuring the amount or concentration of size/property classes after fractionating the particle system)
- spectroscopic ensemble techniques (measuring the spectral or parametric response of a representative particle ensemble of the total particle system)

Counting techniques inherently yield number weighted distributions (Q_0) of a certain particle property or of a physical quantity that is related to a certain particle property (e.g. the average displacement as a measure of the diffusion coefficient). They rely on the individualisation of the particle sample, which can be either achieved by analysing microscopy images (e.g. from electron microscopes) or by sufficient sample dilution.² The number of detected particles per each size class is a stochastic quantity that obeys a Poisson distribution. That means that the relative uncertainty in class frequency is inversely proportional to the square root of particle counts. The probed particle property may be either geometric (in particular for image analysis), optical (e.g. scattering cross section), or related to mobility (diffusion coefficient).

Fractionating (ensemble) techniques include the two steps of fractionation and detection. The former can either result in a physical separation of the different size classes or in the depletion of coarse or fine particles in the measurement zone. In the case of colloidal suspensions, the fractionating effect is usually related to the mobility of the particles (e.g. settling velocity). The detection system monitors the fractionation process and, thus, serves for evaluating the class frequencies. It frequently employs the phase shift, extinction, or scattering of some radiation (e.g. X-rays). The applied detection system determines the type of quantity in which the size fractions are intrinsically weighted (e.g. extinction of X-rays is mass proportional $\rightarrow Q_3$).

The immediate result of a spectroscopic ensemble technique is a signal spectrum, i.e. the variation of the measured signal g over the spectral parameter s (time, space or frequency). Each size fraction x possesses a characteristic spectrum $k_r(s, x)$, which in general covers the whole spectral range. Assuming that each size fraction contributes independently and linearly to the measured signal spectrum, the determination of the size distribution requires the inversion of a linear integral equation (Fredholm type):

$$g(s) = b(s, c_r) + c_r \cdot \int k_r(s, x) q_r(x) dx, \quad (2.2)$$

where c_r is the particle concentration for the type of quantity r and $b(s, c_r)$ is a size-independent baseline signal. When s is varied over a sufficiently wide range, the spectrum can be normalised, which eliminates the concentration influence.³

²“Sufficient” means a vanishing likelihood of having two or more particles in the measurement volume.

³Note that the impact of concentration c_r is lost if $g(s)$ refers to the phase shift rather than to the magnitude of a measured quantity.

Unlike counting or fractionating techniques, the *intrinsic type of quantity* is not necessarily obvious. Indeed, Eq. (2.2) can be expressed and solved for any type of quantity r . Yet, the intrinsic type of quantity of spectroscopic techniques refers to the impact of a single particle to the integrated signal spectrum.

If the integral over the signal spectrum of one particle is proportional to the particle volume, the intrinsic type of property is the volume ($r = 3$); proportionality to the partial scattering cross section implies that the signal is intrinsically weighted by scattering intensity.

Ideally, if the value of the intrinsic type of quantity is kept constant, a variation in size will only shift the spectrum $g(s)$ along the s -axis without changing its height or shape (Babick and Ripperger 2002). Note that in measurements only a limited range of the spectral parameter s is covered, which may affect the real sensitivity to certain size fractions. The probed particle property of the spectroscopic technique can be easily described by the terms of Table 2.1. However, a profound correlation to morphological parameters is much more complicated.

The inversion of Eq. (2.2) is an essential feature of spectroscopic techniques, which requires appropriate numerical algorithms (e.g. Twomey 1977; Kandlikar and Ramachandran 1999). Moreover, any measured spectrum bears only limited information on the size distribution, i.e. only a few details of size distributions are accessible by the measurement (Fig. 2.2). This results from the discreteness and the restricted range of the spectral parameter s as well as from the uncertainty of the measured signal g . The information content is further affected by the physics of the measurement principle, which is expressed by the kernel function $k_r(s, x)$: the more structured the shape of this function, the higher the achievable resolution of the size distribution $q_r(x)$. The information content can be quantified, but just for a given set of instrument parameters. Such data have only been published for a few techniques (dynamic light scattering: Finsy et al. 1992; electroacoustic mobility spectroscopy: Knösche 2001; ultrasonic spectroscopy: Babick and Ripperger 2002).

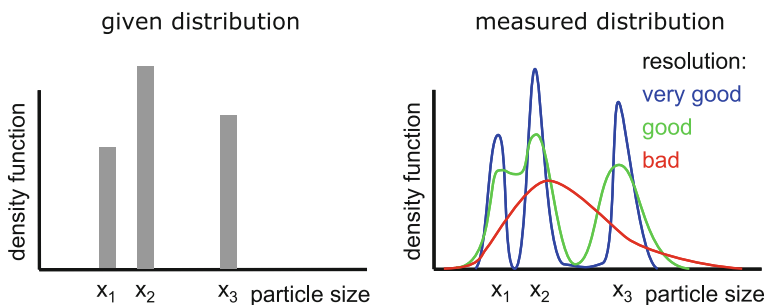


Fig. 2.2 Schematic representation of the meaning of resolution at the example of a tridisperse size distribution: truth and possible measurement results; low resolution results from low information content in the case of spectroscopic techniques

Inversion is not an issue for most counting and fractionating techniques, where the immediate measurement results can be ideally considered as scaled density and sum functions of the size distribution. However, when counting techniques measure a physical property that does not unambiguously correspond to size or when a fractionation is not perfect, the integral Eq. (2.2) also has to be applied.

In summary, every particle sizing technique is characterised by the particle property probed and its intrinsic type of quantity. Experimental size distributions, which are commonly derived for the assumption of spherical particles, may bear very different physical meanings and most often disagree (e.g. the volume weighted distribution Q_3 of the Stokes diameter x_{Stokes} differs from the number weighted distribution Q_0 of the hydrodynamic diameter x_h). For the purpose of comparison, it is in theory possible to recalculate measured distribution functions by converting the particle properties and the type of quantity. However, such a conversion requires models on the correlation between the different particle properties and the different types of quantities, which are available only for few ideal particle shapes. Moreover, the limited resolution of experimental size distributions and the uncertainty in class frequencies affect the quality of such a conversion as well (e.g. the uncertainty about the coarse particle fraction in a number weighted distribution is over-proportionally magnified when converted to volume weighted size distributions, Witt et al. 2007). Last but not least, the comparability of differently measured size distributions may be impeded by specific limitations of the covered size ranges. Such limitations occur when signals of very coarse or very fine particles cannot be separated from noise (e.g. negligible turbidity of non-absorbing nanoparticles may set a lower limit of detection for particle sizing with analytical photocentrifugation). Additionally, they can be related to a rapid migration of particles out of the measurement zone (e.g. due to sedimentation in light scattering experiments). Hence, a perfect agreement of experimental size distributions is illusory even after conversion. Yet, the intrinsic differences between the measurement methods offer the opportunity to study different aspects of particle systems (e.g. selective analysis of coarse particles) or to derive quantitative information on the shape of particles and structure of particle aggregates.

The inevitable imperfection of particle sizing compels a cautious interpretation of measured size distributions. Any computation or any conversion increases the uncertainty. Hence, data should be presented in a way that best resembles the original measurement with regard to the particle property, the type of quantity, and the distribution function (Q_r , q_r or q_r^*). Highest accuracy can be expected for the characteristic location parameters, like $x_{\text{mod},r}$ or $x_{50,r}$, whereas the values of minimum and maximum particle sizes are least reliable. The polydispersity is generally less accurately accessible than the location parameters. This holds particularly true for spectroscopic (ensemble) techniques, where the details of the size distribution (e.g. number of modal values/sizes) significantly depend on the employed inversion algorithm and its parameterisation (Stock and Ray 1985; Riebel and Löffler 1989; Koo and Hirleman 1992; Babick and Ripperger 2002).

2.3 Selected Characterisation Techniques

This section gives a brief survey on characterisation techniques that can be used to determine size distributions and interfacial properties of colloidal suspensions. They are grouped according to the classification scheme in Fig. 2.1 (counting, fractionating, and spectroscopy) and the main physical principle (e.g. imaging, scattering). Some methods that are considered most relevant for colloidal suspensions are discussed more extensively than others. The survey starts with the ultramicroscopy; not only because it belongs to the counting methods, but because of its historical relevance for colloid science. The section is concluded by a comparison of the major characterisation techniques.

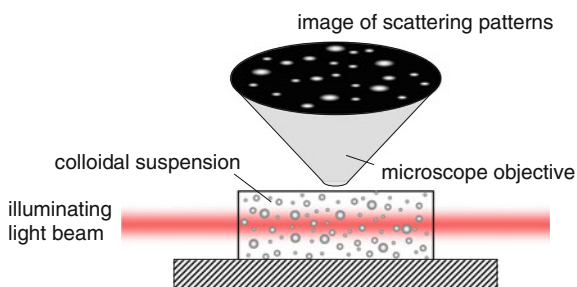
2.3.1 Ultramicroscopy

Fine colloidal particles are usually smaller than the spatial resolution of an ordinary light microscope, which means that they are invisible with regard to an affine projection. However, when colloidal particles are laterally illuminated by very intense light against a dark background (dark field microscopy), it is possible to see the scattering patterns with an optical microscope (Fig. 2.3). Since such an instrument facilitates the indirect visualisation of fine particles beyond the optical limit, it was named *ultramicroscope*.

The first ultramicroscope was developed by the Austrian-Hungarian physicist Richard Zsigmondy and the German technician Henry Siedentopf. It was based on an illumination with sunlight, which was focussed and collimated by using a pair of fine slits (Siedentopf and Zsigmondy 1903; cf. Fig. 2.4). Later, Zsigmondy proposed several optical modifications (e.g. immersion objectives) which increased the illuminance and, thus, improved the resolution (Zsigmondy 1913; Zsigmondy und Bachmann 1914).

The invention of the ultramicroscope finished a long debate of the nineteenth century on the true composition of “colloidal solutions” as it eventually disclosed their heterogeneous, disperse nature. For this reason, this technique attracted

Fig. 2.3 Principal set-up of the ultramicroscope



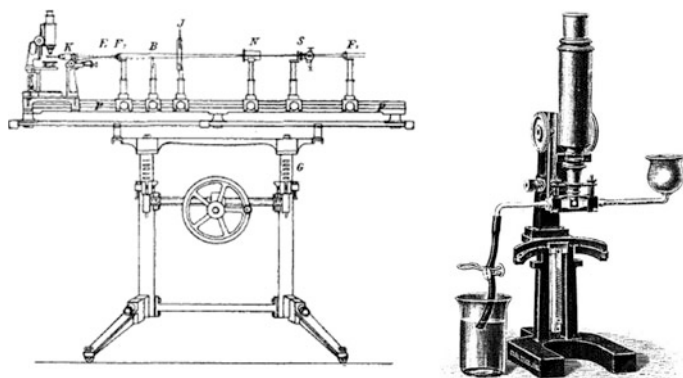


Fig. 2.4 Slit ultramicroscope (original drawing from Siedentopf and Zsigmondy 1903) and advertisement for an commercial instrument by ZEISSWERK Jena from 1907 (© Zeiss Archiv, Jena)

attention by many scientists, in particular since the discontinuity of matter and the statistical interpretation of thermodynamic phenomena had not yet been universally accepted at that time (Bigg 2008).

The instrument soon became a basic tool for colloidal scientists; it raised colloid science from a speculative theory to an independent academic discipline. The Nobel prize that was awarded to Zsigmondy in 1925 explicitly acknowledges his achievements “for elucidating the heterogeneous nature of colloidal solutions as well as for the thus employed methods, which are fundamental to modern colloid chemistry”.

Characterisation of Colloidal Suspensions by Ultramicroscopy

Already in the first publication on the ultramicroscope, Siedentopf and Zsigmondy (1903) described its application to the characterisation of colloidal systems, specifically of gold ruby, i.e. glasses in which colloidal gold particles are embedded. They showed that neither the diameter nor the colour of the diffraction patterns correlated to particle size. Instead, they estimated the size of the gold particles from the particle number concentration (obtained by counting the illuminated particles within a defined volume) based on the known mass concentration of gold. Reissig (1908), however, pointed to the fact that there is a non-linear correlation between the gold content and the detected particle number concentration. This results from the fact that the scattered light of coarse gold particles completely surpasses the scattering signals of neighbouring fine particles. For this principal reason it is difficult to accurately determine the particle number concentration by this measurement technique.

When ultramicroscopy is used for particle sizing nowadays, one evaluates the Brownian motion of the scattering centres (i.e. particles). According to Einstein (1905), the mean square displacement $\overline{\Delta r^2}$ is proportional to the translational diffusion coefficient D_t :

$$\overline{\Delta r^2} \sim D_t \cdot t. \quad (2.3)$$

The diffusion coefficient, in turn, is inversely proportional to the translational hydrodynamic diameter $x_{h,t}$ (Stokes-Einstein equation):

$$D_t = \frac{k_B T}{3\pi\eta x_{h,t}}. \quad (2.4)$$

Particle sizing, thus, involves the quantification of the trajectory lengths (Δr) of the individual scattering centres for a given time step (Δt). This measurement principle is called *dynamic ultramicroscopy* (DUM) or *particle tracking analysis* (PTA). It was first employed by Perrin (1908, 1909) for the quantification of emulsion droplets.

While at Perrin’s time the particle trajectories were recorded by means of a *camera lucida*, contemporary ultramicroscopes produce digital video sequences and evaluate them by image analysis software. The immediate results of such measurements are the average displacements $\overline{\Delta r}$ of the individual scattering objects per time step (i.e. per frame). If averaging was conducted for an infinite number of time steps, the mean displacement of a particle would be identical to the collective average. In practice, however, only a finite number of time steps is evaluated and the average displacement of particles of size $x_{h,t}$ is a stochastic quantity. The measured frequency distribution of the average displacement is, therefore, a “smeared” projection of the number weighted size distribution $q_0(x_{h,t})$:

$$p(\overline{\Delta r}) = \int P(\overline{\Delta r}, x_{h,t}) \cdot q_0(x_{h,t}) dx_{h,t}, \quad (2.5)$$

where the kernel function P depends on the number of time steps. Its shape can usually be approximated by a normal distribution (Saveyn et al. 2010). The size distribution $q_0(x_{h,t})$ can be derived from the distribution of mean displacement $p(\overline{\Delta r})$ by inversion of Eq. (2.5).

The application limits of ultramicroscopy result from the requirements that the particle distances should be much larger than the optical resolution limit of the microscope and that the scattered light of all individual particles is sufficiently strong for detection. While the former can be achieved by appropriate dilution, the latter requirement is missed for particles below a material-specific size limit.

Additionally, there are principal difficulties in detecting weak scatterers in the presence of strong scatterers. That means, though providing number weighted distributions (similar to ordinary microscopy), the dynamic ultramicroscopy has a bias to strongly scattering particles (similar to dynamic light scattering; cf. Domingos et al. 2009). This concerns very broad size distributions as well as multi-component particle systems. On the other hand, the method’s high sensitivity to strong scatterers can be used to evaluate the homogeneity or the possible contamination of a colloidal suspension.

2.3.2 Imaging Methods

Images of the particle systems give a clear idea about their morphological characteristic and are of the highest persuasiveness. Apart from a qualitative morphology description, they can be employed for quantitative analyses of size, shape, and structure as well. Particle images may be obtained from light, electron, or scanning force microscopy.

Light microscopy is the oldest and the simplest imaging method. However, the lower resolution limit for conventional light microscopy lies above 200 nm. Its application to colloidal particles is, therefore, restricted to rather large colloids and aggregates of them. Even though recent developments, like stimulated emission depletion (STED) microscopy, have shifted the optical resolution limit below 100 nm (Hell 2007), light microscopy is not really relevant for the characterisation of colloidal suspensions.

With regard to resolution, *electron microscopy* provides a powerful alternative which even allows the detection of single atoms. First instruments were developed in the 1930s by Ruska (e.g. Knoll and Ruska 1932), who later received the Nobel Prize in physics for this achievement, and von Ardenne (1938). Two fundamental types are distinguished:

- the *transmission electron microscope* (TEM), which is operated in wide-field irradiation mode and for which the image results from the local disturbance of the electron field when it passes through an ultra thin specimen, and
- the *scanning electron microscope* (SEM), which employs a very fine electron beam that scans the surface of the specimen and creates the image from backscattered primary electrons and emitted secondary electrons.

In principle, the TEM can be operated in a scanning mode, too—this modification is called transmission scanning electron microscopy (TSEM).

Traditional electron microscopy is conducted in high vacuum, which imposes specific efforts to sample preparation. Particles from colloidal suspensions have to be deposited onto an appropriate substrate (e.g. on carbon or silica films) and dried. Alternatively, the suspensions can be shock-frozen and particles are subsequently excavated from the continuous phase by special cryo-preparation techniques (Schmidt et al. 1994, pp. 694–705). The sample preparation can be considerably reduced with environmental scanning electron microscopes (ESEM), which are operated up to 1000 Pa and, thus, even facilitate the analysis of wet surfaces. However, the ease in operation is at the expense of resolution (Danilatos 1993).

A further technique able to image colloidal particles is the *scanning force microscopy*, which was developed by Binnig and his co-workers in the 1980s (e.g. Binnig et al. 1986). The scanning force microscopy (or: *atomic force microscopy*) and its related techniques are based on the interaction between a very fine probe tip with the atoms or molecules at the surface of the sample (Giessibl 2003; Danzebrink et al. 2006; cf. Fig. 2.5). This can be used to resolve surface morphologies or particles on a substrate with lateral resolution of 0.1–10 nm (axial resolution: 10 nm).

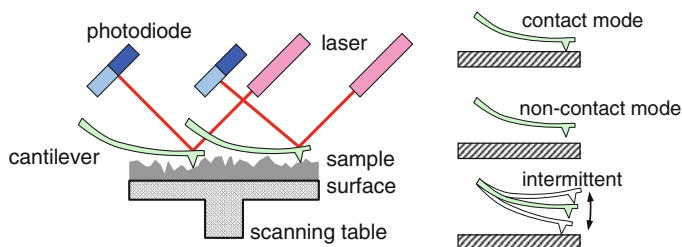


Fig. 2.5 Schematic set-up of scanning force microscopy and modes of operation; variation in surface properties are detected via the deflection of the cantilever with probing tip

The SFM is usually employed for the characterisation of films and surfaces (e.g. roughness), whereas the morphological characterisation of particles is of minor relevance. Its real strength is the sensitivity to the forces between probe and sample, which allows an evaluation of surface chemistry (e.g. functional groups, hydrophobicity) and the quantification particle interactions, or interactions between particles and surfaces (e.g. adhesion, friction; Heim et al. 1999; Butt et al. 2007).

The results of imaging methods are (mainly) number weighted distributions. That means that the sample size (number of probed particles) should be sufficiently high for ensuring low uncertainty in class frequencies. Moreover, the sample size required to achieve a certain confidence level increases with polydispersity. The accuracy of the measured particle properties depends on a variety of factors (e.g. magnification or spatial resolution of the scanning mode, or image processing). Most crucial, however, is the representativity of the imaged particles for the whole particle system. That requires that the particle deposition on the substrate is neither size-selective nor inhomogeneous (Fiala et al. 2011). In general, sample preparation is a key issue for imaging methods.

2.3.3 Fractionating Sizing Techniques

Fractionating sizing techniques combine a size-related classification process with the measurement of particle quantities. The classification may yield a physical separation of differently sized particles (e.g. by sieving, cf. Fig. 2.1) or it may successively deplete the disperse system of the coarsest or finest particles (e.g. in a sedimentation column). Accordingly, the measured quantities, which can be absolute amounts or concentration values, represent either a density or a cumulative function of the size distribution. Anyhow, the type of quantification (e.g. weighing) determines the type of quantity of the measured size distribution (e.g. mass), whereas the classification defines the probed particle property. The classification process should be ideal (i.e. with maximum selectivity) and well-defined by a monotone correlation between the particle property (e.g. settling velocity) and the

parameter(s) of the classification process (e.g. settling time). This relationship is either known from first principle or has to be determined by means of calibration. If both approaches fail to provide sufficiently accurate size information, the concentration measurement can be supplemented with a spectroscopic sizing technique. This notably increases the costs of analysis, yet finally provides accurate and highly resolved particle size distributions. Even more, such a measurement setup—classification followed by particle sizing technique(s)—facilitates, in principle, the experimental correlation between different particle properties and, thus, offers an opportunity to quantify particle shape and structure.

This section addresses two basic principles of classification—*sedimentation* and *field-flow fractionation*—and the corresponding sizing techniques. Additionally, a chromatographic technique is briefly introduced. The focus lies on sedimentation or centrifugation analysis, which corresponds to its practical relevance for the characterisation of colloidal suspensions.

2.3.3.1 Analytical Sedimentation and Centrifugation

Analytical sedimentation counts among the most popular techniques of particle sizing. To a major extent, this can be attributed to the good comprehensibility of the employed classification principle: Isolated particles settle in a quiescent liquid with a stationary velocity, which solely depends on their individual size, shape, and density. The corresponding changes in local particle concentration, which are observed along the settling path and over time, therefore reflect the size distribution of the particle system (Edelmann 1962, pp. 74–86; Bernhardt 2010).

This basic concept can be varied with respect to the force field, the concentration measurement, or the mode of operation. For that reason, several types of sedimentation instruments have been developed (Leschonski 1982); those that are based on centrifugation are of particular relevance for colloidal suspensions. The set-up of an analytical centrifuge for colloids was first described by Svedberg and co-workers (Svedberg and Nichols 1923; Svedberg and Rinde 1924). They called the instrument “ultra-centrifuge” and successfully tested its performance for the size analysis of colloidal gold sols. Nowadays, two fundamental types of centrifuges are distinguished: disc centrifuges and cuvette centrifuges.

Disc centrifuges consist of a hollow disc (“tyre”) which contains the suspension medium. Upon rotation, the liquid forms a stagnant layer on which a thin layer of the particle system is injected (line-start technique, cf. Fig. 2.6). The particles migrate according to their settling velocity to the bottom of the disc.⁴ All particles of a certain size (or settling velocity) move in a narrow band with growing distance from the initial position. In the case of multidisperse particle systems, one can observe several of such bands in analogy to chromatographic techniques. The radial

⁴For the sake of convenience only the case $\rho_p > \rho_m$ is considered throughout this section.

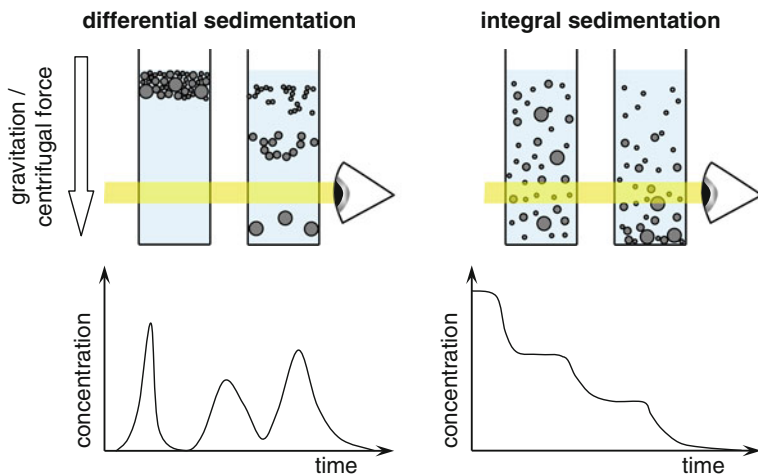


Fig. 2.6 Principles of differential sedimentation (line-start technique) and integral sedimentation (homogeneous technique); the former is employed for disc centrifuges, the latter for cuvette centrifuges; below: the corresponding time-curves of local particle concentration

concentration profile is, hence, a distorted projection of the density function of the size distribution ($q(x_{\text{Stokes}})$). The line start technique requires a density gradient in the suspension medium (e.g. by sugar) before the particles are injected; otherwise there was a convective transport of particles within strands of the (heavy) suspension layer. The density gradient sets some practical limits to the measurement (e.g. duration) and has to be calibrated before conducting size measurements.

A different set-up and even mode of operation is found in *cuvette centrifuges*, where the particle sedimentation is observed in small cuvettes that are fixed on a rotating table. In this case, the particles are homogeneously suspended in the continuous phase before the centrifugation starts (homogeneous technique). During the centrifugation, all particles migrate towards the bottom of the cuvette, which results in the formation of a sediment, in a steady decline of local particle concentrations above the sediment, and in a monotone decrease of particle concentration in the direction from the sediment to the meniscus. These two types of variation in particle concentration, the temporal evolution, and the radial profile, can be considered as distorted projections of the cumulative function of the particle size distribution ($Q(x_{\text{Stokes}})$).

In order to quantify the changes in the local particle concentration, several techniques can be employed. For instance, one can quantify the growth rate of the sediment by means of a sedimentation balance. This indirect way of concentration measurement was proposed by Odén (1916) in one of the earliest papers on analytical sedimentation. In contrast, modern analytical centrifuges directly probe the concentration in the suspension phase. Four important principles of detection are discussed below.

(a) Optical extinction

The extinction of light is a characteristic behaviour of particle systems, which is governed by particle size and concentration—apart from material properties. For dilute, weakly scattering particle systems, the extinction obeys Lambert-Beer law, which states a linear dependency between turbidity τ and particle concentration:

$$\tau = E/L = -\ln T = c_N C_{\text{ext}}, \quad (2.6)$$

where T denotes the transmission of the suspensions, E the natural extinction, c_N the particle number concentration, and C_{ext} the (average) extinction cross section of the particles. The latter is a function of particle size, shape, and optical properties. In general, it is not possible to unambiguously relate the light extinction in suspensions to a geometrical particle property. However, in the case of very fine colloids at the nanoscale, one can apply the scattering rules of the Rayleigh limit (Appendix B.2.2). When such particles absorb light (e.g. soot particles or metal colloids), the extinction cross section C_{ext} is proportional to the particle volume and the turbidity is a multiple of the particle volume concentration. Non-absorbing materials, on the other hand, extinguish light according to the squared particle volume:

$$\text{Rayleigh limit, absorbing particles : } E \sim c_N x^3 \sim c_V, \quad (2.7)$$

$$\text{Rayleigh limit, non-absorbing particles : } E \sim c_N x^6 \sim c_V x^3. \quad (2.8)$$

That means, an optical detection of sedimenting Rayleigh scatterers leads to either volume weighted (q_3 or Q_3) or squared volume weighted distributions (q_6 or Q_6) of the Stokes diameter x_{Stokes} . For the general case, one should prefer the term extinction weighted size distribution (e.g. $Q_{\text{ext}}(x_{\text{Stokes}})$), even though this term is meaningless without additional pieces of information on the employed radiation and the optical properties. Optical extinction is probably the most popular quantification principle for analytical centrifugation. However, its sensitivity to very fine particles is rather low for non-absorbing materials, which means that these size fractions may be disregarded in the case of large polydispersity.

(b) Extinction of X-rays

The extinction of X-rays in a colloidal suspension follows the same fundamental rules as the extinction of light. Nonetheless, its separate treatment is quite common, since the sensor techniques differ considerably. Besides this, X-rays have much shorter wavelengths (approx. 0.01–0.1 nm) than visible light and hardly interact with matter ($|m-1| \ll 1$, cf. Sect. 2.3.4). The scattering of X-rays with colloidal particles can, therefore, be considered as Rayleigh-Debye-Gans scattering with significant absorption (van de Hulst 1981, p. 85), for which the extinction is proportional to volume concentration:

$$\text{extinction of X-rays at colloids : } E \sim c_N x^3 \sim c_V. \quad (2.9)$$

Accordingly, X-ray sedimentometers yield volume weighted size distributions (q_3 or Q_3). However, X-ray absorption is strongly affected by the subatomic structure of the involved elements. The mass specific absorption cross section grows approximately with the third power of the atomic number for light elements (up to potassium), when typical X-ray sources (i.e. with emission energies of several keV) are employed.⁵ An X-ray detection may, therefore, be inappropriate for the characterisation of organic substances. Instrumental aspects are, e.g., discussed by Conlin et al. (1967) and Enomoto et al. (1979).

- (c) (Interferometric) determination of the suspension's refractive index
The interaction of light with colloidal particles does not only affect the intensity of the transmitted beam, but also its phase velocity, and, thus, the refractive index of the suspension (m_{sus}). This quantity depends linearly on the particle concentration for dilute suspensions (appendix B.2):

$$m_{\text{sus}} - m_{\text{m}} \approx c_V \cdot \frac{\partial m_{\text{sus}}}{\partial c_V} \approx c_m \cdot \frac{\partial m_{\text{sus}}}{\partial c_m}, \quad (2.10)$$

where m_{m} is the refractive index of the suspension medium. The increment $\partial m_{\text{sus}}/\partial c_V$ ($\partial m_{\text{sus}}/\partial c_m$) is, in general, a function of the particle size. Yet, the size dependency vanishes for very fine, nanosized colloidal particles, in which case the shift in refractive index is a measure of the change in particle volume concentration and the detected size distribution becomes, therefore, volume weighted (q_3 or Q_3). Interferometric detection systems are mainly employed for analytical ultracentrifuges (e.g. Schilling 1999).

- (d) Manometric determination of the hydrostatic pressure

The hydrostatic pressure results from the weights of the continuous and dispersed phase and can, thus, serve as a measure for the particle mass or volume concentration. In the context of analytical sedimentation, it was already utilised by Ostwald and Hahn (1922), who quantified the rate of sedimentation of flocculated suspensions by means of a hydrostatic pressure gauge. More recent papers report on the manometric determination of the hydrostatic pressure in analytical cuvettes centrifuges with electronic pressure transmitters (Bickert 1997; Beiser 2005). In contrast to the detection systems portrayed above, these *manometer centrifuges* do not measure a local particle concentration, but the total mass of all particles that are suspended above the point of measurement. The cumulative function of the volume weighted size distribution ($Q_3(x_{\text{Stokes}})$) can be, thus, computed from the time derivative of the hydrostatic pressure. In that regard, the manometric detection shows similarity to the sedimentation balance.

⁵Comprehensive tables on X-ray absorption are e.g. provided by Henke et al. (1993).

The various analytical sedimentation techniques differ not only with respect to the immediate measurement results (scaled density or cumulative function, type of quantity), but also with regard to their practical limits of application. Cuvette centrifuges, for instance, require sufficiently high particle concentrations, which yield extinction signals well above the noise for finely resolving the steady decrease in concentration. On the other hand, the particle concentration should be low enough to exclude multiple scattering and hydrodynamic concentration effects.

A reasonable value for the initial sample transmission lies typically in the range between 5 and 95 %. Let us assume an illumination with red light (670 nm), a cuvette of 10 mm thickness, and a suspension of silica particles. An initial particle concentration of 0.1 wt% would then yield a size-dependent turbidity which is too high for particles >400 nm and which is too low for particles <70 nm. While high turbidity can be easily dealt with by dilution or utilisation of thinner cuvettes; analogous measures are restricted for the fine particles. In particular, an increase in particle concentration at this level would inevitably raise the significance of viscous coupling for the settling motion and eventually affect the mean size and the width of the measured distribution function. Note that such limits are material-specific; for titania suspensions, a lower size limit of 15 nm would be obtained for the assumed conditions and concentration, while a colloidal gold sol would be completely opaque then—irrespective of size.

The immediate result of centrifugation analysis is the temporal change or spatial distribution of the particle concentration.⁶ Time and space then correspond to values of the stationary settling velocity, which can be calculated via:

$$v_{\text{sett}} = \frac{a_c \Delta \rho}{18\eta} x_{\text{Stokes}}^2 \approx \frac{a_c \Delta \rho}{18\eta} \frac{x_V^3}{x_{h,t}} \quad (\text{with } a_c = \omega^2 r) \quad (2.11)$$

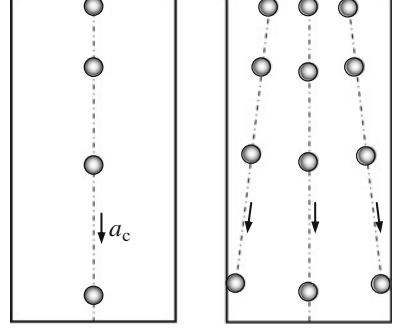
for friction-dominated settling (i.e. $Re < 1$). This condition holds true for the centrifugation of virtually all colloidal suspensions. The equivalent diameter of settling is called Stokes diameter x_{Stokes} and is related to the volume and hydrodynamic equivalent diameters. Values of the settling velocity are meaningful only when reference is made to the centrifugal acceleration. Alternatively, the settling behaviour of particles can be described by the sedimentation coefficient according to Svedberg:

$$s = \frac{v_{\text{sett}}}{\omega^2 r} = \frac{\Delta \rho}{18\eta} x_{\text{Stokes}}^2. \quad (2.12)$$

During centrifugation, the settling particles are steadily accelerated in the centrifugal field. As a result, the sedimentation distance Δr grows exponentially with time:

⁶An alternative to the analysis of time curves or radial profiles is to evaluate the shift of the radial profile with time (e.g. Salinas-Salas 2007, pp.76–80; Paciejewska 2010, pp. 62–64).

Fig. 2.7 Particle depletion in centrifugal fields due to radial acceleration and radial trajectories



$$\ln \frac{r_0 + \Delta r}{r_0} = s \cdot \int \omega^2 dt \propto x^2 t \quad (2.13)$$

and the fractional particle concentration at a given location steadily decreases before the suspension level has reached this point. Moreover, the radial trajectories of the settling particles result in depletion as well (Fig. 2.7).

The depletion effect occurs uniformly along the radial coordinate. It is a function of the sedimentation coefficient (i.e. particle size)

$$\ln \frac{c}{c_0} = -2s \cdot \int \omega^2 dt \quad (2.14)$$

and has to be considered, when converting concentration values to class frequencies. Details can be taken from the literature (Kamack 1972; Leschonski 1982; Detloff et al. 2006).

When dealing with the sedimentation of colloidal particles, it is principally necessary to regard the Brownian motion of the particles, which results in diffusive particle transport and, thus, acts against the migration in the gravitational or centrifugal field. The relevance of the Brownian motion can be roughly estimated by means of a Peclet-number:

$$Pe = \frac{D_t}{v_{\text{sett}} x} = \frac{6}{\pi} \frac{k_B T}{a_c \Delta \rho x^4} = \frac{k_B T}{a_c \Delta \rho x V}. \quad (2.15)$$

It is easily shown that for gravitational settling this Pe-number lies well above 1 for almost the complete colloidal size range (i.e. $\leq 1 \mu\text{m}$), which means that diffusion does matter. In centrifugal fields, the critical particle size is shifted to lower values, yet even for centrifugal accelerations of $10^6 \times g$ this value would remain above 10 nm. The particle diffusion broadens the sedimentation profiles and leads to an overestimation of the distribution width, if not properly accounted for in data analysis. However, its influence on the concentration profiles is decreasing with ongoing sedimentation (Fig. 2.8) because the diffusive particle displacement

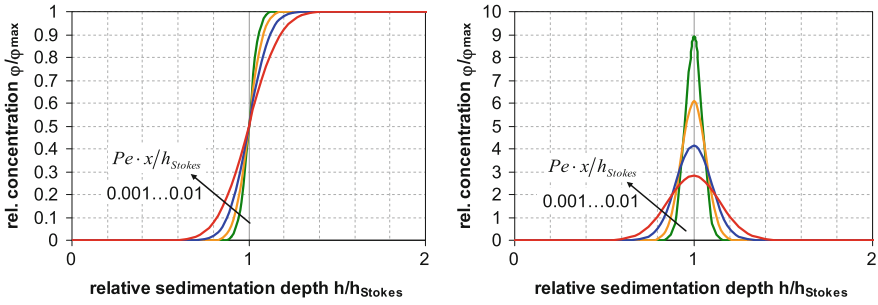


Fig. 2.8 Impact of diffusion on the concentration profiles in sedimentation experiments for a monodisperse particle system; *left* homogeneous technique, *right* line-start technique

grows with the square root of the sedimentation time, whereas the settling distance is linearly related to time.

After the sedimentation process has finished, the diffusion is still present and leads to a fuzzy interface between the sediment and the particle-free supernatant. The thickness of this layer depends on particle size. It may even extend over the whole vessel (cuvette), which means that the particles are not separated, but obey an sedimentation-diffusion equilibrium, which is characterised by an exponential concentration profile (cf. Sect. 3.1.2):

$$c(z) = c_b \cdot \exp(-z/l_g) \quad \text{with} \quad l_g = \frac{k_B T}{\Delta \rho V \bar{a}_c}. \quad (2.16)$$

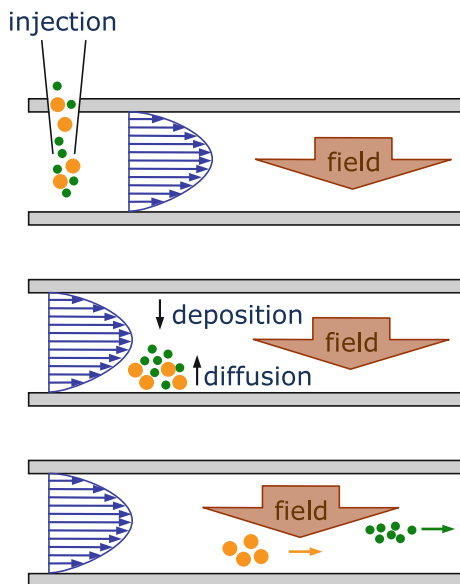
where c_b denotes the particle concentration at the bottom just above the sediment, z the distance from the sediment and \bar{a}_c the average centrifugal acceleration within this distance. The evaluation of such concentration profiles offers a further opportunity to quantify the (average) particle size via centrifugation.

2.3.3.2 Field-Flow Fractionation

The term *field-flow fractionation* (FFF) refers to a class of preparation techniques which classify particle systems with regard to size in a laminar flow channel. A subsequent quantification of the particle concentrations in the eluent transforms FFF into an analytical tool for particle sizing.

Common to all FFF techniques is the application of an external “field” that acts perpendicular to the direction of flow. Particles that are injected into the channel migrate in this field and are, thus, accumulated at one wall of the channel. At the same time, they are subject to Brownian motion, which counteracts the migration. The two effects eventually cause size-dependent, stationary concentration profiles. Typically, coarse particles are less evenly distributed across the channel than fine particles. They accumulate near the channel wall, where the flow velocities are

Fig. 2.9 Classification of particle systems by field-flow fractionation (FFF)



lower than at the channel centre. Hence, coarse particles need more time to leave the channel than fine ones. Due to the size-dependency of the residence time distribution, it is possible to effectively separate the different size fractions when the injection occurs as an impulse function (Fig. 2.9).

The classification into different size fractions can be realised by gravitation (sedimentation FFF), by centrifugal fields (centrifugation FFF), by thermophoresis in temperature gradients (thermal FFF), by electric fields (electrical FFF), or by hydrodynamic fields, i.e. crossflow through the wall(s) (flow FFF). Even though the main fields of application are colloidal systems, one can also employ FFF for the classification of micrometre particles ($x > 1 \mu\text{m}$). In that case, diffusion can be usually neglected, yet hydrodynamic lift forces and steric effects counteract the external field and cause a reversal of the size dependency.

The particle concentration of the eluent is normally measured by means of infrared or ultraviolet photometers. Additionally, fluorescence photometer, interferometric measurements (for the refractive index), or mass-spectroscopic methods (e.g. induced coupled plasma mass spectroscopy—ICP-MS, Plathe et al. 2010) are employed. The combination of different detection systems offers an opportunity for a detailed characterisation of multi-component particle systems. Note that the classification by FFF is not ideal and the relevant material properties are not always known; moreover, the calibration of FFF is rather difficult. The attribution of particle size to residence time, thus, bears some degree of uncertainty. Recent developments of FFF instrumentation, therefore, include a particle-sizing technique additional to the flow channel and the quantity measurement (usually static and dynamic light scattering, Wyatt 1998; Cho and Hackley 2010).

solution, yet could be successfully applied to the characterisation of solid nanoparticles, in particular to gold nanoparticles (Wei et al. 1999; Liu 2009). Unlike FFF, the classification is related to geometric and not hydrodynamic particles properties, whereas the quantification can be conducted with the same methods. Liu (2009) cited several studies in which SEC was coupled with an optical extinction measurement. This means that, for the characterisation of metal nanoparticles, volume weighted size distributions are obtained (cf. with remarks to sedimentation).

Ideally, the particles should not interact with the stationary phase in SEC. In reality, however, electrostatic interaction and adsorption exist and have to be appropriately considered. Indeed, as these kinds of interactions are material-specific it is difficult to find a universal analytical description or an appropriate way of calibration. For that reason, it is highly recommended to supplement the classical SEC set-up with a particle sizing technique (e.g. DLS, Yamaguchi et al. 2006).

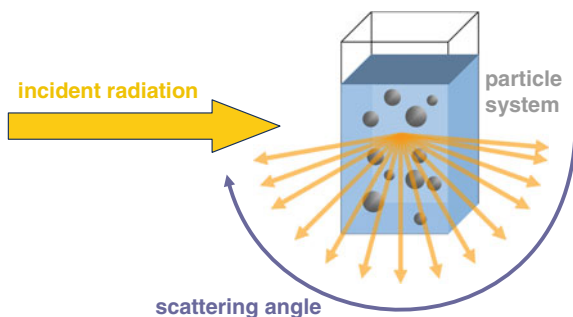
2.3.4 Static Scattering Techniques

Scattering is the dispersal of radiation at an object (particle) that differs in the relevant material properties from its environment (continuous phase). Static scattering experiments record the scattering signal as a function of the angle of observation θ or—more generally—as function of the scattering vector \mathbf{q} :

$$q = |\mathbf{q}| = 2k \cdot \sin(\theta/2), \quad (2.17)$$

where k is the wavenumber ($k = 2\pi/\lambda$). The resulting scattering function depends on the concentration, the size and the shape of the scatterers. Basically, scattering experiments can resolve morphological details with dimensions in the order of magnitude of $1/q$. By variation of the wavelength λ and the angle θ (Fig. 2.11) it is possible to characterise disperse systems over a broad range of size levels, e.g. with regard to interparticle distances, to particle shape, or to surface roughness).

Fig. 2.11 Principal scheme for static scattering techniques



Scattering experiments can be conducted with any kind of radiation (e.g. sound, electromagnetic waves, neutron radiation). This book will be confined to the scattering of light and X-rays, as these two types are most frequently used for the characterisation of colloidal suspensions.⁷ Both belong to electromagnetic radiation, yet the mechanisms of interaction with matter are completely different. This difference becomes manifest in the refractive indices, which deviate qualitatively. For this reason, both types of radiation are separately discussed.

Silica particles have a refractive index of approximately 1.45 in the domain of visible light. That is significantly different to the refractive index of water (1.33), which often serves as suspension medium. In contrast, there is only a weak contrast between the two substances in the domain of X-radiation. At a wavelength of 1 Å, one finds a complex refractive index of $0.999997-1.7 \times 10^{-8}i$ for silica and $0.999999-2.1 \times 10^{-9}i$ for water (cf. Henke et al. 1993).

Moreover, light scattering measurements have been historically realised by two different concepts of instrumentation which cover distinct size ranges. These are the *static light scattering* (SLS), which is conventionally employed for fine colloids, and the *laser diffraction*, which was originally used for micrometre particles only. Even though the measurement ranges of both techniques have actually converged in the recent past, there still remain qualitative differences in the sensor set-up and in data analysis, which justify their separate treatment.

2.3.4.1 Analysis of Static Scattering Experiments

The various static scattering techniques rely on different types of interaction between particles and radiation. Additionally, they are used for the determination of rather dissimilar measurands (e.g. average molecular weight, particle size distribution, shape parameters). This diversity of physical basis and experimental objective has led to very specific ways of data analysis, yet all of them are based on the following principal dependency of the scattering signal:

$$I_{\text{sca}}(q) \propto S_{\text{sus}}(q, \varphi_V) \cdot S_{\text{agg}}(q, x_{\text{agg}}) \cdot P(q, x_p), \quad (2.18)$$

wherein S_{sus} and S_{agg} denote the static structure factors of the suspension and of particle aggregates, respectively, and P is the form factor of the primary (i.e. constituent) particles. The structure factor of the suspension S_{sus} equals 1 for dilute suspensions, i.e. for very large interparticle distances. If aggregates are present, then S_{agg} reflects their size and structure as q -dependency for relatively small scattering vectors ($q < 1/x_p$); otherwise S_{agg} is set to 1. The morphology (shape) of the primary

⁷Additionally, *small angle neutron scattering* (SANS) has some relevance for the characterisation of colloidal particle systems, in particular for dense suspensions (Romer et al. 2001; Qiu et al. 2005). With regard to particle characterisation, SANS is mainly used for disclosing the structure of particle aggregates (Hurd et al. 1987; Bugnicourt et al. 2007). A brief introduction to SANS is, for example, given by Glatter and May (2006).

particles is reflected in the form factor P and can be resolved for large q -values ($q \geq 1/x_p$).

When employed for particle sizing scattering experiments are usually conducted in dilute suspensions ($S_{\text{sus}} = 1$) and possible aggregates are typically ignored ($S_{\text{agg}} = 1$). The spectral scattering signal $I_{\text{sca}}(q)$ of the suspension is then considered as a linear superposition of all individual scattering signals:

$$I_{\text{sca}}(q) = I_{\text{sca}}(0) \cdot \int P(q, x) dQ_0. \quad (2.19)$$

This is an inversion problem as defined in Eq. (2.2). Firstly, this means that its solution requires specifically adapted numerical algorithms and, secondly, that details of the size distribution can be resolved only to a certain extent.

2.3.4.2 Static Light Scattering

Static light scattering (SLS) is an established measurement technique in colloid and polymer science. The time averaged angular distribution of scattered light is commonly employed for the characterisation of macromolecules (molecular weight, radius of gyration, the second virial coefficients), but can be used to study suspensions of inorganic colloids as well (e.g. Poon et al. 1995; Heimer and Težak 2002; Wyss et al. 2004). However, the angular distribution of scattered light is insensitive to particle size for very fine particles. In that case, it cannot be exploited with regard to particle size distribution. Regardless, SLS instruments are frequently combined with a fractionating sample preparation in order to determine the concentration and mean radius of gyration of the individual size fractions (cf. Sect. 2.3.3).

The maximum scattering vector q_{max} primarily depends on the laser wavelength and the refractive index of the solvent. The minimum q -value is additionally affected by the minimum scattering angle θ_{min} . A typical commercial SLS instrument resolves an approximate angular range from 10° to 150° . Hence, for a HeNe laser (wavelength: 632.8 nm) and an aqueous solvent, a q -range from 2.3 to $26 \mu\text{m}^{-1}$ can be covered. That corresponds to a resolution of structural properties with size dimensions being not much smaller than 40 nm and not much larger than 400 nm.

The measured light intensity spectrum is usually expressed as excess Rayleigh ratio R_q (e.g. Xu 2000, p. 92):

$$R_q = \frac{I_{\text{sus}} - I_{\text{m}}}{I_0 \cdot f} \cdot \frac{r^2}{V_{\text{meas}}}, \quad (2.20)$$

which allows for comparison between different experimental setups ($I_{\text{sus/m}}$ = measured intensities of the suspension and the blank medium, r = distance

to measurement volume V_{meas} , f = polarisation factor⁸). The excess Rayleigh ratio R_q depends on the scattering behaviour of the single particles as well as on the particle concentration. For dilute suspensions, one gets:

$$R_q = \frac{c_N}{4\pi} \frac{C_{\text{psca}}(q)}{f}, \quad (2.21)$$

where c_N denotes the particle number concentration and C_{psca} the partial scattering cross section. Alternatively, R_q can be related to the mass concentration c_m , the average molar mass \bar{M} , and the form factor $P(q)$ of very fine particles or macromolecules:

$$R_q = H \bar{M} c_m \cdot P(q), \quad (2.22)$$

$$H = \frac{k^4}{4\pi^2 m_{\text{f}}^2 N_{\text{A}}} \cdot \left(\frac{\partial m_{\text{sus}}}{\partial c_m} \right)^2. \quad (2.23)$$

While the expression (2.21) might be more familiar to the particle sizing community, Eq. (2.22) is customary in colloid and polymer science. The contrast factor H contains the refractive index increment $\partial m_{\text{sus}} / \partial c_m$, which is independent of size and concentration for very fine particles.

The linear relationship between scattering intensity (excess Rayleigh ratio) and particle concentration holds true only for extremely dilute suspensions. For fine, colloidal particles, a declining concentration impact can be observed, which is related to the osmotic pressure in the colloidal suspension and, therefore, depends on the virial coefficients (Einstein 1910; Zimm 1945; Debye 1947):

$$\frac{R_q}{HMP(q)c_m} = \frac{4\pi f R_q}{c_N C_{\text{p,sca}}} = \frac{1}{1 + 2A_2 M c_m + 3A_3 M c_m^2 + \dots}. \quad (2.24)$$

Depending on the objective of SLS measurements, different methods of data processing can be utilised. According to Eq. (2.18), the dependency between R_q and q depicts the scaled structure or form factors of suspension, aggregates, or primary particles. A better distinction is possible with log-log plots. Plots of $\log(R_q)$ versus q^2 are called Guinier plots—they allow for the determination of the radius of gyration. Debye-plots show Hc_m/R_q versus c_m —they yield the average molar mass M and the second virial coefficient A_2 . If measurements for different dilutions are presented in a Zimm plot, i.e. as Hc_m/R_q versus $q^2 + K \cdot c$, the average R_g can also be derived (Zimm 1948).

The calculation of the Rayleigh ratio R_q from Eq. (2.20) requires some knowledge about the instrument's optical configuration (measurement volume, detector distance, polarisation), which is difficult to obtain exactly. Besides this, the

⁸1 for vertical polarisation, $\cos^2\theta$ for horizontal polarisation, $\frac{1}{2}(1 + \cos^2\theta)$ for unpolarised light.

conversion from detector signals to intensity values depends on the detector geometry and electronic settings. For this reason, SLS instruments are calibrated with particle-free scattering standards (e.g. toluene, benzene, and cyclohexane). And the result is calculated from $R_q = (I_{\text{sus}} - I_{\text{med}})/I_{\text{std}} \cdot R_{q,\text{std}}$ (I_{std} is measured intensity from standard). Since usually very fine, i.e. weakly scattering, particles are measured, the SLS technique is very sensitive to contamination by coarse dust particles or particle agglomerates. That requires careful sample preparation procedures (e.g. filtration of solvent and colloidal suspension, sample preparation in laminar flow box).

Like other optical characterisation techniques, SLS exhibits size-dependent concentration limits. At high concentrations, the suspension may become opaque or multiple scattering may occur which affects the angular intensity distribution. Dilution may solve the problem, but then osmotic concentration effects (virial coefficients, particle interactions) are not accessible. Conversely, very fine, weakly scattering particles may require such a high particle concentration that the mentioned concentration effects cannot be neglected and will complicate the determination of morphological structure parameters.

2.3.4.3 Laser Diffraction Spectroscopy

The term *laser diffraction* (LD) spectroscopy comprises static light scattering techniques, which are primarily designed to resolve the scattering pattern at small scattering angles. Historically, LD instruments and software were restricted to the characterisation of micrometre objects for which the scattering pattern is mainly caused by diffraction and can be explained by Fraunhofer's theory (1821). Yet, considerable enhancements in instrumentation as well as in data analyses have extended the applicability to the colloidal size range, where diffraction theory does not apply. Even though the term laser diffraction “does no longer reflect the current state of the art” (Xu 2000, p. 111) and may be replaced by *small angle light scattering* or *angular light scattering*, it is still widely accepted by the international particle sizing community.

The classical set-up of laser diffraction instruments is shown in Fig. 2.12 (left). A monochromatic light beam—typically, but not necessarily from a laser source—is passed through the particle sample and focussed on the centre of the forward scattering detector by means of a (set of) positive lens(es) (ISO 13320 2009). All light scattered in a specific direction is projected in one point of the focal plane independent of the particle's position in the measurement cell. For spherical particles, a typical diffraction pattern consists of concentric rings with outwards decreasing intensity (Fig. 2.12, right), where the radius of the rings (e.g. first minimum) depends on the sphere diameter. From a mathematical point of view the diffraction pattern can be regarded as the Fourier transform of the particle's projection image. It, therefore, reflects the particle size and shape.

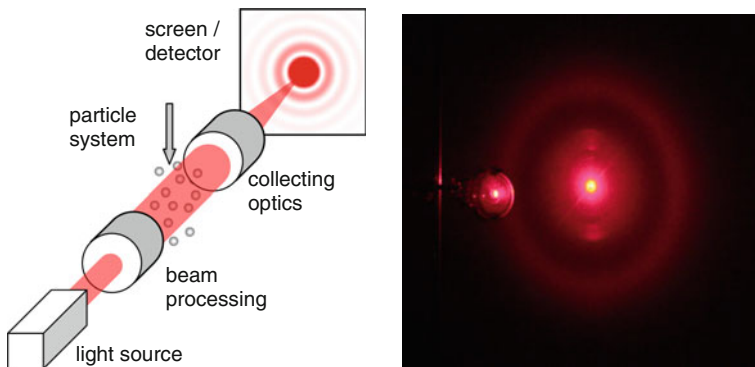


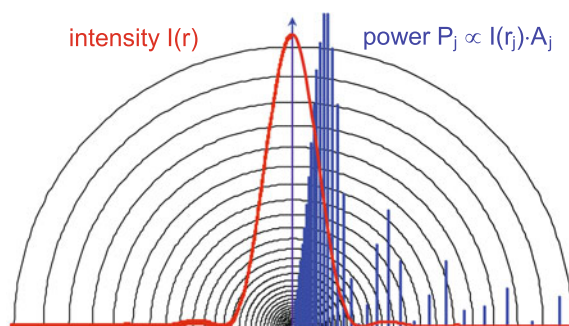
Fig. 2.12 Classical set-up of laser diffraction instruments (*left*) and demonstration of laser diffraction by illuminating a thin layer of monodisperse silica powder (© Benno Wessely 2004)

In the early stages of laser diffraction, the diffraction pattern was recorded by photographic plates (Stromgren 1975, Büchtemann et al. 1982). Today multi-element photodetectors of varying geometry are employed (Heuer and Leschonski 1985, Xu 2000, pp. 135). That means that a discrete power spectrum is measured which deviates significantly in shape from the continuous intensity spectrum (spatial intensity distribution).

For instance, a detector array of concentric half-rings with steadily increasing ring widths—as depicted in Fig. 2.13—yields a power spectrum with size-dependent, off-centre maxima and a total signal strength which is proportional to the cumulated squared particle size. Hence, for this detector configuration, the intrinsic type of quantity of measured size distribution is the particle surface. Nevertheless, size distributions from laser diffraction instruments are commonly calculated as volume weighted distributions. Note that such an interpretation changes with the detector geometry and may become rather abstract when additional detector arrays for collecting sideward and backward scattered light are installed.

The size obtained from laser diffraction is sometimes called diffraction equivalent diameter. However, in contrast to the implication of that term, it is not possible

Fig. 2.13 Intensity distribution and power spectrum for a ring-detector; cf. de Boer et al. (1987)



to reconstruct the diffraction pattern of a non-spherical particle by that of a sphere. Anisotropy in macro-shape (particle proportions) is clearly reflected by anisotropy in the diffraction pattern. Averaging the diffraction pattern over all spatial orientations of the particle (or obtained from an ensemble of randomly aligned monodisperse particles) broadens and smoothes the intensity spectrum similar to the way that a distribution in size does (Jones 1987; Gabas et al. 1994; Heffels et al. 1996; Stevens et al. 2007). In practice, the anisotropy of particles is commonly ignored and the analysis assumes spheres. Size distributions of nonspherical particles, therefore, typically show a pronounced mode around the minor dimension (e.g. rod diameter) and a long tail up to the size of the major dimension (e.g. rod length; cf. Matsuyama et al. 2000; Tinke et al. 2008).

The analysis of the angular spectrum (from laser diffraction instruments) traditionally refers to either Fraunhofer's diffraction theory (Fraunhofer 1821; van de Hulst 1981, p. 108, 209) or to Mie's scattering theory (Mie 1908; van de Hulst 1981, p. 114) for spherical particles. Since Fraunhofer diffraction is a limiting case of Mie's general solution, the latter is often preferred as first choice. However, Mie's theory as employed in standard instruments software firstly assumes homogenous materials and secondly requires the knowledge of the complex refractive index. Besides this, Mie calculation may run unstably for large particles if not installed numerically in the appropriate manner (Stübinger et al. 2010). Hence, for large, strongly scattering particles, Fraunhofer may perform better. However, for the characterisation of colloidal suspensions, where the measured scattering pattern is only partly due to diffraction, Mie theory should be compulsory.

First, laser diffraction instruments were developed in the 1960s (Lodi and Osmolovskaya 1975; Stromgren 1975; Thompson 1977) and were accompanied by corresponding improvements in data processing. Commercial instruments have been available since the 1970s. Today, laser diffraction instruments belong to the standard characterisation tools for particles systems. They can be applied to aerosols as well as to liquid dispersions. Measurements are quick and highly reproducible. Moreover, laser diffractometers can be run at flowing media. Hence, they offer a possibility for on-line or at-line monitoring of industrial processes. On the other hand, the particle concentration is usually restricted to values far below 1 vol % in order to avoid multiple scattering, which would affect the intensity spectrum.

The upper concentration limit depends on the particle system (size, refractive index) and the instrument (detector, optics). Some authors state transmission values above which multiple scattering can be neglected (e.g. Xu 2000, p.163: $T_{\min} = 85\%$, Yamauchi and Ohyama 1982: 75 %, Chigier 1984: $T_{\min} = 40\%$). Ludwig (2010) observed a weak linear correlation between sample transmission and measured size distribution, which resulted in an impact of 3 % for mean particle sizes at transmission values of 40 % (for 30 μm glass beads). If we assume an optical path of 1 mm and an aqueous solvent, then a transmission value of 40 % coincides with a solid content of 0.03 vol% for 1 μm titania spheres or 0.09 vol% of 1 μm silica spheres.

In the micrometre range, which is diffraction dominated, size distribution can be determined with high accuracy and good resolution (Knösche 2001 pp. 40–42; Mori et al. 2007; Witt et al. 2012). In order to extend the instrument applicability to

colloidal particle systems, several modifications have been realised, e.g. variation of wavelength and polarisation or inclusion of wide angle scattering (Xu 2000, pp. 111–181; ISO13320). These modifications have evidently enhanced the sensitivity to colloidal particles far below 1 μm , but not in a uniform way as inter-laboratory comparisons prove (Mori et al. 2008, Kuchenbecker et al. 2012). Even so, laser diffraction may serve as a useful tool for the characterisation of colloidal suspensions, in particular for monitoring dispersion procedures or product changes.

2.3.4.4 Small Angle X-ray Scattering

Shortly after its discovery, X-radiation was already being employed to study the inner structure of matter. This is possible because of the very small wavelengths of X-rays (typically in the order of 1 \AA). In 1938, André Guinier proposed to evaluate X-ray scattering at small angles (i.e. in the forward direction) in order to study colloidal suspensions. He further related the intensity distribution to the radius of gyration of the scattering objects (Guinier 1938). Today, *small angle X-ray scattering* (SAXS) is an established technique for determining the size and shape of colloidal particles, analysing the conformation of macromolecules, or studying the structure of particle aggregates. Its applicability is typically limited to the range below 100 nm (Dörfler 1994, p 554, Glatter and May 2006).

SAXS instruments are usually distinguished with regard to the X-ray source. In (standard) laboratory instruments, X-ray tubes are employed which emit a broad spectrum of X-radiation with characteristic lines (e.g. at 1.54 \AA for Copper anodes) and which are usually coupled with a monochromator. The emitted beam is of rather weak intensity and needs a collimation optic (e.g. pin-hole, slit, or block collimation; cf. Ilavsky et al. 2002; Anderegge et al. 1955; Kratky and Stabinger 1984, respectively). In contrast, X-radiation from synchrotron beamlines allow for a narrow adjustment of wavelengths and deliver highly intensive and well collimated beams for the SAXS measurement. Unlike laboratory instruments, the smearing of the measured spectrum is negligible and the structural parameter can be resolved in detail. However, synchrotron instrumentation is not applicable to routine analysis.

Similar to data processing in SLS, the analysis of SAXS spectra requires preliminary steps like background subtraction and—if necessary—extrapolation to zero concentration. Additionally, the turbidity of the sample may have to be considered (Kammler et al. 2004), but usually this effect is negligible. In general, the thus obtained spectrum is still a smeared version of the true scattering curve. Smearing results from the difficulty of collimating X-rays. In order to achieve sufficiently high signal-noise ratios, the detection optics collects all photons over a two-dimensional section of the scattering pattern, i.e. over a certain range of scattering angles (Fig. 2.14). In case of polychromatic irradiation there is a further smearing contribution. The knowledge of the detector geometry and the spectral distribution of the X-radiation facilitate the de-smearing, which first includes a data smoothing procedure (Glatter and May 2006; Glatter and Kratky 1982, pp. 119–165).

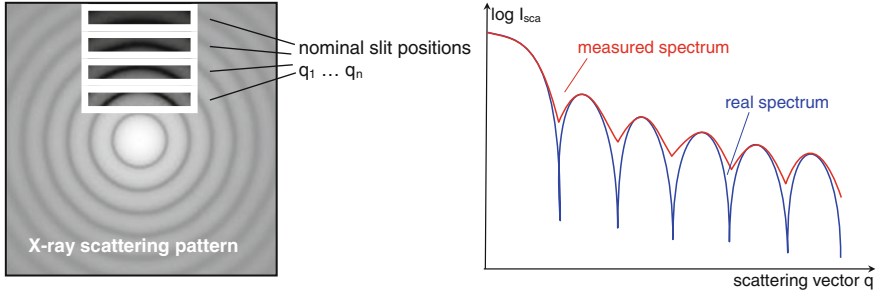


Fig. 2.14 Illustration of smearing for point source illumination and a slit detection system

Eventually, the de-smearred, “true” scattering function can be used to assess the morphological and structural properties of the colloidal suspension. Frequently, this involves some bias, e.g. on the morphology the particles (spheres, rods, core-shell, etc.) or on their size (when studying particle interactions). The algorithms of de-smearing and inversion are manifold (Glatter and May 2006; Fritz and Glatter 2006). There are, however, integral parameters that can be determined without specific assumptions on the particle shape. Based on Porod’s invariant parameter Q

$$Q = \int I_{\text{sca}} q^2 dq \quad (2.25)$$

it is possible to calculate the total particle volume and the specific surface area (supposing the particle surface is smooth):

$$V = 2\pi^2 \frac{I(0)}{Q}, \quad (2.26)$$

$$S_V = \pi \cdot B/Q, \quad (2.27)$$

where B is derived from the asymptotic form of $I_{\text{sca}}(q)$ at large scattering angles ($B = \lim_{q \rightarrow \infty} I_{\text{sca}}/q^4$). The parameter B can be graphically obtained by plotting $I \times q^4$ versus q^4 , which yields the following expression: $\lim_{q \rightarrow \infty} I_{\text{sca}} q^4 = B + \text{const} \cdot q^4$. Here, const is supposed to be background and should, therefore, be zero for background corrected data. A significant deviation of const from zero indicates a fractal or porous particle surface (Schmidt et al. 1991).

De-smearred scattering curves of monodisperse particle systems are well structured (cf. Fig. 2.14) and allow for an accurate determination of size and shape. For polydisperse systems, smooth spectrums are obtained. The resolution of size distributions is rather low (peak distance for bidisperse distribution approx. 25 %,

Glatter and May 2006). If the particle shape is known, SAXS yields distributions of geometric particle properties (e.g. rod length), otherwise it probes essentially the radius of gyration. The distributions are intensity weighted, which typically means that they are weighted by the particle surface ($I_{\text{sca}} \propto x^2$).

When colloidal suspensions are probed by SAXS, the X-ray absorption in the solvent has to be considered because it attenuates the scattered intensities. Maximum scattering intensities are achieved for a sample transmission of 37 %, which is approximately the transmission through a 1 mm sheet of water when a typical copper anode (wavelength: 1.54 nm) is used. Because of this intrinsic background turbidity, SAXS characterisation of colloidal suspensions has to be conducted in relatively small measurement volumes.

While typical SAXS instrumentation works at scattering vector in the range of approx. $0.05\text{--}2\text{ nm}^{-1}$, *ultra small angle X-ray scattering* (USAXS) instruments cover the range from 0.001 to 4 nm^{-1} and can be, therefore, applied to larger particles and particle aggregates up to the micrometre region (Ilavsky et al. 2002; Kammler et al. 2004). Since they rely on the intense radiation of synchrotrons and require special cameras they are not available as standard laboratory equipment (Glatter and May 2006).

2.3.5 Dynamic Scattering

The time-averaged signals from a scattering experiment provide a powerful tool to study the micro-structure of colloidal suspensions (i.e. size and shape of a particle as well as the pair correlation), as was shown in the previous section. However, scattering signals are not constant in time; they exhibit high-frequency fluctuations which are due to the dynamics of the microstructure, e.g. to the Brownian motion of the colloidal particles. Dynamic scattering techniques probe these temporal variations and, thus, add to the characterisation methods for colloidal suspensions. The most popular of these techniques is *dynamic light scattering* (DLS), which will be a focus of this section. In addition to this, diffusive wave spectroscopy, X-ray photon correlation and fluorescence correlation spectroscopy are briefly introduced.

2.3.5.1 Dynamic Light Scattering

Dynamic light scattering (DLS) techniques evaluate the fluctuations in scattered light (Fig. 2.15). These fluctuations may be caused by any changes in the microstructure of the suspension, e.g. by particle motion or vibrations of particle networks. For this reason, there are manifold applications for DLS, e.g. to particle sizing (Finsy 1994), molecular weight determination (Jena and Bohidar 1993; Siddiq and Wu 1996), studying particle aggregation (Bolle et al. 1987; Herrington and Midmore 1991; di Biasio et al. 1994), monitoring phase transition in colloidal

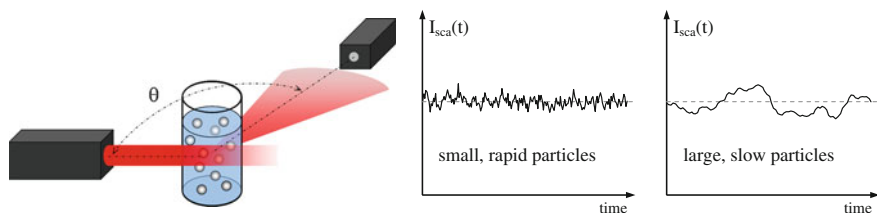


Fig. 2.15 Dynamic light scattering experiment and intensity fluctuation

suspensions (Kroon et al. 1996; Ruzicka et al. 2004; Kätzel et al. 2007), or measuring the strength of colloidal gels (Manley et al. 2005).

First, DLS measurements were conducted in the 1960s by analysing the intensity fluctuations in terms of a frequency spectrum (*frequency analysis*—FA; Cummins et al. 1964; Arrechi et al. 1967; Chu and Schones 1968; Dunning and Angus 1968). The width of the frequency spectrum is a measure of the relaxation time of the microstructural processes and can be employed for the determination of the particle diffusion coefficients (Pecora 1964). An alternative for evaluating the fluctuation of scattered light intensity is *photon correlation spectroscopy* (PCS), which has been used for the characterisation of colloidal suspensions since the end of the 1960s (Jakeman and Pike 1969; Jakeman 1970; Foord et al. 1970). PCS requires a different hardware than FA, but it can be shown that the results of both techniques are equivalent (Jakeman 1970; Xu 2000, pp. 86–89).

Today, a large variety of commercial or “self-made” DLS instruments are used. Apart from data processing (FA or PCS), they can be distinguished with regard to laser optics and signal modulation. The latter refers to the question of whether the scattered light is superposed with a reference (laser) beam. According to Fig. 2.16, three principal set-ups can be distinguished⁹:

- *direct* or *self-beating* measurement: no reference beam; probes interparticle distances, insensitive to mean particle velocity
- *homodyne*: reference beam with same frequency as incident beam, sensitive to the absolute position of the particles
- *heterodyne*: reference beam with frequency shift to the incident light; facilitates the measurement of particle migration velocities

The study of microstructural processes is almost exclusively accomplished by the self-beating and homodyne technique. The light scattering experiment may be realised with conventional or fibre optics (Auwetter and Horn 1985; Bremer et al. 1993). Further differences exist with regard to scattering angle or the range of

⁹There is some confusion in the literature regarding the terms *homodyne* and *heterodyne* (cf. Xu 2000, pp. 84–86). The terminology used here agrees with the modern convention in laser technology (e.g. Paschotta 2008).

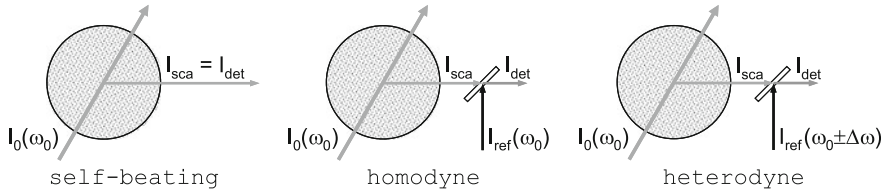


Fig. 2.16 Principal set-ups for detecting laser signals; the superposition with a reference beam allows a control of signal phase, which means for DLS measurements that the absolute particle velocity can be detected

scattering angles and with regard to cross correlation (i.e. conducting and correlating two DSL experiments in parallel at the same sample volume).

The primary result of a DLS experiment is the power spectrum of the scattering intensity which is obtained by FA (Ishii and Iwai 2008):

$$P_I(\omega) = \left| \int_0^\infty I_{\text{det}}(t) e^{i\omega t} dt \right|^2 = \int_0^\infty \langle I_{\text{det}}(t) I_{\text{det}}(t + \tau) \rangle e^{i\omega \tau} d\tau \quad (2.28)$$

or the (normalised) intensity autocorrelation function as produced by PCS

$$g^{(2)}(\tau) = \langle I_{\text{det}}(t) \cdot I_{\text{det}}(t + \tau) \rangle / \langle I_{\text{det}}(t) \rangle^2. \quad (2.29)$$

Both types of data analysis are equivalent because the spectral power function $P_I(\omega)$ is a Fourier transform of the corresponding autocorrelation function $g^{(2)}(\tau)$ (Wiener-Khinchine-theorem; Wiener 1930; Khinchine 1934). In the following, only PCS will be discussed.

If the light fluctuation is caused by Brownian motion, one can relate the normalised autocorrelation function of the detected light intensity $g^{(2)}$ to that of the scattered field $g^{(1)}$ by the following equations (Siegert 1943; Xu 2000, pp. 86–89):

$$\text{self-beating: } g^{(2)}(\tau) = 1 + \beta |g^{(1)}(\tau)|^2, \quad (2.30)$$

$$\text{homodyne: } g^{(2)}(\tau) = 1 + 2X\beta \cdot |g^{(1)}(\tau)| = 1 + a \cdot |g^{(1)}(\tau)|, \quad (2.31)$$

where β is a factor describing the coherence of the light received by the detector ($\beta < 1$), and X is the fraction of scattered to total light on the receiver/detector ($X \ll 1$).

The field correlation function $g^{(1)}$ directly reflects any changes in the microstructure of the suspension. In the case of purely diffusive processes, i.e. when the displacement of scattering objects follows Fick's second law, an exponential time dependency is found.

$$g^{(1)}(\tau) = \int_0^\infty \exp(-\Gamma\tau) dQ_{\text{int}}(\Gamma), \quad (2.32)$$

where Γ denotes the decay rate and dQ_{int} the relative contribution of the corresponding diffusion process to the scattering intensity.

In quiescent, dilute suspensions, the light fluctuations result essentially from the Brownian displacement of the single particles. Thus, the decay rate Γ can be traced back to the particles' translational diffusion coefficient D_t :

$$\Gamma = 1/\tau_{\text{decay}} = q^2 D_t. \quad (2.33)$$

For spherical particles, this parameter (D_t) is inversely proportional to the sphere diameter (cf. Eq. (2.4)). Thus, Eq. (2.32) expresses an integral equation for the particle size distribution (Finsy 1994). The reliable, meaningful, and robust inversion of Eq. (2.32) has been tackled by several authors (e.g. Stock and Ray 1985; Finsy et al. 1989). Most often, regularisation approaches (Provencher 1982; Maier et al. 1999) with a non-negative constraint on the weights dQ_{int} (Lawson and Hanson 1995; Geers and Witt 2008) are employed.

The primary result of such a data analysis is the intensity weighted distribution Q_{int} of the translational hydrodynamic diameter $x_{h,t}$. Instrument software usually allows for conversion in volume or number weighted distributions, but this requires a model on the relationship between $x_{h,t}$ and the scattering intensity. Furthermore, distribution details that do not contribute significantly to the correlation function (e.g. very fine size fractions) and that are consequently ignored in the measured Q_{int} also cannot be revealed by numerical conversion.

Alternative routes for data analysis that avoid the inversion of Eq. (2.32) are the method of cumulants (Koppel 1972) and the Williams-Watts-analysis (Williams and Watts 1970). The former is based on a series expansion of the logarithmised autocorrelation function $g^{(1)}$, which is commonly stopped after the second term:

$$\ln(g^{(1)}) = \ln g^{(1)}(0) - \langle \Gamma \rangle \cdot \tau + \frac{1}{2} PDI \cdot \langle \Gamma \rangle^2 \cdot \tau^2. \quad (2.34)$$

The mean decay rate $\langle \Gamma \rangle$, which can be measured with high accuracy, corresponds to the intensity weighted harmonic mean of the size distribution (x_{cum})

$$x_{\text{cum}} = \text{const.} \cdot \langle \Gamma \rangle = \int x_{h,t}^{-1} dQ_{\text{int}}, \quad (2.35)$$

while the polydispersity index PDI can be understood as the normalised harmonic variance:

$$PDI = x_{\text{cum}}^2 \times \int \left(x_{\text{h,t}}^{-1} - x_{\text{cum}}^{-1} \right)^2 dQ_{\text{int}}. \quad (2.36)$$

Hence, it offers an opportunity to quickly evaluate the distribution width.

PDI values below 0.05 indicate a very narrow, quasi monodisperse distribution, while values above 0.2 usually imply a relatively broad, possibly multimodal distribution. Values above 0.5 mean that the experimental data are poorly reproduced by Eq. (2.34). For log-normal size distributions, one can easily relate the PDI to the geometric standard deviation of the distribution function (Babick et al. 2012).

The method of cumulants performs rather weakly for very broad distributions of the decay rate. In this case, the autocorrelation functions are better fitted by stretched exponentials (Williams and Watts 1970). The Williams-Watts analysis is mainly employed for phase transition in colloidal suspensions (Ruzicka et al. 2004; Kätzel et al. 2007) and for polymer suspensions.

When applied to dilute solutions of macromolecules, DLS reveals the molar mass M which is related to the diffusion coefficient D_t by a power-law (Mark-Hoodwink-Kuhn-Sakurada equation):

$$D_t \propto M^{-\varepsilon}. \quad (2.37)$$

This relation reflects the conformation of the macromolecules and is, therefore, specific for each molecule-solvent combination. For random coils, the exponent is approx. 0.55, while for rigid rods and compact spheres it amounts to 0.85 and 1/3, respectively (Jena and Bohidar 1993; Harding 1995).

During the last two decades, dynamic light scattering has evolved into a major characterisation technique for colloidal suspensions. A recent interlaboratory study into the characterisation of colloidal silica (Braun et al. 2011) showed that state-of-the-art DLS instrumentation facilitate a highly reproducible and very reliable acquisition of correlation function and corresponding mean particle size x_{cum} .

The study involved 17 participants from the EU and the USA, which provided 19 independent data sets from 6 different commercial instruments covering sideward scattering (90°) and backscattering. Suspensions of colloidal silica of spherical particles with a mean diameter of approx. 19 nm and narrow distribution width were sent in several aliquots to each participant and measured by uniform SOP. There was only one outlier with regard to the mean particle size. The overall uncertainty of that parameter was expressed as 95 %-confidence interval of ± 3 %. A considerably higher amount of uncertainty exists with regard to the mean values of the volume weighted distributions because of the twofold error magnification by inversion ($g^{(2)}$ in Q_{int} and conversion Q_{int} in Q_3). A parallel study with a different test material essentially confirmed the high interlaboratory comparability (Lamberty et al. 2011).

The study further confirmed high agreement with the results of electron microscopy and centrifugation analysis. However, such agreement cannot be expected for non-spherical particles. That is because the hydrodynamic diameter deviates from e.g. Stokes diameter. Additionally, there is a significant contribution

of the particle rotation to the intensity fluctuation, which increases with scattering angle (Aragón and Pecora 1977; Hoffmann et al. 2009). DLS then measures an apparent hydrodynamic diameter $x_{h,app}$ which is smaller than the translational one ($x_{h,t}$). The impact of rotation on the autocorrelation function can be computed straightforwardly if the particles are very fine and their shape is known (Aragón and Pecora 1977; Xu 2000, pp. 259). If a depolarised scattering multi-angle DLS setup¹⁰ is employed, it may even be possible to separate the impact of rotation and translation and to determine shape parameters (Nakamura et al. 2006; Hoffmann et al. 2009).

Limits for the applicability of DLS are mainly set by size and concentration of particles. First of all, the concentration should be low enough to avoid strong multiple scattering. Multiple scattering reduces the signal coherence, i.e. the signal-to-noise-ratio, affects the correlation function and contributes to depolarisation. It is of particular relevance for large particles with high contrast in the refractive index. Multiple scattering can be effectively reduced by backscattering techniques (Wiese and Horn 1991; Peters et al. 1998) and largely suppressed by cross correlation techniques (e.g. 2-colour cross-correlation: Dhont and de Kruif 1983; Drewel et al. 1990; Segrè et al. 1995; 2-dimensional cross-correlation: Phillis 1981a, b; 3-dimensional cross-correlation: Schätzel 1991; Aberle et al. 1998; Overbeck and Sinn 1999; Urban and Schurtenberger 1999), where two simultaneous scattering experiments at the same sample volume are conducted. The amplitude of the cross correlation function is proportional to the squared single scattering fraction (Aberle et al. 1998). That means that cross correlation techniques can be used as long as there is a significant portion of single scattered light in the detected signal.

When multiple scattering is discarded from the measured signal, DLS can be used to study the dynamics of concentrated suspensions, in which the Brownian motion of individual particles (self-diffusion) differs from the diffusive mass transport (gradient or collective diffusion), which causes local density fluctuations, and where the diffusion on very short time-scales ($\tau < a^2/D$) deviates from those on large time scales ($\tau \gg a^2/D$; Jones and Pusey 1991; Banchio et al. 2000). These different diffusion coefficients depend on the microstructure of the suspension, i.e. on the particle concentration and on the interparticle forces. For an unknown suspension it is not possible to state a priori which of them is probed by a DLS experiment. For this reason, a further concentration limit must be obeyed when DLS is used for basic characterisation tasks such as particle sizing. As a rule of thumb, such concentration effects vanish below concentrations of 0.01–0.1 vol%, but certainty can only be gained by experiment.

Apart from upper concentration limits, there is a further one at the lower edge, where the intensity fluctuations start to become affected by the statistic variation of

¹⁰DLS instruments typically employ vertically polarised light (I_{vv} ; Xu 2000, p. 230). Depolarised scattered light (I_{vh}) results from anisometry or multiple scattering—signals are usually very weak.

particle number in the measurement zone. According to Willemse et al. (1997), a minimum of 100 particles should stay in the measurement zone. This is fulfilled for most colloidal suspensions; problems may arise for micrometre particles (i.e. $\geq 1 \mu\text{m}$).

Assuming a scattering volume of $10^6 \mu\text{m}^3$ (Willemse et al. 1997) and particles of $1 \mu\text{m}$ diameter, then a minimum concentration of 0.01 vol% is needed for ensuring 300 scattering particles. For strongly scattering particles of that size, such a concentration may already exceed the upper limit set by multiple scattering (cf. Itoh and Takahashi 1991), which means that there is no concentration range, in which the DLS measurement should be conducted. The absence of such a range is the particularly likely for particles $> 1 \mu\text{m}$.

Sedimentation sets a further limit to the detection of coarse particles because the particle displacement of micrometre particles is governed by sedimentation rather than by diffusion (cf. Sect. 2.3.3.1). This is of particular importance for polydisperse particle systems, where diffusion and sedimentation are coupled (Batchelor 1982; Batchelor and Wen 1982). Moreover, sedimentation may affect the size distribution in the measurement zone. However, in the colloidal size range ($x \leq 1 \mu\text{m}$) there is virtually no impact of sedimentation on DLS results (e.g. Paul and Pusey 1981). A lower size limit exists only inasmuch as the scattering intensity of the particles should considerably exceed that of the fluid molecules. Xu (2000, p. 241) proposes a minimum factor of 2.5; yet, for highly reliable DLS this value should be multiplied by 10.

Occasionally, DLS is compared with the DUM (cf. Sect. 2.3.1) because both methods measure the diffusion of colloidal particles. However, the two methods are not equivalent; thus, identical results cannot be expected.

Differences between the two methods exist with regard to particle property and type of quantity: DUM only evaluates the translational diffusion ($x_{h,t}$) and probes number frequencies, whereas DLS is also sensitive to the diffusive rotation ($x_{h,app}$) and yields intensity weighted distribution functions. Furthermore, the methods usually differ in sample size: Typical sample concentrations in DLS are in the range of 0.01 vol%. These are, for instance, 50,000 particles \hat{a} 100 nm in a measurement volume of $10^6 \mu\text{m}^3$, which are all observed in the order of minutes (Willemse et al. 1997), whereas with DUM, the total number of traced particles is smaller by factor 10–100, with an observation time in the order of seconds for each. Last but not least, DLS allows for a temporal resolution in the range from ns to ms, whereas DUM is subject to video processing, typically with 30 frames per second, and is, therefore, not sensitive to very fast relaxation processes (like gradient diffusion).

2.3.5.2 Diffusing Wave Spectroscopy

For the interpretation of DLS measurements, it is prerequisite that multiple scattering has been avoided by sufficiently high sample dilution or even suppressed by technical means. In contrast, *diffusing wave spectroscopy* (DWS) evaluates the light fluctuations in the presence of strong multiple scattering. The decay of the

autocorrelation function is then related to the loss of coherence by multiple scattering, i.e. by the large number of scattering events a photon experiences when travelling through the suspension. In DWS the autocorrelation function reflects the Brownian motion of single particles (short-time self-diffusion) as well as the mean free path of photon transport l^* , which depends on the particle concentration and on the suspension structure (Maret and Wolf 1987; Pine et al. 1988). Consequently, DWS can be used for measuring average diffusion coefficients and mean particle size (Scheffold 2002; Rochas-Ochoa et al. 2002), for investigating aggregation processes and phase transition (Wyss et al. 2001; Alexander and Dalgleish 2007), or for probing the microrheology of gels (Mason and Weitz 1995; Ruis et al. 2008).

2.3.5.3 X-Ray Photon Correlation Spectroscopy

In principle, there is no reason why dynamic scattering techniques should be restricted to radiation in the visible domain of the electromagnetic spectrum. However, practical limits are set by the requirement of coherent radiation (at least for single particle detection) and low sample turbidity, as well as the availability of appropriate radiation sources and sensor technique. In practice, only X-radiation is employed as a further dynamic scattering technique, which is called X-ray photon correlation spectroscopy (XPCS) or X-ray intensity fluctuation spectroscopy (XIFS). In comparison to visible light X-rays allow for a greater spatial resolution of suspension microstructures (larger q -values) and virtually avoid multiple scattering because of the weak interaction of X-radiation with matter (cf. Sect. 2.3.4). On the other hand, only third generation synchrotrons provide the necessary X-radiation of high coherence and intensity. XPCS has been i. a. used to measure diffusion processes of particles in solution, to study the dynamics of polymer blends, or to characterise liquid-crystal membranes (see Sutton 2008; Nugent 2010 and references therein).

2.3.5.4 Fluorescence Correlation Spectroscopy

A further group of dynamic scattering techniques comprises such methods that analyse the fluctuation of inelastic scattering events such as Raman scattering or fluorescence. In particular, fluorescence correlation spectroscopy is widely used for studying bio-molecules (e.g. nucleic acids, proteins) in vitro or in vivo (Elson and Magde 1974; Magde et al. 1974; Krichevsky and Bonnet 2002). X-ray fluorescence correlation spectroscopy has been employed for the characterisation of colloidal suspensions, but is currently still in the stage of development and has not yet attracted wide attention in the colloidal community (Wang et al. 1998; Leupold et al. 2007).

2.3.6 Further Spectroscopic Techniques

Static and dynamic scattering techniques are spectroscopic characterisation methods in the sense of Sect. 2.2. These techniques evaluate the functional dependency of measurement signals on a spectral parameter, i.e. on time, space, or classically on wavelength or frequency. The major advantage of spectroscopic methods is the reduced sample preparation (no fractionation), but they involve the inversion problem. That is, the spectrum is a—most frequently incomplete and discrete—nonlinear projection of the size distribution. Beside the scattering techniques, there are further spectroscopic methods which are based on the extinction of radiation or on any other response of the particle system to an external field. This section describes optical, acoustic, and electroacoustic methods that have gained relevance for the characterisation of colloidal suspensions.

2.3.6.1 Optical Spectroscopy

The term *optical spectroscopy* refers to the evaluation of the wavelength dependency of transmitted light for the quantification of dissolved or dispersed matter (Fig. 2.17, left). Optical spectrometers deliver transmission or turbidity spectra, which commonly range from the ultraviolet (UV) to the near infrared (NIR) domain. They are standard analytical tools which are mainly used to identify solutes and to determine their concentration. The impact of particle size on the shape of the transmission spectra has been known for long and was, for instance, subject of Gustav Mie's (1908) renowned paper on the theory of light scattering. Accordingly, optical spectroscopy has been employed for the measurement of particle size distributions in many experimental studies. It is mainly applied to fine colloids, e. g. to submicron polymer latices (Zollars 1980; Gulari et al. 1987, Celis et al. 2008), to crystallisation processes (Crawley et al. 1997), to fine abrasive particles in polishing slurries (Kuntzsch 2004, pp. 58–60) or to metal nanoparticles (Haiss et al. 2007).

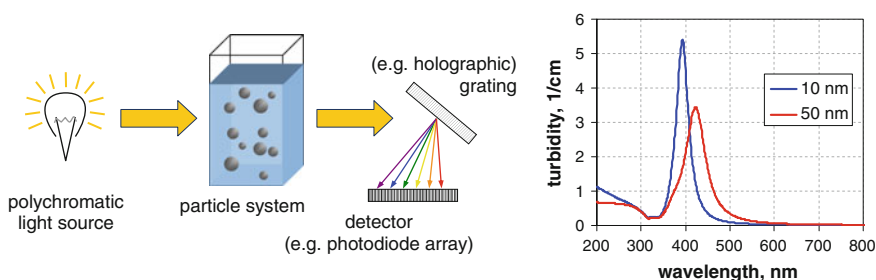


Fig. 2.17 Principle of optical spectroscopy (*left*) and turbidity spectrum for 0.0001 vol% of colloidal Ag in water (*right*)

All these applications rely on the fact that the light transmission through a colloidal suspensions depends on the morphology, the concentration and the optical properties (i.e. the complex refractive index function) of the dispersed phase. In dilute suspensions, the particles contribute independently to the extinction of light, and the transmission T obeys the Lambert-Beer law:

$$T(\lambda) = \exp\left(L \cdot c_N \cdot \int C_{\text{ext}}(x, \lambda, m(\lambda)) q_0(x) dx\right). \quad (2.38)$$

After conversion to turbidity τ and natural extinction E this leads to

$$\tau(\lambda) = E(\lambda)/L = c_N \cdot \int C_{\text{ext}}(x, \lambda, m(\lambda)) q_0(x) dx, \quad (2.39)$$

where L is the optical path, c_N the number concentration, C_{ext} the extinction cross section, and $q_0(x)$ the number weighted density function. The specific shape of an optical spectrum results from the general impact of wavelength λ on C_{ext} as well as from the material-specific wavelength dependency of the relative refractive index. The particle size distribution is obtained by inversion of the two Eqs. (2.38) and (2.39) (Elicabe and Garcia-Rubio 1989).

The optical spectroscopy is commonly applied to such colloidal suspensions that obey the Rayleigh limit or the Rayleigh-Debye-Gans limit of scattering (cf. Appendix B.2). In this case the spectra usually have a smooth and monotone shape, from which only a few details of the size distribution can be deduced. Yet, for metals with a surface plasmon resonance in the optical domain (e.g. Ag or Au), one observes a distinct, size dependent maximum in the turbidity spectra of nanoparticles (Fig. 2.17; cf. Njoki et al. 2007). The presence of such a maximum can clearly enhance the information content of the spectrum.

Size distributions from optical spectroscopy actually reflect the distribution of the extinction cross section C_{ext} , which is a function of the particles morphology and their optical properties. For very fine colloids <100 nm, i.e. for Rayleigh scatterers, the total optical behaviour is determined by the particle volume.¹¹ The method then yields volume equivalent diameters. In order to identify the type of quantity in which the different size fractions are weighted, one needs to determine the impact of single particles to the total signal (i.e. the integrated spectrum). The results depend on the covered frequency range and on the signal representation (transmission or extinction spectrum).

It turns out that, in the case of absorbing colloidal particles, the total signal strength correlates approximately with the third power of the particle size for both types, transmission and extinction, of spectra. They are, thus, volume weighted. For non-absorbing

¹¹with C_{ext} being proportional to the particle volume for absorbing substances and to the squared volume for non-absorbing ones.

particles in the Rayleigh limit of scattering, the transmission spectra can be roughly considered as volume-weighted as well, whereas an ideal extinction spectrum is weighted by the squared particle volume.

Optical spectroscopy requires that both transmission and extinction are well above the electronic noise. This sets a lower size limit to the detection of non-absorbing colloidal particles ($C_{\text{ext}} \propto x^6$), since the maximum optical path is usually defined by the instrument and the particle concentration should be sufficiently low to avoid osmotic concentration effects (cf. Sect. 3.1.1). Such a problem does not occur for absorbing particles, where measurements can be conducted at volume concentrations in the order of ppm. However, for absorbing nanoparticles below 10 nm, the spectra are solely affected by the mass concentration and the influence of size vanishes (Njoki et al. 2007)—unless the optical properties change with size as for quantum dots (Segets et al. 2009) or for metal nanoparticles <10 nm (Römer and Fragstein 1961; Scaffardi and Tocho 2006; Santillán et al. 2013). Last but not least, the data analysis has to adequately regard the contribution of solute or adsorbed matter (ions, polymers) to the optical spectra, which is of particular relevance in the UV domain (e.g. Gaffney et al. 1992).

Although several studies have demonstrated that optical spectroscopy reliably measures the size and concentration of suspended nanoparticles, the method is only of minor relevance for particle sizing. Recent developments try to considerably increase the method's sensitivity, precision, and resolution by employing pulsed laser light with tuneable wavelength (Li et al. 2010) or to realise online-capable instrumentation, e.g. by measuring at a few selected wavelengths, which usually suffices to capture the shape of the spectrum (Melik and Fogler 1983; Gabsch et al. 2005; Steinke et al. 2009).

2.3.6.2 Ultrasonic Spectroscopy

Even though optical particle sizing techniques are very popular, most of them require sufficiently dilute suspensions with less than 1 vol% solid content. That is because dense suspensions are opaque or because light transmission and scattering are subject to unwanted (i.e. poorly understood) concentration effects like multiple scattering. In such situations, acoustic fields may serve as an alternative probe for the state of dispersion. *Ultrasonic spectroscopy* is the generic term for all particle sizing techniques that are based on the frequency dependent measurement of sound velocity or attenuation in the ultrasonic domain (mostly within 100 kHz to 200 MHz). While velocity spectroscopy is mainly used for the study of inter- and intramolecular processes, attenuation spectroscopy has found its major application in particle sizing (McClements 1996; Kachanovskaya et al. 1996). The most promising feature of acoustic characterisation techniques is their applicability to highly concentrated particle systems (up to 70 vol%) under non-equilibrium conditions (McClements 1991). That means it offers the opportunity to monitor the state of dispersion of dense product streams (Scott et al. 1998), to control the

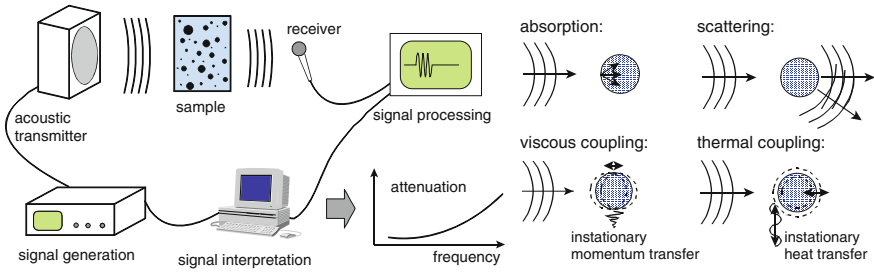


Fig. 2.18 Principle of ultrasonic attenuation spectroscopy (*left*) and kinds of particle-wave interaction in sound fields (*right*)

deagglomeration of suspension or the homogenisation of emulsions, and to study polymerisation or crystallisation processes (Hipp et al. 2000; Mougins et al. 2001).

All of these applications benefit from the size-dependency of sound-particle interactions (Fig. 2.18), which result in sound scattering and dissipation. Scattering is predominant for micrometre particles, but becomes of minor importance for colloidal particles, which are usually much smaller than the sound wavelength (in water: 15 μm at 100 MHz). In that case, sound propagation is governed by the dissipation of sound energy due to momentum and heat exchange between the oscillating and pulsating particles and the surrounding liquid. Additionally, there is always size-independent absorption of sound in the particles and in the liquid (Challis et al. 2005).

First instruments for the detection of ultrasonic velocity and attenuation were built by Pellam and Galt 1946 and Pinkerton 1947 in the middle of the 20th century. Andreae and his co-workers (Andrea et al. 1958; Andrea and Joyce 1962; Edmonds et al. 1962) eventually realised the first spectrometer for measuring ultrasonic attenuation. Today, there are several (commercial) suppliers of ultrasonic spectrometers (e.g. Hinze et al. 2000) that provide on-line instrumentation as well as laboratory instruments.

The immediate result of such instruments is the frequency spectrum of the sound velocity or the attenuation coefficient α , which is defined as the relative decrease of sound pressure per an infinitesimally small distance. The latter is often presented as ratio α/f versus the logarithm of frequency because such a spectrum has one or more size-specific peaks and its total area depends on the volume concentration only. For dilute suspensions, the data analysis reduces to a linear inversion problem (cf. Sect. 2.2):

$$\tilde{\alpha}(f, \varphi_V) = \alpha(f, \varphi_V)/f = \tilde{\alpha}_{\text{abs}}(f, \varphi_V) + \varphi_V \cdot \int k(f, x) \cdot q_3(x) dx. \quad (2.40)$$

The kernel function $k(f, x)$, which quantifies the influence of size and frequency on attenuation, can be derived from the combined universal theory for the inelastic

scattering of sound at spherical particles; the ECAH theory (Epstein & Carhart 1953; Allegra and Hawley 1972).¹² However, this linear theory fails for dense dispersions of colloidal particles because neighbouring particles affect each other with respect to the acoustophoretic motion and to the thermal fluctuation. The non-linearity is tackled by advanced multiple-scattering theories (Hipp et al. 2002), by effective medium approaches (Isakovich 1948; Hemar et al. 1997), or by coupled phase models (Dukhin and Goetz 1996; Babick 2005), but all of them keep restricted to the colloidal size range ($x \ll \lambda$).

In colloidal suspensions, the sound propagation is typically governed by the acoustophoretic motion of particles. For monodisperse spheroids that do not deviate too much from spherical shape (aspect ratio $<10/1$), the attenuation spectrum essentially reflects the volume specific surface area of the particles¹³ (Babick and Richter 2006). Similar results would probably be obtained for any convex particle shape. For particle aggregates, the inner structure is decisive. Regarding the type of quantity, acoustically measured size distributions are ideally volume weighted distributions (see comments in Sect. 2.2).

It could be shown that the results of ultrasonic spectroscopy agree fairly well with those of other characterisation methods and are hardly affected by the extent of sample dilution (Dukhin and Goetz 1996; Babick et al. 1998; Babick 2005). Moreover, an interlaboratory comparison showed excellent agreement for colloidal particles (Dukhin et al. 2012). That is why ultrasonic spectroscopy is considered as a powerful tool for monitoring colloidal processes. However, the method does not allow for a very sharp resolution of size distributions in the colloidal size range (Babick and Ripperger 2002). In addition, the analytical models contain a variety of material parameters. This is of particular relevance for emulsions (14 properties), whereas for aqueous suspensions only the viscosity and sound speed of liquid and the density contrast have to be known (Babick et al. 2000). Lacking knowledge on the model parameters can be coped with by simultaneously evaluating sound speed and attenuation or by employing statistical data processing (e.g. neural networks; cf. Li et al. 2004; Babick et al. 2006).

In summary, the great potential of ultrasonic spectroscopy is the reliable characterisation of concentrated suspensions. For well-defined colloidal suspensions it may be used for fast off-line determinations of the size distribution, although the resolution is rather coarse. Its application to process monitoring is principally possible, yet this may require the development of an appropriate data analysis for the specific process. However, a sufficiently high sensitivity to relevant changes in product quality or process performance can outweigh this additional effort.

¹²The same applies to the calculation of sound dispersion, i.e. frequency impact on sound speed.

¹³Even so, the spectrum can only be reproduced as sphere-spectrum by assuming polydispersity.

2.3.6.3 Electroacoustic Mobility Spectroscopy (EMS)

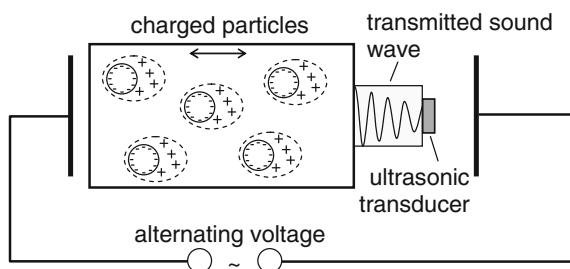
The *electroacoustic mobility spectroscopy* (EMS) is a measurement technique that allows for the simultaneous determination of the particle size distribution and the effective zeta-potential of colloidal suspensions (O'Brien et al. 1995). Its primary signal is the acoustic response of a colloidal suspension to a high-frequency alternating electric field. It is called *electrokinetic sonic amplitude* (ESA) and is directly related to the dynamic electrophoretic mobility of the colloidal particles. The ESA signal results from the simultaneous electrophoretic motion of all charged particles. The corresponding oscillatory flux of momentum is transferred to the walls and subsequently transmitted as a sound wave (Fig. 2.19). Prerequisite for the existence of an ESA-signal is a surface charge and a density contrast between particles and continuous phase (O'Brien 1988).

The EMS can be applied to concentrated suspensions (>1 vol%) of particles above 50 nm and below 10 microns (Hunter 1998). Exact analytical models are available for solid concentrations below approximately 3 vol% and for thin double layers. Although there has been considerable progress in theoretical treatment of higher concentrated systems, empirical correction terms are usually used to account for the hydrodynamic and electrostatic particle-particle interactions. Depending on the quality of the data basis used for deriving these interpolating equations, very satisfactory results can be obtained (Knösche 2001; Babick et al. 2001).

Even though the particle motion originates from the polarisation of the double layer in the electric field, its magnitude and phase is decisively affected by the density contrast and the hydrodynamic drag. Hence, from the point of particle sizing, the dynamic electrophoretic mobility is closely related to the acoustophoretic mobility. The latter has been shown to be governed by the volume-specific surface when regarding spheroids with moderate aspect ratios ($\leq 10/1$, see above); acc. to Loewenberg and O'Brien (1992), this also applies to first approximation to the dynamic electrophoretic mobility.

Since the ESA signal indicates the momentum flux that is related to particle oscillation, mobility spectra are intrinsically volume weighted functions. However, size analysis is conducted at the frequencies at which a volume unit of coarse particles contributes less to the ESA signal than one of fine particles. This may lead to an underestimation of coarse size fractions. The size distribution is obtained by

Fig. 2.19 Generation of the ESA signal in highly frequent electric fields



inversion of the mobility spectrum, yet in contrast to other spectroscopic methods, the spectral signal is a complex (i.e. two-parametric) quantity and does not only depend on the size distribution, but also on the zeta-potential. A profound analysis by Knösche (2001) revealed that, for typical measurement situations, one can extract up to 7 independent pieces of information on the size distribution. However, the ESA signal loses its sensitivity to particle size beyond the size range indicated above (50 nm to 10 μm).

EMS has the potential advantage of being applicable in highly concentrated suspensions, which opens the way for on-line applications (Carasso et al. 1995; Hunter 1998). It delivers reliable analysis data in many circumstances, in particular for solid particles with thin diffuse layers and low polarisabilities. However, the interpretation of mobility spectra requires detailed knowledge of the particulate system, e.g. of particle shape and material properties (like dielectric constant) and sometimes of surface conductance.

2.3.7 Zeta-Potential and Interfacial Properties

When colloidal particles are dispersed in a liquid solvent, it is very likely that they acquire a surface charge (cf. Sect. 3.1.5) which has to be compensated for by a corresponding countercharge in the vicinity of the surface. Both regions, charged surface and counter-charged solvent, form the *electric double layer* (EDL). The charge separation between the two layers creates an electric potential between the particle surface and the bulk solvent, which is responsible for attractive or repulsive interactions between the colloidal particles.

Important measurands for the characterisation of the EDL are the surface charge density and the electrokinetic potential or *zeta-potential*. The zeta-potential is the electric potential at a hypothetical shear plane, which separates the mobile solvent from solvent molecules that adhere to the particle surface. The zeta-potential can be probed by imposing a relative motion between bulk solvent and particle (Delgado et al. 2007).

Such a relative motion can be induced by external electric fields or by pressure gradients or bulk forces (e.g. gravity). It is possible that particles move in a quiescent solvent or that the solvent flows through a fixed bed of particles. A detailed description on electrokinetic phenomena is e.g. given by Hunter (1988). Zeta-potential measurements on colloidal suspensions are frequently conducted via electrophoresis or by means of electroacoustics. Besides this, there are recent techniques based on non-linear optics that are sensitive to interfacial changes.

2.3.7.1 Electrophoretic Zeta-Potential Measurement

If an electric field is applied to a suspension of charged colloidal particles, the mobile ions within the double layer become spatially separated according to the

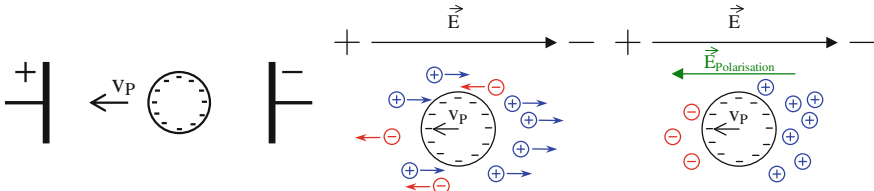


Fig. 2.20 Electrophoresis and double layer polarisation

sign of their charge (double layer polarisation), and the particles start to move along the lines of the electric field (Fig. 2.20). This electrophoretic motion is characterised by the electrophoretic mobility:

$$\mu_{ep} = \frac{\mathbf{v}}{\mathbf{E}}, \quad (2.41)$$

which is a function of the zeta-potential ζ and the Debye-Hückel-parameter κ (the inverse double layer thickness $1/\kappa$):

$$\mu_{ep} = \frac{2}{3} \cdot \frac{\varepsilon_m \varepsilon_0 \zeta}{\eta} \cdot f(\kappa a, \zeta) \quad (2.42)$$

$$\text{with } \kappa^2 = \frac{F^2}{\varepsilon_m \varepsilon_0 \cdot RT} \cdot \sum z_i^2 c_i^\infty. \quad (2.43)$$

The double layer thickness is decisive for the retarding impact of double layer polarisation on the electrophoretic motion. Equation (2.42) yields simple linear relationships only for the two limiting cases of very thin double layers ($\kappa a \rightarrow \infty$) and infinitely thick ones ($\kappa a \rightarrow 0$). The correction function $f(\kappa a)$ then simplifies to a constant value of $3/2$ and 1 , respectively (Fig. 2.21; von Smoluchowski 1903; Debye and Hückel 1924; O'Brien and White 1978).

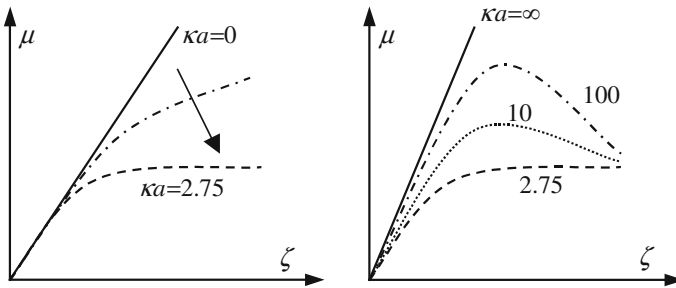


Fig. 2.21 Nonlinear relationship between zeta-potential and electrophoretic mobility acc. to O'Brien and White (1978)

The electrophoretic motion is either measured microscopically or by light scattering. The former way is called *microelectrophoresis* and usually employs ultramicroscopes when dealing with colloidal particle systems. The optical instrumentation can be identical to that of DUM, while the software has to be modified because only the displacement in the direction of the electric field is relevant. The method yields a number weighted distribution of zeta-potentials. Similar to DUM, a sufficiently large number of trajectories has to be evaluated in order to keep the statistical uncertainty within an acceptable level. Moreover, the method may be insensitive to weak scatterers within a polydisperse colloidal suspension.

An instrumental alternative to microelectrophoresis is *electrophoretic light scattering* (ELS). The light scattering at migrating particles leads to phase shift (Doppler effect), which can be detected by a heterodyne DLS set-up (i.e. reference-beating with frequency shift). The method yields an intensity weighted distribution of the zeta-potential.

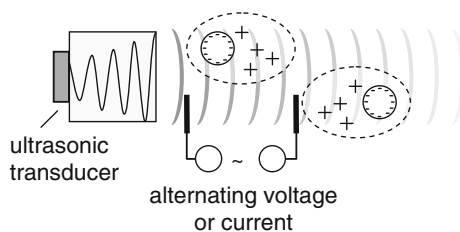
The electrophoretic motion of colloidal particles is superposed by their Brownian motion. Ideally, both can be separated because of their different space-time correlations, in practice however, diffusion broadens the measured zeta-potential distribution. In microelectrophoresis, the Brownian contribution can be minimised by long observation times ($t \gg D_t/v_{ep}^2$). For ELS, diffusion is least pronounced at small scattering angles (Xu 2008).

2.3.7.2 Electroacoustic Zeta-Potential Measurement

Electroacoustic techniques are either based on the acoustic response of a suspension to an alternating electric field or on its electric response to a sound field. The former signal is the *electrokinetic sonic amplitude* (ESA), which can be employed for particle sizing (cf. Sect. 2.3.6.3) and for the determination of the zeta-potential. The latter signal is the *colloid vibration potential* (analogously the *colloid vibration current*), which is defined as the alternating electric potential between two electrodes that are separated by the half acoustic wavelength. This potential arises from the particle oscillation in the sound field (acoustophoretic motion) which coincides with a polarisation of the double layer (Fig. 2.22) (Dukhin and Goetz 2001).

The existence of the colloidal vibration potential (CVP) was predicted in the 1930s (Debye 1933; Hermans 1938a, b; Rutgers 1938) and intensively investigated—both experimentally and theoretically after the Second World War (Rutgers 1946; Enderby

Fig. 2.22 Generation of the colloid vibration potential (CVP) or current (CVI) in ultrasonic fields



1951; Booth and Enderby 1952; Yeager et al. 1953). The discovery of the electrokinetic sonic amplitude (ESA) occurred comparatively late, in the 1980s (Oja et al. 1985), yet this effect was soon employed in commercial instruments for zeta-potential measurements. Subsequent theoretical treatments showed that both signals can be traced back to the dynamic electrophoretic mobility and that they form a reciprocal couple of the Onsager type (O'Brien 1988; O'Brien et al. 1994).

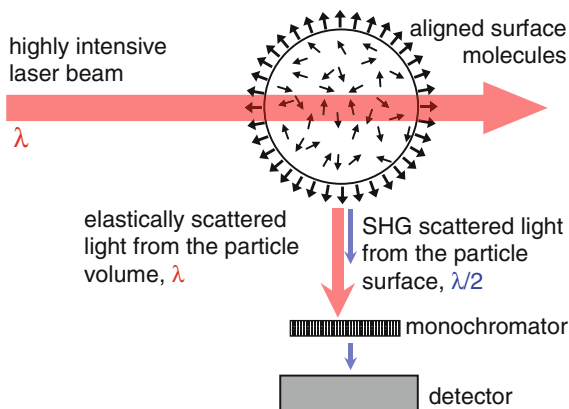
The electroacoustic techniques provide a powerful means to measure the zeta-potential in concentrated suspensions that are optically opaque (Hunter 2001, Dukhin et al. 2001, Greenwood 2003). Thus, laborious sample preparation, which aims at conserving the state of double layer during dilution, can be avoided. Yet, modelling electroacoustics for dense suspensions is not straightforward, since the hydrodynamic interaction and double layer overlap has to be adequately considered (e.g. Dukhin et al. 1999; Rasmussen 2001; O'Brien et al. 2003). Available models are based on several assumptions (e.g. on particle shape and the suspension structure) and require model parameters like particle size or surface conductance. Since the electroacoustic raw signals do not only depend on the suspension properties, but are affected by the acoustic coupling between suspension and sensor and by the instrument geometry, calibration is typically required (Hunter 1998; Dukhin et al. 2001). Last but not least, it should be noted that electroacoustic signals are essentially volume weighted. That means they provide a better sensitivity to very fine colloidal particles than an optical detection system and may be more appropriated for the electrokinetic characterisation of multi-component suspensions (containing weak and strong scatterers).

2.3.7.3 Surface Characterisation with Second Harmonic Generation

The zeta-potential, which is traditionally measured with electrokinetic and electroacoustic techniques, is an important parameter for the computation of particle-particle interactions and the corresponding electroviscous effects. However, it does not reveal the complete structure of the electric double layer, in particular its immobile part (Stern layer). New arising techniques that are sensitive to the real interface without affecting the double layer equilibrium may facilitate a complementary characterisation.

One such technique is the second harmonic generation (SHG), which relies on the effect that a minute portion of light is scattered with twice the frequency (i.e. energy) of the incident radiation (Fig. 2.23). This can be understood as the spontaneous re-emission of one double-energy photon after the simultaneous absorption of two normal photons (Hollis 1988). In contrast to fluorescence, there is no phase lag. Hence, the SHG is a coherent scattering event, which—like Rayleigh scattering—would be completely cancelled by destructive interference in a homogenous medium with randomly aligned molecules for any direction besides forwards. At interfaces with symmetry breaks and molecule orientation, the second harmonics superpose constructively and produce a corresponding scattering field (prerequisite that the interface curvature is not much smaller than the wavelength).

Fig. 2.23 Second harmonic generation at particle interface



In order to attain measurable SHG signals, pulsed femtosecond lasers with large intensities are usually employed (Yan et al. 1998; Schneider et al. 2007). It was possible to show that the SHG scales with surface potential and the independently measured zeta-potentials can be reproduced by adopting appropriate models for the electric double layer (Yan et al. 1998). More generally, SHG is directly related to the surface excess of adsorbate as shown for malachite green on polystyrene (Eckenrode et al. 2005). This technique offers the opportunity for online and in situ characterisation of colloidal suspensions with particle sizes considerably larger than 5 nm (Schneider and Peukert 2007; Schürer and Peukert 2010).

SHG is far from being a mature characterisation technique of colloidal interfaces. But with regard to the on-going developments in instrumental set-up and the growing number of application experiences its potential benefits seems very promising.

2.3.8 Final Remarks on Particle Sizing

This chapter introduced important characterisation techniques for colloidal suspensions. The focus was on particle sizing methods, which are specified by the particle property employed to distinguish the different size fractions as well as by the type of quantity intrinsically used to quantify the size fractions. Additionally, they differ in the degree to which details of size distributions can be resolved and in their sensitivity to certain parts of the size distribution (e.g. sensitivity towards coarse, contaminant particles). Further differences concern the ranges of particle size and concentration in which sizing is possible. Table 2.2 summarises the discussed sizing methods with regard to the mentioned aspects.

The differences between the various sizing techniques mean that a measured size distribution is inevitably affected by the employed characterisation method. That frequently causes confusion on the correctness of measurements when deviations

Table 2.2 Characteristics of selected particle sizing methods

Method	Classification	Particle property	Equiv. diameter or related geometric parameter	Type of quantity (index, index for nanoparticles)	Size and concentration range (conservative)	Comments
Dynam. ultramicroscopy (DUM)	Counting	Diffusion coeff.	$X_{h,t}$	Number (0)	10 nm–1 μ m \ll 1 vol%	Requires inversion, statistics
Image analysis (IA)	Counting	Any length/area of projected image	e.g. perimeter, area	Number (0)	1 nm to \ll 1 vol%	Various imaging methods
Optical centrifugation (OCA)	Fractionating	Settling velocity	$X_{Stokes} = X_V^3/X_{h,t}$	Extinction (ext, NP: 3 or 6)	10 nm–1 μ m $<$ 1 vol%	Different realisations
Field-flow fractionation (FFF)	Fractionating	e.g. diffusion coeff., settling velocity	e.g. $X_{h,t}$, X_{Stokes}	e.g. scattering intensity (int, NP: 6)	10 nm–1 μ m \ll 1 vol%	Different fields, different detection systems
Static light scattering (SLS)	Spectroscopic	Volume, diameter of gyration molecular weight	X_V , X_g	Scattering intensity (int, NP: 6)	10 nm–1 μ m \ll 1 vol%	Impact of colloid concentration
Laser diffraction spectroscopy (LD)	Spectroscopic	Main proportions of projected image	(Orientation averaged) Feret diameters	e.g. projection area (2)	500 nm–1 mm \ll 1 vol%	Not only diffraction, impact of detection optics
Small angle X-ray scattering (SAXS)	Spectroscopic	Volume, diameter of gyration	$X_V X_g$	Scattering intensity (int, NP: 2)	1 nm–50 nm 0.1–10 vol%	Best quality with synchrotron X-ray sources

(continued)

Table 2.2 (continued)

Method	Classification	Particle property	Equiv. diameter or related geometric parameter	Type of quantity (index, index for nanoparticles)	Size and concentration range (conservative)	Comments
Dynamic light scattering (DLS)	Spectroscopic	(Apparent) diffusion coefficient	$X_{h,r}$ or $X_{h,app}$	Scattering intensity (int, NP: 6)	1 nm–1 nm < 1 vol%	Correlation spectroscopy or frequency analysis
Optical spectroscopy (OS)	Spectroscopic	Volume, diameter of gyration	X_1X_g	Extinction (ext, NP: 3 or 6)	10 nm–1 μm < 0.1 vol%	Plasmon resonance for metals
Ultrasonic spectroscopy (US)	Spectroscopic	Scattering, acoustoph. mobility	Approx.: volume, specific surface	Volume (3)	10 nm–100 μm 1–70 vol%	Evaluation of sound speed or attenuation

between differently determined size distributions are observed. Again, apart from uncertainties due to sample preparation and measurement, there are intrinsic differences between particle sizing techniques. It is, therefore, necessary to ask for the most appropriate characterisation technique for a specific characterisation task. For that purpose, one has to clarify the objective(s) of measurement in advance (cf. Polke et al. 2003):

- which property defines the quality of the suspension or its process behaviour (particle volume, particle diffusivity, ...)?
- which parameters of the size distribution are required (mean size, modal values, amount of nanoparticles, ...)?
- where will the measurement be conducted (at process line, in laboratories, ...)?
- what level of accuracy and precision is required?

The answers to those questions define the requirements on the measurement instrument and reduce the list of applicable characterisation techniques. It might be even possible that the characterisation aims at the quantification of two or more independent or weakly correlating parameters of the size distribution (e.g. maximum size and average size). In that case, it is quite likely that at least two methods have to be employed.

Ruscitti et al. (2008) reported on the performance of different sizing techniques with regard to the qualification of product quality after comminution. The product quality was described by a set of three macroscopic suspension properties, two of which correlate with “average” particle size (below 1 μm) and one with the maximum size (above 1 μm). The outcome of this study was twofold: On the one hand, it was not possible to determine average and maximum particle size with one inline-capable sizing technique. On the other hand, the authors significantly improved their understanding of the process, in particular with regard to the interdependency between the quality parameters.

In general, by combining different characterisation techniques, one can benefit from their specific characteristics, e.g. probed particle property, and gain (more) comprehensive insight into the microstructure of colloidal suspensions.

References

General Matter

- R. Polke, M. Schäfer, N. Scholz, Charakterisierung disperser Systeme, in *Handbuch der Mechanischen Verfahrenstechnik, Bd. 1*; Chapter 2, ed. by H. Schubert (Wiley-VCH, Weinheim, 2003), pp. 7–100. ISBN 3-527-30577-7
- R. Xu, *Particle Characterization: Light Scattering Methods* (Kluwer Academic Publishers, Dordrecht, 2000). ISBN 0-7923-6300-0

Sizing

- F. Babick, S. Ripperger, Information content of acoustic attenuation spectra. Part. Part. Syst. Charact. **19**(3), 176–185 (2002). doi:[10.1002/1521-4117\(200207\)19:3<176::AID-PPSC176>3.0.CO;2-8](https://doi.org/10.1002/1521-4117(200207)19:3<176::AID-PPSC176>3.0.CO;2-8)
- R. Finsy, N. De Jaeger, R. Sneyers, E. Geladé, Particle sizing by photon correlation spectroscopy. Part III: Mono and Bimodal Distributions and Data Analysis. Part. Part. Syst. Charact. **9**(1–4), 125–137 (1992). doi:[10.1002/ppsc.19920090117](https://doi.org/10.1002/ppsc.19920090117)
- ISO 9276-1:1998, *Representation of Results of Particle Size Analysis—Part 1: Graphical Representation* (Beuth-Verlag, Berlin, 2004)
- M. Kandlikar, G. Ramachandran, Inverse methods for analysing aerosol spectrometer measurements: a critical review. J. Aerosol Sci. **30**(4), 413–437 (1999). doi:[10.1016/0021-8502\(98\)00066-4](https://doi.org/10.1016/0021-8502(98)00066-4)
- C. Knösche, *Möglichkeiten und Grenzen der elektroakustischen Spektroskopie zur Gewinnung von Partikelgrößeninformationen*. PhD thesis, Technische Universität Dresden, 2001
- J.H. Koo, E.D. Hirleman, Synthesis of integral transform solutions for the reconstruction of particle-size distributions from forward-scattered light. Appl. Opt. **31**(12), 2130–2140 (1992). doi:[10.1364/AO.31.00213](https://doi.org/10.1364/AO.31.00213)
- K. Leschonski, Representation and evaluation of particle size analysis data. Part. Part. Syst. Char. **1**(1–4), 89–95 (1984). doi:[10.1002/ppsc.19840010115](https://doi.org/10.1002/ppsc.19840010115)
- U. Riebel, F. Löffler, The fundamentals of particle size analysis by means of ultrasonic spectrometry. Part. Part. Syst. Charact. **6**(1–4), 135–143 (1989). doi:[10.1002/ppsc.19890060124](https://doi.org/10.1002/ppsc.19890060124)
- H. Rumpf, K.F. Ebert, Darstellung von Kornverteilungen und Berechnung der spezifischen Oberfläche. Chem. Ing. Tech. **36**(5), 523–537 (1964). doi:[10.1002/cite.330360516](https://doi.org/10.1002/cite.330360516)
- M. Stintz, *Technologie-relevante Charakterisierung von Partikeln und Partikelsystemen* Habilitation thesis, Technische Universität Dresden, 2005
- M. Stintz, F. Babick, G. Roebben, *Metrology for nanoparticle characterisation: instruments, standard methods and reference materials* (Workshop report, Nuremberg, 28./29.04.2010). Co-nanomet Consortium, c/o euspen, Cranfield, 2010. ISBN 978-0-9566809-3-8
- R.S. Stock, W.H. Ray, Interpretation of photon correlation spectroscopy data: A comparison of analysis methods. J. Polym. Sci. Part B: Polym. Phys. **23**(7), 1393–1447 (1985). doi:[10.1002/pol.1985.180230707](https://doi.org/10.1002/pol.1985.180230707)
- S. Twomey, *Introduction to the mathematics of inversion in remote sensing and indirect measurements* (Elsevier Scientific Publishing Company, Amsterdam, 1977). ISBN 0-444-41547-5
- W. Witt, U. Köhler, J. List, Current limits of particle size and shape analysis with high speed image analysis. On the CD-ROM: *PARTEC 2007, International Congress for Particle Technology*, Nuremberg, 27–29 Mar 2007. (available from NürnbergMesse GmbH, Messezentrum, 90471 Nürnberg, Germany), paper S35_2

Ultramicroscopy

- C. Bigg, Evident atoms: visuality in Jean Perrin's Brownian motion research. Stud. Hist. Phil. Sci. **39**(3), 312–322 (2008). doi:[10.1016/j.shpsa.2008.06.003](https://doi.org/10.1016/j.shpsa.2008.06.003)
- R.F. Domingos, M.A. Baalousha, Y. Ju-Nam, M.M. Reid, N. Tufenkji, J.R. Lead, G.G. Leppard, K.J. Wilkinson, Characterizing manufactured nanoparticles in the environment: multimethod determination of particle sizes. Environ. Sci. Technol. **43**(19), 7277–7284 (2009). doi:[10.1021/es900249m](https://doi.org/10.1021/es900249m)

- A. Einstein, Über die von der molekularteoretischen Theorie der Wärme geforderten Bewegung von in ruhenden Flüssigkeiten suspendierten Teilchen. *Ann. Phys. IV* **17**(8), 549–560 (1905). doi:[10.1002/andp.19053220806](https://doi.org/10.1002/andp.19053220806)
- J. Perrin, L'agitation moléculaire et le mouvement brownien. *CR Hebd. Seance Acad. Sci.* **146** (19), 967–970 (1908)
- J. Perrin, Mouvement brownien et réalité moléculaire. *Ann. Chim. Phys.* **8**(18), 1–114 (1909)
- J. Reissig, Ultramikroskopische Beobachtungen. *Ann. Phys. IV* **27**(11), 186–212 (1908). doi:[10.1002/andp.19083321110](https://doi.org/10.1002/andp.19083321110)
- H. Saveyn, B. De Baets, O. Thas, P. Hole, J. Smith, P. Van der Meeren, Accurate particle size distribution determination by nanoparticle tracking analysis based on 2-D Brownian dynamics simulation. *J. Colloid Interface Sci.* **352**(2), 593–600 (2010). doi:[10.1016/j.jcis.2010.09.006](https://doi.org/10.1016/j.jcis.2010.09.006)
- H. Siedentopf, R. Zsigmondy, Über Sichtbarmachung und Größenbestimmung ultramikroskopischer Teilchen, mit besonderer Anwendung auf Goldrubingläser. *Ann. Phys. IV* **10**(1), 1–39 (1903). doi [10.1002/andp.19023150102](https://doi.org/10.1002/andp.19023150102)
- R. Zsigmondy, Über ein neues Ultramikroskop. *Phys. Z.* **14**, 975–979 (1913)
- R. Zsigmondy, W. Bachmann, Handhabung des Immersionsultramikroskops. *Kolloid Z.* **14**(6), 281–295 (1914). doi:[10.1007/BF01423340](https://doi.org/10.1007/BF01423340)

Imaging

- M. V. Ardenne, Das Elektronen-Rastermikroskop. Theoretische Grundlagen. *Z. Phys.* **109**(9–10), 553–572 (1938). doi:[10.1007/BF01341584](https://doi.org/10.1007/BF01341584)
- G. Binnig, C.F. Quate, C. Gerber, Atomic force microscope. *Phys. Rev. Lett.* **56**(9), 930–933 (1986). doi:[10.1103/PhysRevLett.56.930](https://doi.org/10.1103/PhysRevLett.56.930)
- H.-J. Butt, R. Berger, E. Bonaccorso, Y. Chen, J. Wang, Impact of atomic force microscopy on interface and colloid science. *Adv. Colloid Interface Sci.* **133**(2), 91–104 (2007). doi:[10.1016/j.cis.2007.06.001](https://doi.org/10.1016/j.cis.2007.06.001)
- G.D. Danilatos, Bibliography of environmental scanning electron microscopy. *Microsc. Res. Tech.* **25**(5–6), 529–534 (1993). doi:[10.1002/jemt.1070250526](https://doi.org/10.1002/jemt.1070250526)
- H.-U. Danzebrink, L. Koenders, G. Wilkening, A. Yacoot, H. Kunzmann, Advances in scanning force microscopy for dimensional metrology *Ann. CIRP* **55**(2), 841–878 (2006). doi:[10.1016/j.cirp.2006.10.010](https://doi.org/10.1016/j.cirp.2006.10.010)
- P. Fiala, D. Göhler, E. Buhr, T. Dziomba, T. Klein, *Realisierung und Optimierung von Präparationsmethoden für zuverlässige Größenmessungen mit AFM und TSEM*. DIN-INS report,-Technische Universität Dresden, Physikalisch-Technische Bundesanstalt Braunschweig, 2011
- F.J. Giessibl, Advances in atomic force microscopy. *Rev. Mod. Phys.* **75**(3), 949–983 (2003). doi:[10.1103/RevModPhys.75.949](https://doi.org/10.1103/RevModPhys.75.949)
- L.-O. Heim, J. Blum, M. Preuss, H.-J. Butt, Adhesion and friction forces between spherical micrometre-sized particles. *Phys. Rev. Lett.* **83**(16), 3328–3331 (1999). doi:[10.1103/PhysRevLett.83.3328](https://doi.org/10.1103/PhysRevLett.83.3328)
- S.W. Hell, Far-field optical nanoscopy. *Science* **316**(5828), 1153–1158 (2007). doi:[10.1126/science.1137395](https://doi.org/10.1126/science.1137395)
- M. Knoll, E. Ruska, Das Elektronenmikroskop. *Z. Phys.* **78**(5–6), 318–339 (1932). doi:[10.1007/BF01342199](https://doi.org/10.1007/BF01342199)
- P. F. Schmidt et al., *Praxis der Rasterelektronenmikroskopie und Mikrobereichsanalyse*. In series: *Kontakt & Studium*, ed. by W. J. Bartz, vol. 444 (Messtechnik. expert Verlag, Renningen-Malmsheim, 1994). ISBN 3-8169-1038-6

Sedimentation

- M. Beiser, *Sedimentationsverhalten submikroner Partikeln in Abhängigkeit physikalisch-chemischer Einflüsse und ihr Separationsverhalten in Dekantierzentrifugen*. PhD thesis, Universität Fridericiana Karlsruhe (TH), 2005
- C. Bernhardt, Sedimentation in particle size analysis, in *Encyclopedia of analytical chemistry*, ed. by R. A. Meyers (Wiley, 2010). doi:[10.1002/9780470027318.a1513](https://doi.org/10.1002/9780470027318.a1513)
- G. Bickert, *Sedimentation feinsten suspendierter Partikeln im Zentrifugalfeld*. PhD thesis, Universität Fridericiana Karlsruhe (TH), 1997
- S.G. Conlin, W.J. Levene, W.F. Volume, An instrument for size analysis of fine powders by X-ray absorption. *J. Sci. Instrum.* **44**(8), 606–610 (1967). doi:[10.1088/0950-7671/44/8/306](https://doi.org/10.1088/0950-7671/44/8/306)
- T. Detloff, T. Sobisch, D. Lerche, Particle size distribution by space or time dependent extinction profiles obtained by analytical centrifugation. *Part. Part. Syst. Charact.* **23**(2), 184–187 (2006). doi:[10.1002/ppsc.200601028](https://doi.org/10.1002/ppsc.200601028)
- K. Edelman, *Lehrbuch der Kolloidchemie*, vol. I (Verlag der Wissenschaften, Berlin, 1962)
- S. Enomoto, T. Hiroshi, N. Tachikawa, M. Senoo, Particle size determination by use of ⁵⁵Fe X-ray absorption. *Int. J. Appl. Radiat. Isot.* **30**(1), 51–54 (1979). doi:[10.1016/0020-708X\(79\)90097-8](https://doi.org/10.1016/0020-708X(79)90097-8)
- B. L. Henke, E. M. Gullikson, J. C. Davis, X-Ray Interactions: Photoabsorption, scattering, transmission, and reflection at E = 50–30,000 eV, Z = 1–92. *At. Data Nucl. Data Tables* **54**(2), 181–342 (1993). doi:[10.1006/adnd.1993.1013](https://doi.org/10.1006/adnd.1993.1013)
- H.J. Kamack, A note on centrifugal particle size analysis. *J. Phys. D Appl. Phys.* **5**(10), 1962–1968 (1972). doi:[10.1088/0022-3727/5/10/330](https://doi.org/10.1088/0022-3727/5/10/330)
- K. Leschonski, *Hochschulkurs Grundlagen und Moderne Verfahren der Partikelmesstechnik*. Technische Universität Clausthal, Institut für Mechanische Verfahrenstechnik und Umweltverfahrenstechnik, 1982
- S. Odén, Eine neue Methode zur Bestimmung der Körnerverteilung in Suspensionen. *Kolloid Z.* **18**(2), 33–48 (1916). doi:[10.1007/BF01432659](https://doi.org/10.1007/BF01432659)
- W. Ostwald, F.-V. V. Hahn, Ueber kinetische Flockungsmesser, I. *Kolloid-Z.* **30**(1), 62–70, 1922. doi:[10.1007/BF01430381](https://doi.org/10.1007/BF01430381)
- K. M. Paciejewska, *Untersuchung des Stabilitätsverhaltens von binären kolloidalen Suspensionen*. PhD thesis, Technische Universität Dresden, 2010. <http://nbn-resolving.de/urn:nbn:de:bsz:14-qucosa-65050>
- G. E. Salinas Salas, *Sedimentationsverhalten von Submikrometerpartikeln in wässrigen Suspensionen*. PhD thesis, Technische Universität Dresden, 2007
- K. Schilling, *Charakterisierung mizellarer Systeme mit der Analytischen Ultrazentrifuge—Synthese von Titandioxid in mizellaren Reaktionsräumen*, PhD thesis, Universität Potsdam, 1999
- T. Svedberg, J.B. Nichols, Determination of size and distribution of size of particle by centrifugal methods. *J. Am. Chem. Soc.* **45**(12), 2910–2917 (1923). doi:[10.1021/ja01665a016](https://doi.org/10.1021/ja01665a016)
- T. Svedberg, H. Rinde, The ultra-centrifuge, a new instrument for the determination of size and distribution of size of particle in amicroscopic colloids. *J. Am. Chem. Soc.* **46**(2), 2677–2693 (1924). doi:[10.1021/ja01677a011](https://doi.org/10.1021/ja01677a011)
- H. C. van de Hulst, *Light Scattering by Small Particles* (Dover Publications, New York, 1981). ISBN 0-486-64228-3

Field-Flow Fractionation (FFF)

- T.J. Cho, V.A. Hackley, Fractionation and characterization of gold nanoparticles in aqueous solution: asymmetric-flow field flow fractionation with MALS, DLS, and UV-Vis detection. *Anal. Bioanal. Chem.* **398**(5), 2003–2018 (2010). doi:[10.1007/s00216-010-4133-6](https://doi.org/10.1007/s00216-010-4133-6)

- J.C. Giddings, A new separation concept based on a coupling of concentration and flow nonuniformities. *Separ. Sci.* **1**(1), 123–125 (1966). doi:[10.1080/01496396608049439](https://doi.org/10.1080/01496396608049439)
- J.C. Giddings, Nonequilibrium theory of field-flow fractionation. *J. Chem. Phys.* **49**(1), 81–85 (1968). doi:[10.1063/1.1669863](https://doi.org/10.1063/1.1669863)
- J.C. Giddings, G. Karaiskakis, K.D. Caldwell, M.N. Myers, Colloid characterization by sedimentation field-flow fractionation. I. Monodisperse population. *J. Colloid Interface Sci.* **92**(1), 66–80 (1983). doi:[10.1016/0021-9797\(83\)90117-0](https://doi.org/10.1016/0021-9797(83)90117-0)
- E. Grushka, K.D. Caldwell, M.N. Myers, Marcus, J. C. Giddings, Field flow fractionation. *Sep. Purif. Rev.* **2**(1), 127–151 (1974). doi:[10.1080/03602547408068793](https://doi.org/10.1080/03602547408068793)
- J. Laudan, *Untersuchung von ultrahochmolekularen Polymeren mittels asymmetrischer Fluss Feld-Fluss-Fraktionierung und Lichtstreu-/Konzentrationsdetektor-Kombination*. PhD thesis, Universität Hamburg, 2004
- Y. Mori, B. Scarlett, H.G. Merkus, Effects of ionic strength of eluent on size analysis of submicrometre particles by sedimentation field-flow fractionation. *J. Chromatogr. A* **515**, 21–35 (1990). doi:[10.1016/S0021-9673\(01\)89298-0](https://doi.org/10.1016/S0021-9673(01)89298-0)
- K.L. Plathe, F. von der Kammer, M. Hasselov, J. Moore, M. Murayama, T. Hofmann, M.F. Hochella Jr, Using FFFF and aTEM to determine trace metal-nanoparticle associations in riverbed sediment. *Environ. Chem.* **7**(1), 82–93 (2010). doi:[10.1071/EN09111](https://doi.org/10.1071/EN09111)
- T. Schauer, Symmetrical and asymmetrical flow field-flow fractionation for particle size determination. *Part. Part. Syst. Charact.* **12**(6), 284–288 (1995). doi:[10.1002/ppsc.19950120606](https://doi.org/10.1002/ppsc.19950120606)
- P.J. Wyatt, Submicrometre particle sizing by multiangle light scattering following fractionation. *J. Colloid Interface Sci.* **197**(1), 9–20 (1998). doi:[10.1006/jcis.1997.5215](https://doi.org/10.1006/jcis.1997.5215)
- F.-S. Yang, K.D. Caldwell, J.C. Giddings, Colloid characterization by sedimentation field-flow fractionation. II. Particle size distribution. *J. Colloid Interface Sci.* **92**(1), 81–91 (1983). doi:[10.1016/0021-9797\(83\)90118-2](https://doi.org/10.1016/0021-9797(83)90118-2)

Size-Exclusive Chromatography (SEC)

- P.S. Fedotov, N.G. Vanifatova, V.M. Shkinev, B.Y. Spivakov, Fractionation and characterization of nano- and microparticles in liquid media. *Anal. Bioanal. Chem.* **400**(6), 1787–1804 (2011). doi:[10.1007/s00216-011-4704-1](https://doi.org/10.1007/s00216-011-4704-1)
- F.-K. Liu, Analysis and applications of nanoparticles in the separation sciences: a case of gold nanoparticles. *J. Chromatogr. A* **1216**(52), 9034–9047 (2009). doi:[10.1016/j.chroma.2009.07.026](https://doi.org/10.1016/j.chroma.2009.07.026)
- G.T. Wei, F.-K. Liu, C.R.C. Wang, Shape separation of nanometre cold particles by size-exclusion chromatography. *Anal. Chem.* **71**(11), 2085–2091 (1999). doi:[10.1021/ac990044u](https://doi.org/10.1021/ac990044u)
- T. Yamaguchi, Y. Azuma, K. Okuyama, Development of a photon correlation spectroscopy instrument to measure size distributions of nanoparticles. *Part. Part. Syst. Charact.* **23**(2), 188–192 (2006). doi:[10.1002/ppsc.200601029](https://doi.org/10.1002/ppsc.200601029)

Static Light Scattering (SLS)

- P. Debye, Molecular-weight determination by light scattering. *J. Phys. Colloid Chem.* **51**(1), 18–32 (1947). doi:[10.1021/j150451a002](https://doi.org/10.1021/j150451a002)
- A. Einstein, Theorie der Opaleszenz von homogenen Flüssigkeiten und Flüssigkeitsgemischen in der Nähe des kritischen Zustandes (Theory of opalescence of homogenous liquids and liquid mixtures near critical conditions). *Ann. Phys. IV* **33**(16), 1275–1298 (1910). doi:[10.1002/andp.19103381612](https://doi.org/10.1002/andp.19103381612)

- S. Heimer, D. Težak, Structure of polydispersed colloids characterised by light scattering and electron microscopy. *Adv. Colloid Interface Sci.* **98**(1), 1–23 (2002). doi:[10.1016/S0001-8686\(01\)00090-2](https://doi.org/10.1016/S0001-8686(01)00090-2)
- W.C.K. Poon, A.D. Pirie, P.N. Pusey, Gelation in colloid-polymer mixtures. *Faraday Discuss.* **101**, 65–76 (1995). doi:[10.1039/fd9950100065](https://doi.org/10.1039/fd9950100065)
- H.M. Wyss, J. Innerlohinger, L.P. Meier, L.J. Gauckler, O. Glatter, Small-angle static light scattering of concentrated silica suspensions during in situ destabilization. *J. Colloid Interface Sci.* **271**(2), 388–399 (2004). doi:[10.1016/j.jcis.2003.09.051](https://doi.org/10.1016/j.jcis.2003.09.051)
- R. Xu, *Particle Characterization: Light Scattering Methods* (Kluwer Academic Publishers, Dordrecht, 2000). ISBN 0-7923-6300-0
- B.H. Zimm, Molecular theory of the scattering of light in fluids. *J. Chem. Phys.* **13**(4), 141–145 (1945). doi:[10.1063/1.1724013](https://doi.org/10.1063/1.1724013)
- B.H. Zimm, Apparatus and methods for measurement and interpretation of the angular variation of light scattering; Preliminary results on polystyrene solutions. *J. Chem. Phys.* **16**(12), 1099–1116 (1948). doi:[10.1063/1.1746740](https://doi.org/10.1063/1.1746740)

Laser Diffraction

- A. Büchtemann, H. Dautzenberg, I. Müller, Ermittlung der Größenverteilung sphärischer Teilchen mittels Laserdiffraktion an elektronenmikroskopischen Aufnahmen. *Acta Polym.* **33**(10), 605–612 (1982). doi:[10.1002/actp.1982.010331008](https://doi.org/10.1002/actp.1982.010331008)
- N. Chigier, Comparative measurements using different particle size instruments, in *Liquid particle size measurement techniques, ASTM STP 848*, eds. by J. M. Tishkoff, R. D. Ingelbo, J. B. Kennedy (American Society for Testing and Materials, Philadelphia, 1984), pp. 169–189. ISBN 0-8031-0227-5
- G.B.J. de Boer, C. de Weerd, D. Thoenes, H.W.J. Goossens, Laser diffraction spectrometry: Fraunhofer diffraction versus Mie scattering. *Part. Charact.* **4**(1), 14–19 (1987). doi:[10.1002/ppsc.19870040104](https://doi.org/10.1002/ppsc.19870040104)
- N. Gabas, N. Hiquily, C. Laguérie, Response of laser diffraction particle sizer to anisometric particles. *Part. Part. Syst. Charact.* **11**(2), 121–126 (1994). doi:[10.1002/ppsc.19940110203](https://doi.org/10.1002/ppsc.19940110203)
- C.M.G. Heffels, P.J.T. Verheijen, D. Heitzmann, B. Scarlett, Correction of the effect of particle shape on the size distribution measured with a laser diffraction instrument. *Part. Part. Syst. Charact.* **13**(5), 271–279 (1996). doi:[10.1002/ppsc.19960130504](https://doi.org/10.1002/ppsc.19960130504)
- M. Heuer, K. Leschonski, Results obtained with a new instrument for the measurement of particle size distributions from diffraction patterns. *Part. Charact.* **2**(1–4), 7–13 (1985). doi: [10.1002/ppsc.19850020102](https://doi.org/10.1002/ppsc.19850020102)
- ISO 13320:2009, *Particle Size Analysis—Laser Diffraction Methods* (Beuth-Verlag Berlin, 2009)
- A.R. Jones, Fraunhofer diffraction by random irregular particles. *Part. Part. Syst. Charact.* **4**(4), 123–127 (1987). doi:[10.1002/ppsc.19870040126](https://doi.org/10.1002/ppsc.19870040126)
- C. Knösche, *Möglichkeiten und Grenzen der elektroakustischen Spektroskopie zur Gewinnung von Partikelgrößeninformationen*. PhD thesis, Technische Universität Dresden, 2001
- P. Kuchenbecker, M. Gemeinert, T. Rabe, Interlaboratory study of particle size distribution measurements by laser diffraction. *Part. Part. Syst. Charact.* **29**(4), 304–310 (2012). doi:[10.1002/ppsc.201000026](https://doi.org/10.1002/ppsc.201000026)
- M.N. Lodi, E.P. Osmolovskaya, Laser diffraction systems for measuring small objects. *Meas. Techn.* **18**(7), 1006–1008 (1975). doi:[10.1007/BF00818603](https://doi.org/10.1007/BF00818603)
- M. Ludwig, *Methodeneruierung zur Charakterisierung von Sprühtropfen verschiedener Sprühlösungen*, public report, Technische Universität Dresden, Institut für Verfahrenstechnik und Umwelttechnik, 2010

- T. Matsuyama, H. Yamamoto, B. Scarlett, Transformation of diffraction pattern due to ellipsoids into equivalent diameter distribution for spheres. *Part. Part. Syst. Charact.* **17**(2), 41–46 (2000). doi:[10.1002/1521-4117\(200006\)17:2<41::AID-PPSC41>3.0.CO;2-W](https://doi.org/10.1002/1521-4117(200006)17:2<41::AID-PPSC41>3.0.CO;2-W)
- G. Mie, Beiträge zur Optik trüber Medien, speziell kolloidaler Goldlösungen. *Ann. Phys.* **IV** **25**(3), 377–445 (1908). doi:[10.1002/andp.19083300302](https://doi.org/10.1002/andp.19083300302)
- Y. Mori, H. Yoshida, H. Masuda, Characterization of reference particles of transparent glass by laser diffraction method. *Part. Part. Syst. Charact.* **24**(2), 91–96 (2007). doi:[10.1002/ppsc.200601048](https://doi.org/10.1002/ppsc.200601048)
- Y. Mori, H. Yoshida, H. Masuda, Round robin test results of reference particle candidates of submicrometer size range. On the CD-ROM: *Particulate Systems Analysis 2008*, Stratford-Upon-Avon, 02–04 Sept 2008. (available from PCIG, C/o Particle Technology Ltd, Station Yard Industrial Estate, Hatton, Derbyshire, DE65 5DU, United Kingdom), paper 38
- N. Stevens, J. Shrimpton, M. Palmer, D. Prime, B. Johal, Accuracy assessments for laser diffraction measurements of pharmaceutical lactose. *Meas. Sci. Technol.* **18**(12), 3697–3706 (2007). doi:[10.1088/0957-0233/18/12/004](https://doi.org/10.1088/0957-0233/18/12/004)
- T. Stromgren, Linear measurements of growth of shells using laser diffraction. *Limnol. Oceanogr.* **20**(5), 845–848 (1975). doi:[10.4319/lo.1975.20.5.0845](https://doi.org/10.4319/lo.1975.20.5.0845)
- T. Stübinger, U. Köhler, W. Witt, Verification of Mie scattering algorithms by extreme precision calculations. On the CD-ROM: *WCPT6 2010, World Congress on Particle Technology*, Nuremberg, 2–29 Apr 2010. ISBN 978-3-00-030570-2. (available from NürnbergMesse GmbH, Messezentrum, 90471 Nürnberg, Germany), paper 00272
- B.J. Thompson, Hybrid processing systems—assessment. *Proc. IEEE* **65**(1), 62–76 (1977). doi:[10.1109/PROC.1977.10431](https://doi.org/10.1109/PROC.1977.10431)
- A.P. Tinke, A. Carnicer, R. Govoreanu, G. Scheltjens, L. Lauwerysen, N. Mertens, Particle shape and orientation in laser diffraction and static image analysis. *Powder Technol.* **186**(2), 154–167 (2008). doi:[10.1016/j.powtec.2007.11.017](https://doi.org/10.1016/j.powtec.2007.11.017)
- H. C. van de Hulst, *Light Scattering by Small Particles* (Dover Publications, New York, 1981). ISBN 0-486-64228-3
- J. von Fraunhofer, Neue Modifikation des Lichtes durch gegenseitige Einwirkung und Beugung der Strahlen, und Gesetze derselben. *Denkschr. K. Akad. Wiss. München* **8**, 3–76 (1821)
- W. Witt, T. Stübinger, U. Köhler, J. List, J. Jordan, Partikelgrößenanalyse mit absoluter Genauigkeit. *Chem. Ing. Tech.* **84**(3), 211–222 (2012). doi:[10.1002/cite.201100172](https://doi.org/10.1002/cite.201100172)
- R. Xu, *Particle Characterization: Light Scattering Methods* (Kluwer Academic Publishers, Dordrecht, 2000). ISBN 0-7923-6300-0
- T. Yamauchi, Y. Ohyama, A study on the measurement of particle size distribution with laser diffraction systems. *Bull. Jpn. Soc. Mech. Eng.* **25**(210), 1931–1937 (1982). doi:[10.1299/jsme1958.25.1931](https://doi.org/10.1299/jsme1958.25.1931)

Small Angle Neutron and X-ray Scattering (SANS and SAXS)

- J.W. Anderegg, W.W. Beeman, S. Shulman, P. Kaesberg, An investigation of the size, shape and hydration of serum albumin by small-angle X-ray scattering. *J. Am. Chem. Soc.* **77**(11), 2927–2937 (1955). doi:[10.1021/ja01616a002](https://doi.org/10.1021/ja01616a002)
- E. Bugnicourt, J. Galy, J.-F. Géraud, F. Boué, H. Barthel, Structural investigations of pyrogenic silica–epoxy composites: combining small-angle neutron scattering and transmission electron microscopy. *Polymer* **48**(4), 949–958 (2007). doi:[10.1016/j.polymer.2006.12.012](https://doi.org/10.1016/j.polymer.2006.12.012)
- H.-D. Dörfler, *Grenzflächen- und Kolloidchemie* (Wiley-VCH, Weinheim, 1994). ISBN 3-527-29072-9
- G. Fritz, O. Glatter, Structure and interaction in dense colloidal systems: evaluation of scattering data by the generalized indirect Fourier transformation method. *J. Phys. Condens. Matter* **18** (36), S2403–S2419 (2006). doi:[10.1088/0953-8984/18/36/S14](https://doi.org/10.1088/0953-8984/18/36/S14)

- O. Glatter, R. May, Small-angle techniques, in *International tables for crystallography volume C: Mathematical, physical and chemical tables*, Chapter 2.6, *IUCr Series. International Tables for Crystallography*, ed. by E. Prince (Springer, Luxembourg, 2006), pp. 89–112. ISBN 978-1-4020-1900-5; doi:[10.1107/97809553602060000581](https://doi.org/10.1107/97809553602060000581)
- O. Glatter, O. Kratky (eds.), *Small angle X-ray scattering* (Academic Press, London, 1982). ISBN 0-12-286280-5
- A. Guinier, La diffusion des rayons X sous les très faibles angles appliquée à l'étude de fines particules et de suspensions colloïdales (The diffusion of X-rays under the extremely weak angles applied to the study of fine particles and colloidal suspension). *CR Hebd. Seance Acad. Sci.* **206**(19), 1374–1376 (1938)
- B. L. Henke, E. M. Gullikson, J. C. Davis, X-Ray Interactions: Photoabsorption, scattering, transmission, and reflection at $E = 50\text{--}30,000$ eV, $Z = 1\text{--}92$. *At. Data Nucl. Data Tables* **54**(2), 181–342 (1993). doi:[10.1006/adnd.1993.1013](https://doi.org/10.1006/adnd.1993.1013)
- A.J. Hurd, D.W. Schaefer, J.E. Martin, Surface and mass fractals in vapor-phase aggregates. *Phys. Rev. A* **35**(5), 2361–2364 (1987). doi:[10.1103/PhysRevA.35.2361](https://doi.org/10.1103/PhysRevA.35.2361)
- J. Ilavsky, A.J. Allen, G.G. Long, P.R. Jemian, Effective pinhole-collimated ultrasmall-angle X-ray scattering instrument for measuring anisotropic microstructures. *Rev. Sci. Instrum.* **73** (3), 1660–1662 (2002). doi:[10.1063/1.1425387](https://doi.org/10.1063/1.1425387)
- H.K. Kammler, G. Beaucage, R. Mueller, S.E. Pratsinis, Structure of flame-made silica nanoparticles by ultra-small-angle X-ray scattering. *Langmuir* **20**(5), 1915–1921 (2004). doi:[10.1021/la030155v](https://doi.org/10.1021/la030155v)
- O. Kratky, H. Stabinger, X-ray small angle camera with block-collimation system an instrument of colloid research. *Colloid Polym. Sci.* **262**(5), 345–360 (1984). doi:[10.1007/BF01410252](https://doi.org/10.1007/BF01410252)
- D. Qiu, C.A. Dreiss, T. Cosgrove, A.M. Howe, Small-angle neutron scattering study of concentrated colloidal dispersions: The interparticle interactions between sterically stabilized particles. *Langmuir* **21**(22), 9964–9969 (2005). doi:[10.1021/la050322m](https://doi.org/10.1021/la050322m)
- S. Romer, C. Urban, H. Bissig, A. Stradner, F. Scheffold, P. Schurtenberger, Dynamics of concentrated colloidal suspensions: diffusion, aggregation and gelation. *Phil. Trans. R. Soc. Lond. A* **359**(1782), 977–984 (2001). doi:[10.1098/rsta.2000.0812](https://doi.org/10.1098/rsta.2000.0812)
- P.W. Schmidt, D. Avnir, D. Levy, A. Höhr, M. Steiner, A. Röhl, Small angle X-ray scattering from the surfaces of reversed phase silicas: power-law scattering exponents of magnitudes greater than four. *J. Chem. Phys.* **94**(2), 1474–1479 (1991). doi:[10.1063/1.460006](https://doi.org/10.1063/1.460006)

Dynamic Light Scattering (DLS)

- L.B. Aberle, P. Hülstede, S. Wiegand, W. Schröer, W. Staude, Effective suppression of multiply scattered light in static and dynamic light scattering. *Appl. Opt.* **37**(27), 6511–6524 (1998). doi:[10.1364/AO.37.006511](https://doi.org/10.1364/AO.37.006511)
- S.R. Aragón, R. Pecora, Theory of dynamic light scattering from large anisotropic particles. *J. Chem. Phys.* **66**(6), 2506–2516 (1977). doi:[10.1063/1.434246](https://doi.org/10.1063/1.434246)
- F.T. Arecchi, M. Giglio, U. Tartari, Scattering of coherent light by a statistical medium. *Phys. Rev.* **163**(1), 186–197 (1967). doi:[10.1103/PhysRev.163.186](https://doi.org/10.1103/PhysRev.163.186)
- H. Auweter, D. Horn, Fiber-optical quasi-elastic light scattering of concentrated dispersions. *J. Colloid Interface Sci.* **105**(2), 399–409 (1985). doi:[10.1016/0021-9797\(85\)90313-3](https://doi.org/10.1016/0021-9797(85)90313-3)
- F. Babick, M. Vorbau, M. Stintz, Characterization of pyrogenic powders with conventional particle sizing technique: II. Experimental data. *Part. Part. Syst. Charact.* **29**(2), 116–127 (2012). doi:[10.1002/ppsc.201000025](https://doi.org/10.1002/ppsc.201000025)
- A. Banchio, G. Nägele, J. Bergenholtz, Collective diffusion, self-diffusion and freezing criteria of colloidal suspensions. *J. Chem. Phys.* **113**(8), 3381–3396 (2000). doi:[10.1063/1.1286964](https://doi.org/10.1063/1.1286964)
- G.K. Batchelor, Sedimentation in a dilute polydisperse system of interacting spheres. Part 1. General theory. *J. Fluid Mech.* **119**, 379–408 (1982). doi:[10.1017/S0022112082001402](https://doi.org/10.1017/S0022112082001402)

- G.K. Batchelor, C.-S. Wen, Sedimentation in a dilute polydisperse system of interacting spheres. Part 2. Numerical results. *J. Fluid Mech.* **124**, 495–528 (1982). doi:[10.1017/S0022112082002602](https://doi.org/10.1017/S0022112082002602)
- G. Bolle, C. Cametti, P. Codastefano, P. Tartaglia, Kinetics of salt-induced aggregation in polystyrene lattices studied by quasielastic light scattering. *Phys. Rev. A* **35**(2), 837–841 (1987). doi:[10.1103/PhysRevA.35.837](https://doi.org/10.1103/PhysRevA.35.837)
- A. Braun, K. Franks, V. Kestens, G. Roebben, A. Lamberty, T. Linsinger, *Certification Report. Certification of Equivalent Spherical Diameters of Silica Nanoparticles in Water. Certified Reference Material ERM®-FD100* (Publications Office of the European Union, Luxembourg, 2011). ISSN 1018-5593, doi:[10.2787/33725](https://doi.org/10.2787/33725)
- L.G.B. Bremer, L. Deriemaeker, R. Finsy, E. Gelad, J.G.H. Joosten, Fiber optic dynamic light scattering, neither homodyne nor heterodyne. *Langmuir* **9**(8), 2008–2014 (1993). doi:[10.1021/la00032a019](https://doi.org/10.1021/la00032a019)
- B. Chu, F.J. Schoenes, The laser homodyne “self-beating” technique in light scattering. *J. Colloid Interface Sci.* **27**(3), 424–431 (1968). doi:[10.1016/0021-9797\(68\)90180-X](https://doi.org/10.1016/0021-9797(68)90180-X)
- H.Z. Cummins, Y. Yeh, N. Knable, Observation of diffusion broadening of Rayleigh scattered light. *Phys. Rev. Lett.* **12**(6), 150–153 (1964). doi:[10.1103/PhysRevLett.12.150](https://doi.org/10.1103/PhysRevLett.12.150)
- J.K.G. Dhont, C.G. de Kruif, Scattered light intensity cross correlation. I. Theory. *J. Chem. Phys.* **79**(4), 1658–1683 (1983). doi:[10.1063/1.446009](https://doi.org/10.1063/1.446009)
- A. di Biasio, G. Bolle, C. Cametti, P. Codastefano, F. Sciortino, P. Tartaglia, Crossover region in the aggregation of colloids. *Phys. Rev. E* **50**(2), 1649–1652 (1994). doi:[10.1103/PhysRevE.50.1649](https://doi.org/10.1103/PhysRevE.50.1649)
- M. Drewel, J. Ahrens, U. Podschus, Decorrelation of multiple scattering for an arbitrary scattering angle. *J. Opt. Soc. Am. A* **7**(2), 206–210 (1990). doi:[10.1364/JOSAA.7.000206](https://doi.org/10.1364/JOSAA.7.000206)
- J.W. Dunning Jr, J.C. Angus, Particle-size measurement by doppler-shifted laser light, a test of the Stokes-Einstein relation. *J. Appl. Phys.* **39**(5), 2479–2480 (1968). doi:[10.1063/1.1656588](https://doi.org/10.1063/1.1656588)
- R. Finsy, P. de Groen, L. Deriemaeker, M. van Laethem, Singular value analysis and reconstruction of photon correlation data equidistant in time. *J. Chem. Phys.* **91**(12), 7374–7383 (1989). doi:[10.1063/1.457260](https://doi.org/10.1063/1.457260)
- R. Finsy, Particle sizing by quasi-elastic light scattering. *Adv. Colloid Interface Sci.* **52**, 79–143 (1994). doi:[10.1016/0001-8686\(94\)80041-3](https://doi.org/10.1016/0001-8686(94)80041-3)
- R. Foord, E.R. Pike, E. Jakeman, R.J. Blagove, E. Wood, A.R. Peacocke, Determination of diffusion coefficients of haemocyanin at low concentration by intensity fluctuation spectroscopy of scattered laser light. *Nature* **227**(5255), 242–245 (1970). doi:[10.1038/227242a0](https://doi.org/10.1038/227242a0)
- H. Geers, W. Witt, Direct calculation of the volume based particle size distribution from PCS or PCCS measurements. On the CD-ROM: *Particulate Systems Analysis 2008, Stratford-Upon-Avon*, 02–04 Sept 2008. (available from PCIG, C/o Particle Technology Ltd, Station Yard Industrial Estate, Hatton, Derbyshire, DE65 5DU, United Kingdom), paper 28
- S.E. Harding, On the hydrodynamic analysis of macromolecular conformation. *Biophys. Chem.* **55** (1–2), 69–93 (1995). doi:[10.1016/0301-4622\(94\)00143-8](https://doi.org/10.1016/0301-4622(94)00143-8)
- T.M. Herrington, B.R. Midmore, The rapid aggregation of dilute suspensions—an experimental investigation of Smoluchowski theorem using photon-correlation spectroscopy. *Powder Technol.* **65**(1–3), 251–256 (1991). doi:[10.1016/0032-5910\(91\)80188-O](https://doi.org/10.1016/0032-5910(91)80188-O)
- M. Hoffmann, C.S. Wagner, L. Harnau, A. Wittemann, 3D Brownian diffusion of submicron-sized particle clusters. *ACS Nano* **3**(10), 3326–3334 (2009). doi:[10.1021/nn900902b](https://doi.org/10.1021/nn900902b)
- K. Ishii, T. Iwai, Theoretical analysis of path-length-resolved power spectrum measurement using low-coherence dynamic light scattering. *Jpn. J. Appl. Phys.* **47**(11), 8397–8401 (2008). doi:[10.1143/JJAP.47.8397](https://doi.org/10.1143/JJAP.47.8397)
- M. Itoh, K. Takahashi, Measurement of aerosol particles by dynamic light scattering—I. Effects of non-Gaussian concentration fluctuation in real time photon correlation spectroscopy. *J. Aerosol Sci.* **22**(7), 815–822 (1991). doi:[10.1016/0021-8502\(91\)90076-T](https://doi.org/10.1016/0021-8502(91)90076-T)
- E. Jakeman, E.R. Pike, Spectrum of clipped photon-counting fluctuations of Gaussian light. *Phys. A* **2**(3), 411–412 (1969). doi:[10.1088/0305-4470/2/3/021](https://doi.org/10.1088/0305-4470/2/3/021)
- E. Jakeman, Theory of optical spectroscopy by digital autocorrelation of photon-counting fluctuations. *J. Phys. A* **3**(2), 201–215 (1970). doi:[10.1088/0305-4470/3/2/012](https://doi.org/10.1088/0305-4470/3/2/012)

- S.S. Jena, H.B. Bohidar, Determination of absolute polydispersity and molecular-weight distribution of high-molecular-weight polymers from dynamic light-scattering. *J. Chem. Phys.* **99**(1), 673–681 (1993). doi:[10.1063/1.465739](https://doi.org/10.1063/1.465739)
- R.B. Jones, P.N. Pusey, Dynamics of suspended colloidal spheres. *Ann. Rev. Phys. Chem.* **42**, 137–169 (1991). doi:[10.1146/annurev.physchem.42.1.137](https://doi.org/10.1146/annurev.physchem.42.1.137)
- U. Kätzel, T. Richter, M. Stintz, H. Barthel, T. Gottschalk-Gaudig, Phase transitions of pyrogenic silica suspensions: a comparison to model laponite. *Phys. Rev. E* **76**(3), 031402 (2007). doi:[10.1103/PhysRevE.76.031402](https://doi.org/10.1103/PhysRevE.76.031402)
- A. Khintchine, Korrelationstheorie der stationären stochastischen Prozesse. *Math. Ann.* **109**(1), 604–615 (1934). doi:[10.1007/BF01449156](https://doi.org/10.1007/BF01449156)
- D.E. Koppel, Analysis of macromolecular polydispersity in intensity correlation spectroscopy: the method of cumulants. *J. Chem. Phys.* **57**(11), 4814–4820 (1972). doi:[10.1063/1.1678153](https://doi.org/10.1063/1.1678153)
- M. Kroon, G.H. Wegdam, R. Sprik, Dynamic light scattering studies on the sol-gel transition of a suspension of anisotropic colloidal particles. *Phys. Rev. E* **54**(6), 6541–6550 (1996). doi:[10.1103/PhysRevE.54.6541](https://doi.org/10.1103/PhysRevE.54.6541)
- A. Lamberty, K. Franks, A. Braun, V. Kestens, G. Roebben, T. Linsinger, Interlaboratory comparison for the measurement of particle size and zeta potential of silica nanoparticles in an aqueous suspension. *J. Nanopart. Res.* **13**(12), 7317–7329 (2011). doi:[10.1007/s11051-011-0624-4](https://doi.org/10.1007/s11051-011-0624-4)
- C. L. Lawson, R. J. Hanson, *Solving least squares problems*. In series: *Classics in applied mathematics*, vol. 15 (Society for Industrial Mathematics, Philadelphia, 1995), pp. 158–165. ISBN 0-898-71356-0
- D. Maier, M. Marth, J. Honerkamp, J. Weese, Influence of correlated errors on the estimation of the relaxation time spectrum in dynamic light scattering. *J. Appl. Opt.* **38**(21), 4671–4680 (1999). doi:[10.1364/AO.38.004671](https://doi.org/10.1364/AO.38.004671)
- S. Manley, B. Davidovitch, N.R. Davies, L. Cipelletti, A.E. Bailey et al., Time-dependent strength of colloidal gels. *Phys. Rev. Lett.* **95**(4), 048302 (2005). doi:[10.1103/PhysRevLett.95.048302](https://doi.org/10.1103/PhysRevLett.95.048302)
- M. Nakamura, M. Suzuki, H. Takano, M. Itoh, Simultaneous rotational and translational diffusion measurement of ellipsoidal fine particles by dual-polarization photon correlation spectroscopy. *On the CD-ROM: 10th International Conference on Liquid Atomization and Spray Systems ICLASS-2006*, Kyoto, 27 Aug–01 Sept 2006. (available from Institute for Liquid Atomization and Spray Systems—Japan, 2-14-9, Kasugadenaka, Konohana-ku, Osaka-shi, 554-0022, JAPAN), paper 217
- E. Overbeck, C. Sinn, Three-dimensional dynamic light scattering. *J. Mod. Opt.* **46**(2), 303–326 (1999). doi:[10.1080/09500349908231273](https://doi.org/10.1080/09500349908231273)
- R. Paschotta, *Encyclopedia of Laser Physics and Technology*, vol. A—M (Wiley-VCH, Berlin, 2008). ISBN 978-3-527-40828-3
- G.L. Paul, P.N. Pusey, Observation of a long-time tail in Brownian motion. *J. Phys. A: Math. Gen.* **14**(12), 3301–3327 (1981). doi:[10.1088/0305-4470/14/12/025](https://doi.org/10.1088/0305-4470/14/12/025)
- R. Pecora, Doppler shifts in light scattering from pure liquids and polymer solutions. *J. Chem. Phys.* **40**(6), 1604–1614 (1964). doi:[10.1063/1.1725368](https://doi.org/10.1063/1.1725368)
- R. Peters, Y. Georgalis, W. Sängler, Accessing lysozyme nucleation with a novel dynamic light scattering detector. *Acta Cryst. D* **54**(5), 873–877 (1998). doi:[10.1107/S0907444998002455](https://doi.org/10.1107/S0907444998002455)
- G.D.J. Phillies, Suppression of multiple scattering effects in quasielastic light scattering by homodyne cross-correlation techniques. *J. Chem. Phys.* **74**(1), 260–262 (1981a). doi:[10.1063/1.440884](https://doi.org/10.1063/1.440884)
- G.D.J. Phillies, Experimental demonstration of multiple-scattering suppression in quasielastic-light-scattering spectroscopy by homodyne coincidence techniques. *Phys. Rev. A* **24**(4), 1939–1943 (1981b). doi:[10.1103/PhysRevA.24.1939](https://doi.org/10.1103/PhysRevA.24.1939)
- S.W. Provencher, CONTIN. A general purpose constrained regularization program for inverting noisy linear algebraic and integral equations. *Comput. Phys. Commun.* **27**(3), 229–242 (1982). doi:[10.1016/0010-4655\(82\)90174-6](https://doi.org/10.1016/0010-4655(82)90174-6)
- V. Ruzicka, L. Zulian, G. Ruocco, Routes to gelation in a clay suspension. *Phys. Rev. Lett.* **93**(25), 258301 (2004). doi:[10.1103/PhysRevLett.93.258301](https://doi.org/10.1103/PhysRevLett.93.258301)

- K. Schätzel, Suppression of multiple scattering by photon cross-correlation techniques. *J. Mod. Opt.* **38**(9), 1849–1865 (1991). doi:[10.1080/09500349114551951](https://doi.org/10.1080/09500349114551951)
- P.N. Segré, W. van Megen, P.N. Pusey, K. Schätzel, W. Peters, Two-colour dynamic light scattering. *J. Mod. Opt.* **42**(9), 1929–1952 (1995). doi:[10.1080/09500349514551681](https://doi.org/10.1080/09500349514551681)
- M. Siddiq, C. Wu, B. Li, Dynamic light-scattering characterization of the molecular weight distribution of a broadly distributed phenolphthalein poly(ary1 ether ketone). *J. Appl. Polymer Sci.* **60**(11), 1995–1999 (1996). doi:[10.1002/\(SICI\)1097-4628\(19960613\)60:11<1995:AID-APP24>3.0.CO;2-Z](https://doi.org/10.1002/(SICI)1097-4628(19960613)60:11<1995:AID-APP24>3.0.CO;2-Z)
- A. J. F. Siegert, *On the fluctuations in signals returned by many independently moving scatterers*. MIT Rad. Lab. Rep. 465, Massachusetts Institute of Technology, 1943
- R.S. Stock, W.H. Ray, Interpretation of photon correlation spectroscopy data: a comparison of analysis methods. *J. Polym. Sci. Part B Polym. Phys.* **23**(7), 1393–1447 (1985). doi:[10.1002/pol.1985.180230707](https://doi.org/10.1002/pol.1985.180230707)
- C. Urban, P. Schurtenberger, Application of a new light scattering technique to avoid the influence of dilution in light scattering experiments with milk. *Phys. Chem. Chem. Phys.* **1**(17), 3911–3915 (1999). doi:[10.1039/a903906f](https://doi.org/10.1039/a903906f)
- N. Wiener, Generalized harmonic analysis. *Acta Math.* **55**(1), 117–258 (1930). doi:[10.1007/BF02546511](https://doi.org/10.1007/BF02546511)
- H. Wiese, D. Horn, Single-mode fibers in fiber-optic quasielastic light scattering: a study of the dynamics of concentrated latex dispersions. *J. Chem. Phys.* **94**(10), 6429–6443 (1991). doi:[10.1063/1.460272](https://doi.org/10.1063/1.460272)
- A.W. Willemse, J.C.M. Marijnissen, A.L. van Wuyckhuyse, R. Roos, H.G. Merkus, B. Scarlett, Low-concentration photon correlation spectroscopy. *Part. Part. Syst. Charact.* **14**(4), 157–162 (1997)
- G. Williams, D.C. Watts, Non-symmetrical dielectric relaxation behaviour arising from a simple empirical decay function. *Trans. Faraday Soc.* **66**, 80–85 (1970). doi:[10.1039/tf9706600080](https://doi.org/10.1039/tf9706600080)
- R. Xu, *Particle Characterization: Light Scattering Methods* (Kluwer Academic Publishers, Dordrecht, 2000). ISBN 0-7923-6300-0

Diffusive Wave Spectroscopy (DWS)

- M. Alexander, D.G. Dalgleish, Diffusing wave spectroscopy of aggregating and gelling systems. *Curr. Opin. Colloid Interface Sci.* **12**(4–5), 179–186 (2007). doi:[10.1016/j.cocis.2007.07.008](https://doi.org/10.1016/j.cocis.2007.07.008)
- G. Maret, P.E. Wolf, Multiple light scattering from disordered media. The effect of Brownian motion of scatterers. *Z. Phys. B* **65**(4), 409–413 (1987). doi:[10.1007/BF01303762](https://doi.org/10.1007/BF01303762)
- T.G. Mason, D.A. Weitz, Optical measurement of frequency-dependent linear viscoelastic moduli of complex fluid. *Phys. Rev. Lett.* **74**(7), 1250–1253 (1995). doi:[10.1103/PhysRevLett.74.1250](https://doi.org/10.1103/PhysRevLett.74.1250)
- D.J. Pine, D.A. Weitz, P.M. Chaikin, E. Herbolzheimer, Diffusing wave spectroscopy. *Phys. Rev. Lett.* **60**(12), 1134–1137 (1988). doi:[10.1103/PhysRevLett.60.1134](https://doi.org/10.1103/PhysRevLett.60.1134)
- L.F. Rojas-Ochoa, S. Romer, F. Scheffold, P. Schurtenberger, Diffusing wave spectroscopy and small-angle neutron scattering from concentrated colloidal suspensions. *Phys. Rev. E* **65**(5), 051403 (2002). doi:[10.1103/PhysRevE.65.051403](https://doi.org/10.1103/PhysRevE.65.051403)
- H.G.M. Ruis, P. Venema, E. van der Linden, Diffusing wave spectroscopy used to study the influence of shear on aggregation. *Langmuir* **24**(14), 7117–7123 (2008). doi:[10.1021/la800517h](https://doi.org/10.1021/la800517h)
- F. Scheffold, Particle sizing with diffusing wave spectroscopy. *J. Disp. Sci. Technol.* **23**(5), 591–599 (2002). doi:[10.1081/DIS-120015365](https://doi.org/10.1081/DIS-120015365)
- H.M. Wyss, S. Romer, F. Scheffold, P. Schurtenberger, L.J. Gauckler, Diffusing-wave spectroscopy of concentrated alumina suspensions during gelation. *J. Colloid Interface Sci.* **241**(1), 89–97 (2001). doi:[10.1006/jcis.2001.7668](https://doi.org/10.1006/jcis.2001.7668)

Fluorescence and X-ray Spectroscopy

- E.L. Elson, D. Magde, Fluorescence correlation spectroscopy. I. Conceptual basis and theory. *Biopolymers* **13**(1), 1–27 (1974). doi:[10.1002/bip.1974.360130102](https://doi.org/10.1002/bip.1974.360130102)
- O. Krichевsky, G. Bonnet, Fluorescence correlation spectroscopy: the technique and its applications. *Rep. Prog. Phys.* **65**(2), 251–297 (2002). doi:[10.1088/0034-4885/65/2/203](https://doi.org/10.1088/0034-4885/65/2/203)
- O. Leupold, G. Grübel, S.V. Roth, C. Schroer, W. Roseker, M. Sikorski, A. Robert, X-ray fluorescence correlation spectroscopy—a tool to study element-specific dynamics. *J. Appl. Cryst.* **40**(Suppl. 1), s283–s285 (2007). doi:[10.1107/S0021889807017852](https://doi.org/10.1107/S0021889807017852)
- D. Magde, E.L. Elson, W.W. Webb, Fluorescence correlation spectroscopy. II. An experimental realization. *Biopolymers* **13**(1), 29–61 (1974). doi:[10.1002/bip.1974.360130103](https://doi.org/10.1002/bip.1974.360130103)
- K.A. Nugent, Coherent methods in the X-ray sciences. *Adv. Phys.* **59**(1), 1–99 (2010). doi:[10.1080/00018730903270926](https://doi.org/10.1080/00018730903270926)
- M. Sutton, A review of X-ray intensity fluctuation spectroscopy. *C. R. Physique* **9**(5–6), 657–667 (2008). doi:[10.1016/j.crh.2007.04.008](https://doi.org/10.1016/j.crh.2007.04.008)
- J. Wang, A.K. Sood, P.V. Satyam, Y. Feng, X.-Z. Wu, Z. Cai, W. Yun, S.K. Sinha, X-ray fluorescence correlation spectroscopy: A method for studying particle dynamics in condensed matter. *Phys. Rev. Lett.* **80**(5), 1110–1113 (1998). doi:[10.1103/PhysRevLett.80.1110](https://doi.org/10.1103/PhysRevLett.80.1110)

Optical Spectroscopy

- M.-T. Celis, A. Forgiarini, M.-I. Briceno, L.H. García-Rubio, Spectroscopy measurements for determination of polymer particle size distribution. *Colloids Surf. A* **331**(1–2), 91–96 (2008). doi:[10.1016/j.colsurfa.2008.07.024](https://doi.org/10.1016/j.colsurfa.2008.07.024)
- G. Crawley, M. Cournil, D.D. Benedetto, Size analysis of fine suspensions by spectral turbidimetry. *Powder Technol.* **91**(3), 197–208 (1997). doi:[10.1016/S0032-5910\(96\)03252-4](https://doi.org/10.1016/S0032-5910(96)03252-4)
- G.E. Elicabe, L.H. Garcia-Rubio, Latex particle size distribution from turbidimetry using inversion techniques. *J. Coll. Int. Sci.* **129**(1), 192–200 (1989). doi:[10.1016/0021-9797\(89\)90430-X](https://doi.org/10.1016/0021-9797(89)90430-X)
- S. Gabsch, B. Wessely, S. Ripperger, L. Steinke, Dynamic extinction spectroscopy as a new method to investigate precipitation processes in micro scale, in *VDI Berichte, Band 1901*, ed. by J. Ulrich (VDI Verlag GmbH, Düsseldorf, 2005), pp. 1189–1193. ISBN 3-18-091901-9
- J.S. Gaffney, N.A. Marley, M.M. Cunningham, Measurement of the absorption constants for nitrate in water between 270 and 335 nm. *Environ. Sci. Technol.* **26**(1), 207–209 (1992). doi:[10.1021/es00025a027](https://doi.org/10.1021/es00025a027)
- E. Gulari, G. Bazzi, E. Gulari, A. Annapragada, Latex particle size distributions from multiwavelength turbidity spectra. Part. Part. Syst. Charact. **4**(1–4), 96–100 (1987). doi:[10.1002/ppsc.19870040120](https://doi.org/10.1002/ppsc.19870040120)
- W. Haiss, N. T. K. Thanh, J. Aveyard, D. G. Fernig, Determination of size and concentration of gold nanoparticles from uv-vis spectra. *Anal. Chem.* **79**(11), 4215–4221 (2007). doi:[10.1021/ac0702084](https://doi.org/10.1021/ac0702084)
- T. Kuntzsch, *Erfassung und Beeinflussung des Zustandes von Poliersuspensionen für das chemisch-mechanische Polieren (CMP) in der Halbleiterbauelementfertigung*. PhD thesis, Technische Universität Dresden, 2004
- F. Li, R. Schafer, C.-T. Hwang, C.E. Tanner, S.T. Ruggiero, High-precision sizing of nanoparticles by laser transmission spectroscopy. *Appl. Opt.* **49**(34), 6602–6611 (2010). doi:[10.1364/AO.49.006602](https://doi.org/10.1364/AO.49.006602)
- D.H. Melik, H.S. Fogler, Turbidimetric determination of particle size distributions of colloidal systems. *J. Coll. Int. Sci.* **92**(1), 161–180 (1983). doi:[10.1016/0021-9797\(83\)90125-X](https://doi.org/10.1016/0021-9797(83)90125-X)
- G. Mie, Beiträge zur Optik trüber Medien, speziell kolloidaler Goldlösungen. *Ann. Phys. IV* **25**(3), 377–445 (1908). doi:[10.1002/andp.19083300302](https://doi.org/10.1002/andp.19083300302)

- P.N. Njoki, I.S. Lim, D. Mott, H.-Y. Park, B. Khan, S. Mishra, R. Sujakumar, J. Luo, C.-J. Zhong, Size correlation of optical and spectroscopic properties for gold nanoparticles. *J. Phys. Chem. C* **111**(40), 14664–14669 (2007). doi:[10.1021/jp074902z](https://doi.org/10.1021/jp074902z)
- H. Römer, C. V. Fragstein, Bestimmung des Absorptionskoeffizienten und des Brechungsquotienten von kolloidalem Gold. Ein Beitrag zur Anomalie der optischen Konstanten. *Z. Phys.* **163**(1), 27–43 (1961). doi:[10.1007/BF01328913](https://doi.org/10.1007/BF01328913)
- J.M.J. Santillán, F.A. Videla, M.B. Fernández van Raap, D. Muraca, L.B. Scaffardi, D.C. Schinca, Influence of size-corrected bound-electron contribution on nanometric silver dielectric function. Sizing through optical extinction spectroscopy. *J. Phys. D Appl. Phys.* **46**(43), 435301 (2013). doi:[10.1088/0022-3727/46/43/435301](https://doi.org/10.1088/0022-3727/46/43/435301)
- L.B. Scaffardi, J.O. Tocho, Size dependence of refractive index of gold nanoparticles. *Nanotechnol* **17**(5), 1309–1315 (2006). doi:[10.1088/0957-4484/17/5/024](https://doi.org/10.1088/0957-4484/17/5/024)
- D. Segets, J. Gradl, R. Klupp Taylor, V. Vassilev, W. Peukert, Analysis of optical absorbance spectra for the determination of zno nanoparticle size distribution, solubility, and surface energy. *ACS Nano* **3**(7), 1703–1710 (2009). doi:[10.1021/nn900223b](https://doi.org/10.1021/nn900223b)
- L. Steinke, B. Wessely, S. Ripperger, Optische Extinktionsmessverfahren zur Inline-Kontrolle disperser Stoffsysteme. (Optical extinction measurement procedures to control Inline substance dispersed systems). *Chem. Ing. Tech.* **81**(6), 735–747 (2009). doi:[10.1002/cite.200800129](https://doi.org/10.1002/cite.200800129)
- R.L. Zollars, Turbidimetric method for on-line determination of latex particle number and particle size distribution. *J. Colloid Interface Sci.* **74**(1), 163–172 (1980). doi:[10.1016/0021-9797\(80\)90179-4](https://doi.org/10.1016/0021-9797(80)90179-4)

Ultrasonic Spectroscopy

- J.R. Allegra, S.A. Hawley, Attenuation of sound in suspensions and emulsions: theory and experiments. *J. Acoust. Soc. Am.* **51**(5), 1545–1564 (1972). doi:[10.1121/1.1912999](https://doi.org/10.1121/1.1912999)
- J. Andreae, R. Bass, E. Heasell, J. Lamb, Pulse technique for measuring ultrasonic absorption in liquids. *Acustica* **8**, 131–142 (1958)
- P. Andreae, J.H. Joyce, 30 to 230 megacycle puls technique for ultrasonic absorption measurements in liquids. *Brit. J. Appl. Phys.* **13**(9), 462–467 (1962). doi:[10.1088/0508-3443/13/9/307](https://doi.org/10.1088/0508-3443/13/9/307)
- F. Babick, F. Hinze, M. Stintz, S. Ripperger, Ultrasonic spectrometry for particle size analysis in dense submicron suspensions. Part. Part. Syst. Charact. **15**(5), 230–236 (1998). doi:[10.1002/\(SICI\)1521-4117\(199810\)15:5<230:AID-PPSC230>3.0.CO;2-D](https://doi.org/10.1002/(SICI)1521-4117(199810)15:5<230:AID-PPSC230>3.0.CO;2-D)
- F. Babick, F. Hinze, S. Ripperger, Dependence of ultrasonic attenuation on the material properties. *Colloids Surf. A* **172**(1–3), 33–46 (2000). doi:[10.1016/S0927-7757\(00\)00571-9](https://doi.org/10.1016/S0927-7757(00)00571-9)
- F. Babick, S. Ripperger, Information content of acoustic attenuation spectra. Part. Part. Syst. Charact. **19**(3), 176–185 (2002). doi:[10.1002/1521-4117\(200207\)19:3<176:AID-PPSC176>3.0.CO;2-8](https://doi.org/10.1002/1521-4117(200207)19:3<176:AID-PPSC176>3.0.CO;2-8)
- F. Babick, *Schallspektroskopische Charakterisierung von submikronen Emulsionen*. PhD thesis, Technische Universität Dresden, 2005. <http://nbn-resolving.de/urn:nbn:de:swb:14-1112809488055-07176>
- F. Babick, M. Stintz, A. Richter, Ultrasonic particle sizing of disperse systems with partly unknown properties. Part. Part. Syst. Charact. **23**(2), 175–183 (2006). doi:[10.1002/ppsc.200601027](https://doi.org/10.1002/ppsc.200601027)
- F. Babick, A. Richter, Sound attenuation by small spheroidal particles due to visco-inertial coupling. *J. Acoust. Soc. Am.* **119**(3), 1441–1448 (2006). doi:[10.1121/1.2168427](https://doi.org/10.1121/1.2168427)
- R.E. Challis, M.J.W. Povey, M.L. Mather, A.K. Holmes, Ultrasound techniques for characterizing colloidal dispersions. *Rep. Prog. Phys.* **68**(7), 1541–1637 (2005). doi:[10.1088/0034-4885/68/7/R01](https://doi.org/10.1088/0034-4885/68/7/R01)
- A.S. Dukhin, P.J. Goetz, Acoustic spectroscopy for concentrated polydisperse colloids with high density contrast. *Langmuir* **12**(21), 4987–4997 (1996). doi:[10.1021/la951085y](https://doi.org/10.1021/la951085y)

- A. Dukhin, S. Parlia, D. Klank, M. Lesti, Particle sizing and zeta potential of silica Koestrosol (basis for certified reference material ERM-FD100 for nanoparticles) by acoustics and electroacoustics. *Part. Part. Syst. Charact.* **27**(5–6), 165–171 (2012). doi:[10.1002/ppsc.201100038](https://doi.org/10.1002/ppsc.201100038)
- J. Edmonds, P.D. Pearce, V.F. Andreae, 1.5 to 28.5 Mc/s pulse apparatus for automatic measurement of sound absorption in liquids and some results for aqueous and other solutions. *Brit. J. Appl. Phys.* **13**(11), 551–560 (1962). doi:[10.1088/0508-3443/13/11/310](https://doi.org/10.1088/0508-3443/13/11/310)
- P.S. Epstein, R.R. Carhart, The absorption of sound in suspensions and emulsions. I. Water fog in air. *J. Acoust. Soc. Am.* **25**(3), 553–565 (1953). doi:[10.1121/1.1907107](https://doi.org/10.1121/1.1907107)
- Y. Hemar, N. Herrmann, P. Lemar  chal, R. Hocquart, F. Lequeux, Effective medium model for ultrasonic attenuation due to the thermo-elastic effect in concentrated emulsions. *J. Phys. II France* **7**(4), 637–647 (1997). doi:[10.1051/jp2:1997148](https://doi.org/10.1051/jp2:1997148)
- F. Hinze, S. Ripperger, M. Stintz, Charakterisierung von Suspensionen nanoskaliger Partikel mittels Ultraschallspektroskopie und elektroakustischer Methoden. *Chem. Ing. Tech.* **72**(4), 322–332 (2000). doi:[10.1002/1522-2640\(200004\)72:4<322::AID-CITE322>3.0.CO;2-2](https://doi.org/10.1002/1522-2640(200004)72:4<322::AID-CITE322>3.0.CO;2-2)
- A. K. Hipp, B. Walker, M. Mazzotti, M. Morbidelli, In-situ monitoring of batch crystallization by ultrasound spectroscopy. *Ind. Eng. Chem. Res.* **39**, 783–789 (2000). doi:[10.1021/ie990448c](https://doi.org/10.1021/ie990448c)
- A.K. Hipp, G. Storti, M. Morbidelli, Acoustic characterization of concentrated suspensions and emulsions. I. Model analysis. *Langmuir* **18**(2), 391–404 (2002). doi:[10.1021/la015538c](https://doi.org/10.1021/la015538c)
- M.A. Isakovich, On the propagation of sound in emulsions (in Russian: O rasprostraneni   zvuka v emulsiyakh). *Zh. Eksperim. i Teor. Fiz.* **18**(10), 907–912 (1948)
- L.D. Kachanovskaya, E.V. Datskevich, V.S. Sperkach, Y.D. Usenko, Acoustic studies of aqueous solutions of biomacromolecules. *Colloids Surf. A* **106**(2–3), 103–107 (1996). doi:[10.1016/0927-7757\(95\)03361-0](https://doi.org/10.1016/0927-7757(95)03361-0)
- M. Li, D. Wilkinson, K. Patchigolla, P. Moug  n, K.J. Roberts, R. Tweedie, On-line crystallization process parameter measurements using ultrasonic attenuation spectroscopy. *Cryst. Growth Des.* **4**(5), 955–963 (2004). doi:[10.1021/cg030041h](https://doi.org/10.1021/cg030041h)
- D.J. McClements, Ultrasonic characterisation of emulsions and suspensions. *Adv. Colloid Interface Sci.* **37**(1–2), 34–72 (1991). doi:[10.1016/0001-8686\(91\)80038-L](https://doi.org/10.1016/0001-8686(91)80038-L)
- D.J. McClements, Principles of ultrasonic droplet size determination in emulsion. *Langmuir* **12**(2), 3454–3461 (1996). doi:[10.1021/la960083q](https://doi.org/10.1021/la960083q)
- P. Moug  n, D. Wilkinson, K.J. Roberts, R. Tweedie, Characterization of particle size and its distribution during the crystallization of organic fine chemical products as measured in situ using ultrasonic attenuation spectroscopy. *J. Acoust. Soc. Am.* **109**(1), 274–282 (2001). doi:[10.1121/1.1331113](https://doi.org/10.1121/1.1331113)
- J. Pellam, J.R. Galt, Ultrasonic Propagation in Liquids: I. Application of pulse technique to velocity and absorption measurements at 15 megacycles. *J. Chem. Phys.* **14**(10), 608–614 (1946). doi:[10.1063/1.1724072](https://doi.org/10.1063/1.1724072)
- J.M.M. Pinkerton, A pulse method for measurement of ultrasonic absorption in liquids. *Nature* **160** (4056), 128–129 (1947). doi:[10.1038/160128b0](https://doi.org/10.1038/160128b0)
- D.M. Scott, A. Boxman, C.E. Jochen, In-line particle characterization. *Part. Part. Syst. Charact.* **15** (1), 47–50 (1998). doi:[10.1002/\(SICI\)1521-4117\(199802\)15:1<47::AID-PPSC47>3.0.CO;2-Q](https://doi.org/10.1002/(SICI)1521-4117(199802)15:1<47::AID-PPSC47>3.0.CO;2-Q)

Electroacoustic Mobility Spectroscopy

- F. Babick, C. Kn  sche, M. Sch  fer, F. Stenger, Characterisation of emulsions with the ultrasonic spectroscopy. On the CD-ROM: *PARTEC 2001, International Congress for Particle Technology, Nuremberg*, 27–29 Mar 2001. (available from N  rnbergMesse GmbH, Messezentrum, 90471 N  rnberg, Germany), paper 10/1
- M.L. Carasso, W.N. Rowlands, R.A. Kennedy, Electroacoustic determination of droplet size and zeta potential in concentrated intravenous fat emulsions. *J. Colloid Interface Sci.* **174**(2), 405–413 (1995). doi:[10.1006/jcis.1995.1408](https://doi.org/10.1006/jcis.1995.1408)

- R. J. Hunter, Recent developments in the electroacoustic characterisation of colloidal suspensions and emulsions. *Colloids Surf. A* **141**(1), 37–65 (1998). doi:[10.1016/S0927-7757\(98\)00202-7](https://doi.org/10.1016/S0927-7757(98)00202-7)
- C. Knösche, *Möglichkeiten und Grenzen der elektroakustischen Spektroskopie zur Gewinnung von Partikelgrößeninformationen*. PhD thesis, Technische Universität Dresden, 2001
- M. Loewenberg, R.W. O'Brien, The dynamic mobility of nonspherical particles. *J. Colloid Interface Sci.* **150**(1), 158–168 (1992). doi:[10.1016/0021-9797\(92\)90276-R](https://doi.org/10.1016/0021-9797(92)90276-R)
- R.W. O'Brien, Electro-acoustic effects in a dilute suspension of spherical particles. *J. Fluid Mech.* **190**, 71–86 (1988). doi:[10.1017/S0022112088001211](https://doi.org/10.1017/S0022112088001211)
- R.W. O'Brien, D.W. Cannon, W.N. Rowlands, Electroacoustic determination of particle size and zeta potential. *J. Colloid Interface Sci.* **173**(2), 406–418 (1995). doi:[10.1006/jcis.1995.1341](https://doi.org/10.1006/jcis.1995.1341)

Zeta-Potential and Electrophoresis

- P. Debye, E. Hückel, Bemerkungen zu einem Satze über die kataphoretische Wanderungsgeschwindigkeit suspendierter Teilchen (Remarks on a rate concerning cataphoretic appearances in suspended parts). *Phys. Z.* **25**(3), 49–52 (1924)
- A.V. Delgado, F. González-Caballero, R.J. Hunter, L.K. Koopal, J. Lyklema, Measurement and interpretation of electrokinetic phenomena. *J. Colloid Interface Sci.* **309**(2), 194–224 (2007). doi:[10.1016/j.jcis.2006.12.075](https://doi.org/10.1016/j.jcis.2006.12.075)
- R. J. Hunter, *Zeta Potential in Colloid Science: Principles and Applications*. In Series: *Colloid science*, vol. 2; 3rd edn. (Academic Press, London, 1988). ISBN 0-12-361961-0
- R.W. O'Brien, L.R. White, Electrophoretic mobility of a spherical colloidal particle. *J. Chem. Soc. Faraday Trans. 2* **74**(9), 1607–1626 (1978). doi:[10.1039/F29787401607](https://doi.org/10.1039/F29787401607)
- M. von Smoluchowski, Przyczynek do teorii endosmozy elektrycznej i kilku pokrewnych zjawisk. *Rozprawy Wydziału matematyczno-przyrodniczego Akademii Umiejętności w Krakowie*, T. XLIII, Serja A, 110–127 (1903). (reprint in French: Contribution à la théorie de l'endosmose électrique et de quelques phénomènes corrélatifs. *Bull. Int. Acad. Sci. Cracovie, Cl. Sci. Math. Nat.* **8**, 182–200 (1903))
- R. Xu, Progress in nanoparticles characterization: Sizing and zeta potential measurement. *Particuology* **6**(2), 112–115 (2008). doi:[10.1016/j.partic.2007.12.002](https://doi.org/10.1016/j.partic.2007.12.002)

Electroacoustic Zeta-Potential Measurement

- F. Booth, J.A. Enderby, On electrical effects due to sound waves in colloidal suspensions. *Proc. Phys. Soc. A* **65**(5), 321–324 (1952). doi:[10.1088/0370-1298/65/5/303](https://doi.org/10.1088/0370-1298/65/5/303)
- P. Debye, A method for the determination of the mass of electrolyte ions. *J. Chem. Phys.* **1**(1), 13–16 (1933). doi:[10.1063/1.1749213](https://doi.org/10.1063/1.1749213)
- A.S. Dukhin, V.N. Shilov, H. Ohshima, P.J. Goetz, Electroacoustic phenomena in concentrated dispersions: new theory and CVI experiment. *Langmuir* **15**(20), 6692–6706 (1999). doi:[10.1021/la990317g](https://doi.org/10.1021/la990317g)
- A.S. Dukhin, P.J. Goetz, Acoustic and electroacoustic spectroscopy for characterizing concentrated dispersions and emulsions. *Adv. Colloid Interface Sci.* **92**, 73–132 (2001). doi:[10.1016/S0001-8686\(00\)00035-X](https://doi.org/10.1016/S0001-8686(00)00035-X)
- A.S. Dukhin, P.J. Goetz, S. Truesdail, Titration of concentrated dispersions using electroacoustic zeta-potential probe. *Langmuir* **17**(4), 964–968 (2001). doi:[10.1021/la001024m](https://doi.org/10.1021/la001024m)
- J.A. Enderby, On electrical effects due to sound waves in colloidal suspensions. *Proc. Roy. Soc. A* **207**(1090), 329–342 (1951). doi:[10.1098/rspa.1951.0121](https://doi.org/10.1098/rspa.1951.0121)
- R. Greenwood, Review of the measurement of zeta potentials in concentrated aqueous suspensions using electroacoustics. *Adv. Colloid Interface Sci.* **106**(1–3), 55–81 (2003). doi:[10.1016/S0001-8686\(03\)00105-2](https://doi.org/10.1016/S0001-8686(03)00105-2)

- J.J. Hermans, Charged colloidal particles in an ultrasonic field. *Philos. Mag.* **25**(168), 426–438 (1938a)
- J.J. Hermans, Charged colloid particles in an ultrasonic field. II. Particles surrounded by a thin double layer. *Philos. Mag.* **26**(177), 674–683 (1938b)
- R. J. Hunter, Recent developments in the electroacoustic characterisation of colloidal suspensions and emulsions. *Colloids Surf. A* **141**(1), 37–65 (1998). doi:[10.1016/S0927-7757\(98\)00202-7](https://doi.org/10.1016/S0927-7757(98)00202-7)
- R.J. Hunter, Measuring zeta potential in concentrated industrial slurries. *Colloids Surf. A* **195**(1–3), 205–214 (2001). doi:[10.1016/S0927-7757\(01\)00844-5](https://doi.org/10.1016/S0927-7757(01)00844-5)
- R.W. O'Brien, Electro-acoustic effects in a dilute suspension of spherical particles. *J. Fluid Mech.* **190**, 71–86 (1988). doi:[10.1017/S0022112088001211](https://doi.org/10.1017/S0022112088001211)
- R.W. O'Brien, P. Garside, R.J. Hunter, The electroacoustic reciprocal relation. *Langmuir* **10**(3), 931–935 (1994). doi:[10.1021/la00015a053](https://doi.org/10.1021/la00015a053)
- R.W. O'Brien, A. Jones, W.N. Rowlands, A new formula for the dynamic mobility in a concentrated colloid. *Colloids Surf. A* **218**(1–3), 89–101 (2003). doi:[10.1016/S0927-7757\(02\)00593-9](https://doi.org/10.1016/S0927-7757(02)00593-9)
- T. Oja, G. L.Petersen, D. Cannon, Measurement of electro-kinetic properties of a solution. *US Patent* 4 497 208, 1985
- M. Rasmusson, Volume fraction effects in electroacoustic measurements. *J. Colloid Interface Sci.* **240**(2), 432–447 (2001). doi:[10.1006/jcis.2001.7559](https://doi.org/10.1006/jcis.2001.7559)
- A.J. Rutgers, Comments on the difference of potential caused by ultrasonic waves in solutions. *Physica* **5**(1), 46 (1938). doi:[10.1016/S0031-8914\(38\)80106-3](https://doi.org/10.1016/S0031-8914(38)80106-3)
- A.J. Rutgers, Supersonic vibration potentials and centrifugation potentials. *Nature* **157**(3977), 74–76 (1946). doi:[10.1038/157074b0](https://doi.org/10.1038/157074b0)
- E. Yeager, H. Dietrick, F. Hovorka, Ultrasonic waves and electrochemistry. II. Colloidal and ionic vibration potentials. *J. Acoust. Soc. Am.* **25**(3), 456–460 (1953). doi:[10.1121/1.1907063](https://doi.org/10.1121/1.1907063)

Second Harmonic Generation (SHG)

- H.M. Eckenrode, S.-H. Jen, J. Han, A.-G. Yeh, H.-L. Dai, Adsorption of a cationic dye molecule on polystyrene microspheres in colloids: Effect of surface charge and composition probed by second harmonic generation. *J. Phys. Chem. B* **109**(10), 4646–4653 (2005). doi:[10.1021/jp045610q](https://doi.org/10.1021/jp045610q)
- D.B. Hollis, Review of hyper-Rayleigh and second-harmonic scattering in minerals and other inorganic solids. *Am. Mineral.* **73**(7–8), 701–706 (1988)
- L. Schneider, W. Peukert, Review: Second harmonic generation spectroscopy as a method for in situ and online characterization of particle surface properties. Part. Part. Syst. Charact. **23**(5), 351–359 (2007). doi:[10.1002/ppsc.200601084](https://doi.org/10.1002/ppsc.200601084)
- L. Schneider, H.J. Schmid, W. Peukert, Influence of particle size and concentration on the second-harmonic signal generated at colloidal surfaces. *Appl. Phys. B* **87**(2), 333–339 (2007). doi:[10.1007/s00340-007-2597-7](https://doi.org/10.1007/s00340-007-2597-7)
- B. Schürer, W. Peukert, In situ surface characterization of polydisperse colloidal particles by second harmonic generation. Part. Sci. Technol. **28**(5), 458–471 (2010). doi:[10.1080/02726351.2010.504131](https://doi.org/10.1080/02726351.2010.504131)
- E.C.Y. Yan, Y. Liu, K.B. Eisenthal, New method for determination of surface potential of microscopic particles by second harmonic generation. *J. Phys. Chem. B* **102**(33), 6331–6336 (1998). doi:[10.1021/jp981335u](https://doi.org/10.1021/jp981335u)

Final Remarks

- O. Ruscitti, R. Franke, H. Hahn, F. Babick, T. Richter, M. Stintz, Application of particle measurement technology in process intensification. *Chem. Eng. Technol.* **31**(2), 270–277 (2008). doi:[10.1002/ceat.200700465](https://doi.org/10.1002/ceat.200700465)

Suspensions of Colloidal Particles and Aggregates

Babick, F.

2016, XXI, 341 p. 96 illus., 24 illus. in color., Hardcover

ISBN: 978-3-319-30661-2